Geological Survey of Israel
Ministry of Energy

Geochemical evolution of Lake Lisan brine from interstitial soluble salts

Omri Khalifa

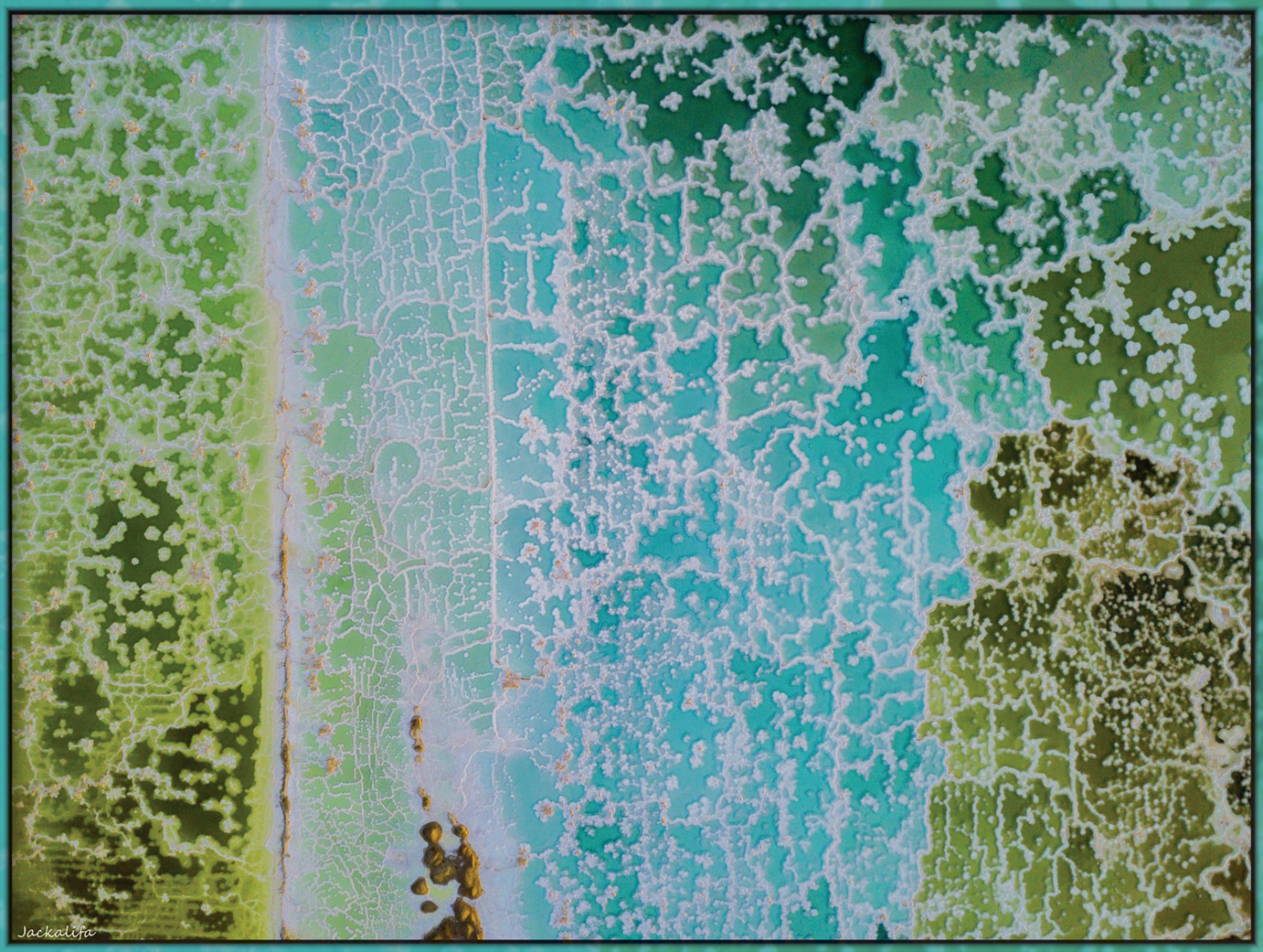

Report GSI/10/2021

November 2021

32 Yeshayahu Leibowitz St. Jerusalem 9692100, Israel

Front Cover:
Aerial view of the southern ponds of the Dead Sea.
The picture was taken by Jacob Khalifa

Back Cover:
Typical laminated section of Lisan Formation's sediments.

Cover design: Tirza Tzuberi

Geological Survey of Israel
Ministry of Energy

Geochemical evolution of Lake Lisan brine from interstitial soluble salts

Omri Khalifa

Thesis for the degree of "Master of science"

Submitted to the senate of the Hebrew University of Jerusalem.

The study was carried out under the supervision of:

Prof. Mordechai Stein, the Hebrew University of Jerusalem, Geological Survey of Israel.

Prof. Boaz Lazar, the Hebrew University of Jerusalem

Report GSI/10/2021 November 2021

Acknowledgments

First and foremost, I would like to thank my supervisors and teachers, Mordechai Stein and Boaz Lazar, from whom I tried to learn as much as possible about science and life. I thank them for their support, guidance, enthusiasm, and for the freedom they provided me along the project.

I wish to thank also Amitai Katz who advised me during the writing of the thesis, for his patience, involvement, and good ideas.
Additional advisors and good friends who I wish to thank are Gil Lapid and Tal Benaltabet for the moral and scientific support along the way.

The lab work and analytical measurements were possible thanks to the help of Ofhir Tirosh from the clean lab in the Institute of Earth Science, The Hebrew University of Jerusalem, and the crew of the geochemical department in the Geological Survey of Israel - Galit Sharabi, Dina Stiber, Olga Berlin and Nadia Teutsch. The help of Eilam Zahavi was also crucial for the preparation and measurements of the samples.

The completion of this work was possible thanks to the persistent help of my parents who supported my along the way.

This work is dedicated to my father, Ezra Khalifa, who encouraged me to learn, to be diligent and to persist but did not get to witness its completion.

Table of Contents

List of Figures

List of Tables

Abstract

A series of hypersaline and terminal lakes filled the tectonic depression of the Dead Sea Basin during the Quaternary. This basin and its lakes are located on the transition between the climatic belts of the hyperarid Sahara to the subtropical Mediterranean. The solutions that filled the lakes comprise Ca-chloride brines that originated in the Pliocene Sedom lagoon. This thesis focuses on the evolution of the brine during the last glacial period (70-14 ka) when Lake Lisan occupied the Dead Sea Basin. The sediments deposited from Lake Lisan comprise the Lisan Formation that consists mainly of sequences of laminated primary aragonite, silty detritus, and occasional gypsum. The primary aragonite was precipitated from the epilimnion solution of the lake, and the silty detritus comprises detrital particles (mainly quartz, calcite, and clays) that were washed to the lake from the surface cover of its watershed. Within the pores of the sediments fluids are trapped, and they are attributed to be a direct remnant of the lake's brine. In exposed sediments this brine was desiccated and precipitated salts. These salts are termed here: " soluble salts" and the investigation of their properties (e.g., the chemical compositions) and the implications for the geochemical and limnological history of the lake stand in the focus of this thesis.

The sediments that are studied in this work were collected from cores that were drilled at the deepest floor of the lake and intermediate depth (modern day shore), during the Dead Sea Deep Drilling Project (DSDDP) held by the ICDP in 2010/11. In addition, samples were collected in exposed sections of the Lisan Fm. at the marginal terraces of the modern Dead Sea, e.g., at Perazim valley and Mt. Sedom.

The measured ions are: $Ca^{2+,}$ Mg^{2+}, K^{+}, Na^{+}, Sr^{2+}, SO_4^{2-}, Br^{-}, Cl^{-}, NO_3^{-}, HCO_3^{-}. and the data are presented as elemental ratios (e.g., $\frac{Na}{Cl}$, $\frac{Sr}{Ca}$). The elemental ratios of the soluble salts are compared to data of pore fluids from the deep core (DSDDP project), and to soluble salts and aragonite chemistry from the marginal terraces.

The main conclusions of the study are:

1. Elements that are not part of the primary (evaporitic) minerals that precipitated from the lake such as aragonite and gypsum dissolve solely from interstitial soluble salts during the water extraction procedure. These elements are: Na, Cl, Br, Mg and NO_3.

   Elements that did participate in precipitation of the primary gypsum and aragonite are Ca, Sr and SO_4. These elements dissolve from primary minerals in addition to their dissolution from soluble salts,thus,

limited information can attain from their ionic ratios before a correction is conducted for the excess portions.

2. The ionic ratios of soluble salts extracted from sediments of the deep basin show high correlation to coeval pore fluids ratios from the same origin. Therefore, these ionic ratios serve as reliable tools for reconstructions of brine's chemical evolution.

3. Potassium shows some excess that may relate to mild dissolution of potash salts and/or adsorption of this ion from clays during the sediment-water interactions of the method.

4. The $\frac{Na}{Cl}$ ratios from the sediments of the deep basin rise from 0.3 to 0.7 in between 100-12 ka BP, which is followed by a sharp drop to 0.48 at 11 ka BP. The $\frac{Mg}{Cl}$ and $\frac{Br}{Cl}$ ratios exhibit a mirror pattern during the same time interval, with $\frac{Mg}{Cl}$ values dropping from 0.5 to 0.2 and then peaking to 0.43 and $\frac{Br}{Cl}$ dropping from 0.01 to 0.005 and peaking to 0.008. These profiles demonstrate the ability of these ratios to document the impact of the major hydro-climatic trends, as glacial-interglacial oscillations, on the lake's chemistry as well as the impact of short-term climatic shifts such as Heinrich events and glacial maximums.

5. During glacial periods (e.g., Lake Lisan period), when the lake level was high $\frac{Na}{Cl}$, $\frac{Mg}{Cl}$ and $\frac{Br}{Cl}$ ratios in the soluble salts of the sediments of intermediate elevations in the lake oscillate within similar ranges of values of the sediments of the deep basin. During interglacials the $\frac{Na}{Cl}$ ratios are higher in the soluble salts of the "intermediate elevation sediments" relative to those of the deep basin (0.5 vs 0.2) and lower in the $\frac{Mg}{Cl}$ and $\frac{Br}{Cl}$ (~0.36 vs 0.55 and ~0.0075 vs 0.011, respectively). This simultaneous behavior indicates that halite used to precipitate from the last interglacial Lake Samra in a similar way as it occurs today in the Dead Sea, where halite massively precipitate and accumulate year-round in the deep brine, while the upper brine remain close to saturation of halite but do not sustain accumulation of this salt on the shallow margins.

6. The $\frac{Na}{Cl}$ ratios in the marginal outcrops vary frequently within the range of 0.07-0.93 with many values that are significantly higher or lower than the coeval deep and shallow cores' ratios. The $\frac{Br}{Cl}$ ratios show a similar mirror behavior, oscillating between 0.0015 to 0.011, but with less distinct outliers. The $\frac{Mg}{Cl}$ ratios show a similar behavior as the $\frac{Br}{Cl}$ ratios, yet the values are lower than the coeval deep and shallow

cores' ratios, ranging between 0.034-0.343. Few of these distinct oscillations are attributed to originate from sediments deposition in a restricted marginal lake that pooled during periods of low lake level while the majority stem from diagenetic desiccation of the pore's brine and the crystallization of halite. The rest of the data is considered as original chemistry of the unstable epilimnion brine.

7. The soluble salts data suggest that chemical changes in the epilimnion were controlled by mixing between freshwater that entered the lake with high $\frac{Na}{Cl}$ values of ~0.9 to the epilimic solution that held an intermediate value of 0.45-0.65. This upper brine mixed with the lower isolated brine through turbulent-mixing and diffusion across the epilimnion-hypolimnion interface and by sinking of dense brine that dissolved halite and made its way to the deep basin. These processes transferred the mean chemical composition of the upper brine to the deep lake and controlled the chemical composition of the deep brine.

8. The presence of nitrate in the marginal sediments and its absence in the deep and intermediate sediments, and its pattern of dissolution, implies that the lake maintained stable stratified configuration during long time intervals of the last glacial period, what led to development of anoxic conditions in the hypolimnion. The epilimnion on the other hand remained oxide and its reduced salinity could sustain some bacteria. In this configuration nitrate and organic matter, that entered the lake with freshwater, could accumulate in the epilimnion. The organic matter was slowly oxidized to nitrate but was not consumed (assimilated) by primary producers that could not sustain in the high salinity of the brine. Some of the accumulated nitrate transported down to the hypolimnion and there it was slowly consumed by denitrifying bacteria present in the reducing deep brine.

תקציר מורחב בעברית

משקעי אגמים הם כלי מרכזי במחקרים לימנולוגיים מאחר והחומר השוקע נושא עימו מידע רב על התכונות השונות של האגם, החל מההרכב הכימי של מימיו וכלה במשטר ההידרולוגי ותנאי האקלים באגם ובאגן הניקוז שלו והשינויים שחלו בכל אלה במהלך הזמן. המידע המתקבל יכול להגיע הן מהחומר המוצק, ממי האגם הנלכדים בחללי המשקעים, ממלחים המושקעים בחללים או תוצרים של תהליכים דיאגנטיים המאוחרים לזמן ההשקעה. באגמים היפר-סליניים נוצרים חתכי משקעים אופייניים אשר מייצגים את התנאים הייחודיים השוררים באגני הניקוז של אגמים שכאלו. אחד התהליכים המתרחשים במשקעי האגמים הללו הוא כניסה של תמלחות האגם לחללי החומר השוקע באזור המגע בין הקרקעית לתמלחת. תמלחות אלו מכילות ריכוז גבוה של מלחים, בהתאם להרכב הכימי של האגם, ולכן חתך משקעים אשר שקע מאגם שכזה ואיננו נחשף או עבר תהליכים דיאגנטים אשר הביאו ליציאת התמלחות או שינוי בהרכבן, יכיל בחלליו הן את אותם נוזלים והן את המלחים המומסים בהם. במידה והחתך נחשף וכתלות באופי הסדימנטים מי התמלחת יכולים להתאדות אך כחלק מתהליך זה יושקעו המלחים המומסים בהם בחללי המשקעים ובשל כך יישארו בחתך.

בעבודה זו נעשה שימוש בהרכב מלחים מסיסים שכאלו בכדי לשחזר את ההתפתחות הגיאוכימית של אגם הלשון ואת התנאים האקלימיים וההידרולוגיים שהתקיימו במרחב אגן הניקוז שלו. אגם הלשון היה אגם היפר-סליני שהתקיים בבקע ים המלח במהלך תקופת הקרח האחרונה (70-14 אלף שנים לפני ההווה). התייבשותו, שהחלה עם היציאה מתקופת הקרח האחרונה והמעבר להולוקן, הביאה להתפתחות גופי המים השאריתיים, ים המלח והכינרת. לאגם זה (ושאר אגמי הבקע) היו מספר תכונות ייחודיות אשר הפכו אותו למערכת טבעית המתעדת שינויי אקלים מקומיים וגלובליים ברגישות רבה: מיקומו באזור המעבר בין רצועת האקלים הצחיח של מדבריות סהרה-ערב לבין רצועת האקלים הסב-טרופי של מזרח הים התיכון, היותו אגם פנים יבשתי ללא מוצא לים, הטופוגרפיה התלולה והדפנות המצוקיים של העמק בו הוא נקווה והיות האגם עמוק (400-600 מטרים). המשקעים אשר הצטברו על קרקעיתו של אגם זה מכונים תצורת הלשון. התצורה מורכבת מחילופי למינות דקות (1± מ"מ) של ארגוניט וחומר דטריטי אשר שקעו במחזורים שנתיים ובניהם, באופן לא סדור, מופיעות שכבות גבס בעובי של ס"מ בודדים עד עשרות סנטימטרים. הארגוניט והגבס הם משקעים כימיים אשר שקעו מגוף המים בעוד החומר הדטריטי הוא בעיקרו חלקיקי קלציט וקוורץ שמקורם באבק מדברי שהוסעו לאגם מרחבי אגן הניקוז ע"י שיטפונות. במהלך שיא תקופת הקרח האחרונה (MIS2) הגיע האגם למפלסו המרבי, 160~ מטרים תחת פני הים, והשתרע בין הכינרת בצפון לאזור מושב חצבה בדרום. כיום מרבית שטח זה חשוף ומופיעים בו חתכים של משקעי התצורה אשר חוו התייבשות ותהליכי בלייה שונים בעוד בקרקעית של ים המלח (והכינרת) קיימים חתכים אשר טרם נחשפו מזמן השקעתם.

לצורך עבודה זו נדגמו שני גלעינים אשר נקדחו במסגרת ה-Dead Sea Deep Drilling Project (DSDDP). תצורת הלשון נדגמה ברזולוציה גבוהה מגלעין אשר נקדח מהנקודה העמוקה ביותר באגם (הקדוח הזה מכונה בעבודה "הקידוח העמוק"). דיגום ה"קידוח העמוק" מייצג את כל תצורת הלשון. כמו כן נדגם ברזולוציה נמוכה יותר גלעין אשר נקדח בעומק ביניים של האגם (בסמוך לחוף ים המלח המודרני, קדוח זה מכונה בעבודה: "הקידוח הרדוד"). חתך זה כולל דוגמאות מהתקופה הבין-קרחונית האחרונה ומשיא תקופה הקרח הקודמת, מעבר לדוגמאות הליסן. בנוסף לכך נדגמו חתכים מטראסות השוליים הגבוהות של תצורת הלשון בנחל פרצים והר סדום אשר משקעיהם מייצגים את האזורים הרדודים של אגם הלשון.

מהסדימנטים שנדגמו הוכנו דוגמאות מעורבבות של ארגוניט וחומר דטריטי אשר מתוכם מוצו המלחים המסיסים ע"י שטיפה במים מזוקקים וסינון התמיסות לצורך הפרדתן מהסדימנט השאריתי. מים אלו נלקחו, לאחר טיפול, למדידה ב-ICP-OES, עבור הקטיונים העיקריים ו-Ion Chromatograph וטיטרציות עבור האניונים. עבודה זו מתמקדת בהרכב היסודות העיקריים של המלחים המסיסים המצויים במשקעי אגם הלשון. יסודות אלו הם Ca^{2+}, Mg^{2+}, K^{+}, Na^{+}, Sr^{2+}, SO_4^{2-}, Br^{-}, Cl^{-}, NO_3^{-}, HCO_3^{-}. בעזרת ריכוזי היסודות והיחסים ביניהם, כדוגמת $\frac{Na}{Cl}, \frac{Br}{Cl}, \frac{Sr}{Ca}$, ניתן לשחזר את הרכב התמלחת של אגם הלשון והשינויים הגיאוכימיים שהתרחשו בו. תוצאות המדידות של הרכב המלחים המסיסים מהקידוח העמוק, מקידוח הביניים ומהמחשופים מושוות ביניהן ולהרכב הכימי של תמלחת מי החללים שהופקו מהסדימנטים של הקידוח העמוק, (מעבודות קודמות), על בסיס כרונולוגיה.

המסקנות העיקריות הנובעות מעבודה זו הן:

1. ע"פ דפוסי ההמסה של היסודות השונים במהלך שטיפות הסדימנט הכרוכות בפרוצדורת מיצוי המלחים המסיסים נמצא כי היסודות Na, Cl, Br, Mg ו-NO_3 מגיעים רובם ככולם מהמסה של מלחים מסיסים. היחסים היונים של יסודות אלו מראים התאמה גבוה מאוד ליחסים מקבילים ממי החללים של הקידוח העמוק. לפיכך, יחסיהם של יסודות אלו יכולים לשמש ככלי אמין לצורך שחזור ההרכב הכימי של תמלחת האגם והתפתחותה.

2. עודף מועט נמצא באשלגן אשר ייתכן ונובע מהמסה של מלחי אשלגן מסיסים מחללי הסדימנט ו/או מספיחה של יסוד זה מחרסיות במהלך התגובה של הסדימנט עם המים של השטיפות.

3. דפוסי ההתמוססות והיחסים היונים של היסודות Ca, Sr ו-SO_4 הראו פאזת המסה נוספת, מעבר להמסת המלחים המסיסים, ועודף בהשוואה ליחסים המקבילים של תמלחת החללים. הוסק כי יסודות אלו משתתפים בהמסה של מינרלים מקוריים של האגם, כגבס וארגוניט, ולכן יחסיהם היוניים יכולים לספק מידע מוגבל אודות ההרכב הכימי של תמלחת האגם בטרם מתבצע תיקון לעודף של יסודות אלו שמקורו אינו במלחים המסיסים. במסגרת עבודה זו מתבצע תיקון לעודף של Ca ומוצעת שיטה לתיקון עודפם של היסודות הנוספים.

4. ערכי היחס $\frac{Na}{Cl}$ מהקידוח העמוק מראים עליה יציבה ומתמדת מערכים של 0.3 ל-0.7 בפרק הזמן של 12-100 אלף שנים לפני ההווה, ומיד לאחר ההגעה לערך השיא מתרחשת נפילה חדה לערך של 0.48, 11 לפני 11 אלף שנים. יחסי $\frac{Mg}{Cl}$ ו-$\frac{Br}{Cl}$ מראים מגמה כמעט זהה אך עם דפוס הפוך (דפוס מראה) באותו פרק הזמן. ערכי ה-$\frac{Mg}{Cl}$ יורדים מ-0.5 ל-0.2 ואז מזנקים ל-0.43 וערכי ה-$\frac{Br}{Cl}$ יורדים מ-0.01 ל-0.005 ומזנקים ל-0.008. יחסים אלו מבססים את יכולת המלחים המסיסים לתעד את השפעת מגמות האקלים הכלליות על ההרכב הכימי באגם כמו גם את השפעותיהם של שינויים אקלימיים קצרי מועד כאירועי היינריך ושיא תקופות הקרח.

5. ערכי היחסים $\frac{Na}{Cl}, \frac{Mg}{Cl}$ ו-$\frac{Br}{Cl}$ במשקעי הקידוח מעומק הביניים נעים במסגרת טווחים כמעט זהים לטווחים שנראו בקידוח העמוק אך ערכים אלו תואמים לערכי תמלחת החללים מהקידוח העמוק רק בפרקי הזמן של תקופות הקרח (שיא תקופת הקרח הקודמת-MIS6 ובמהלך תקופת הקרח האחרונה-MIS4-2), בהן מפלס האגם היה גבוה. דוגמאות מהתקופה הבין-

קרחונית האחרונה (MIS5) מראות כי ערכי היחס $\frac{Na}{Cl}$ גבוהים במשקעי עומק הביניים לעומת הערכים במרכז העמוק של האגם (0.5 לעומת 0.2) ונמוכים יותר ביחסים $\frac{Mg}{Cl}$ ו-$\frac{Br}{Cl}$ (0.36 לעומת 0.55 ו-0.0075 לעומת 0.011). הבדל זה, בערכים בני אותו הזמן, מציע כי מנגנון השקעת ההליט שהתקיים באגם סמרה, אשר אכלס את בקע ים המלח במהלך התקופה הבין-קרחונית האחרונה, היה דומה לאופן בו שוקע הליט כיום בים המלח. ע"פ מנגנון זה הליט שוקע באופן מסיבי מהתמלחת העמוקה והמרוכזת של מרכז האגם ומתאפשרת הצטברות של מלח זה במהלך כל השנה. במקביל, התמלחת העליונה נותרת בדרגת רוויה קרובה לזו של הליט אך לא מאפשרת השקעה והצטברות מאסיביים של חתך הליט באזורי השוליים.

6. ערכי ה-$\frac{Na}{Cl}$ בחתכי השוליים משתנים באופן תדיר במסגרת הטווח 0.07-0.93 עם ערכים רבים שהם גבוהים/נמוכים מהערכים המקבילים בקידוח הביניים והעמוק. יחס ה-$\frac{Br}{Cl}$ מראה דפוס הפוך ומגמה דומה אך יציבה יותר בטווח הערכים 0.0015-0.011, עם פחות חריגות קיצוניות. יחס ה-$\frac{Mg}{Cl}$ מראה מגמה דומה ליחס ה-$\frac{Br}{Cl}$ אך כל ערכיו נמוכים מערכי מרכז האגם ועומק הביניים ונעים בטווח 0.034-0.343. חלק מהתנודות החריפות הללו בערכי המלחים המסיסים מיוחסות לשקיעת הסדימנטים מאגם שאריתי שנקווה על פני מישור עמיעז במהלך תקופות שחונות של מפלס אגם נמוך או מהתייבשות תמלחת החללים והשקעת הליט בחללי הסדימנטים לאחר היחשפותם. שאר המגמות מיוחסות להרכב הכימי המקורי של התמלחת העליונה באגם אשר מראות כי תמלחת זו חוותה תנודות רבות בהרכבה הכימי.

7. תוצאות המלחים המסיסים המיוחסות להרכב המקורי של התמלחת מראות כי ההתפתחות הכימית של התמלחת העליונה נשלטה ע"י ערבוב בין מים מתוקים שנכנסו לאגם עם יחס $\frac{Na}{Cl}$ גבוה של ~0.9 לבין תמלחת האגם שהייתה בעלת ערך ביניים של $\frac{Na}{Cl}$, 0.45-0.65. תמלחת עליונה זו התערבבה עם התמלחת העמוקה ע"י תהליכי ערבוב עדינים ודיפוזיה שהתרחשו לאורך קו המגע שבין התמלחות וע"י שקיעה של תמלחת עליונה צפופה שהמיסה הליט אל הקרקעית העמוקה של האגם. תהליכי ערבוב עדינים אלו בלמו את השפעתם של תהליכי פני השטח אשר הביאו לתנודות בהרכב התמלחת העליונה והעבירו לעומק רק את השפעתם הכוללת על הרכב האגם, ובכך נוצרו מגמות השינוי העקביות והיציבות אשר נצפות בהרכב הכימי של משקעי מרכז האגם.

8. נוכחותו של ניטרט במשקעי המחשופים, בעודו נעדר ממשקעי האגן העמוק ועומקי הביניים, ודפוס ההמסה שלו (ראה מסקנה-1), מחייבים כי אגם הלשון שמר על מבנה משוכב בעמודת המים במהלך מרבית תקופת הקרח האחרונה, מה שהביא להתפתחות תנאים מחזרים בתמלחת העמוקה. מאידך, התמלחת העליונה שמרה על תנאים מחמצנים ומליחותה הפחותה אפשרה את קיומן של בקטריות מסוימות בגוף המים. במצב שכזה, ניטרט וחומר אורגני, אשר נכנסו לאגם ממקורות המים המתוקים, יכלו להצטבר בתמלחת העליונה והחומר האורגני חומצן בהדרגה לניטרט ע"י הבקטריות אך איננו נצרך ע"י יצרנים ראשוניים אשר לא יכלו להתקיים במים בשל מליחותם. חלק מהניטרט שהצטבר בתמלחת העליונה הועבר לתמלחת העמוקה, ע"י מנגנוני הערבוב, ושם הוא חומצן ע"י בקטריות (דה-ניטריפיקציה) אשר התקיימו בתמלחת זו.

1. Introduction

1.1. Quaternary lakes in the Dead Sea Basin

The contemporary lakes of the Jordan Rift Valley, Sea of Galilee (Lake Kinneret) and the Dead Sea, are remnants of several water-bodies that occupied the Dead Sea Basin, Kinnarot Basin and the Jordan Valley during the Quaternary (e.g. Stein, 2001, 2014 a, b and references there). The evolution of those water-bodies began during the Pliocene, with the ingression of Mediterranean Sea waters to the area of the Dead Sea Basin, forming the so called Sedom Lagoon, where the salts of the Sedom Formation were deposited (Stein et al., 2000; Belmaker et al., 2013). The interaction between the ingressing lagoon seawaters and the Cretaceous limestones led to the development of a unique Ca-chloride brine (Zak, 1967; Starinsky, 1974; Stein et al., 2000; Stein et al., 2002; Katz and Starinsky, 2009).

Ca-chloride brine is defined as a solution with equivalent ratios of $\frac{Na^+}{Cl^-} < 1$ and $\frac{Ca^+}{(SO_4^{2-}+HCO_3^-)} > 1$, expressing the excess of chloride over sodium and Ca over dissolved gypsum and $CaCO_3$ (e.g, Starinsky, 1974; Katz and Starinsky, 2009). Around 3 Ma ago the connection of the lagoon to the open sea was permanently closed and the water bodies of the lowest depression in the Jordan Rift Valley (named the Dead Sea Basin – DSB) transformed to be close, inland lakes (Torfstein et al., 2009).

The Quaternary lakes that filled the DSB were characterized with several unique features: (1) The dominant presence of the Ca-chloride brine, which dictated the hyper-salinity nature of the lakes. The high salinity of the brine prevented significant lacustrine life to evolve in these lakes and therefore the thin lamination of the sedimentation could have been preserved in many cases and the influence of biological processes in the lakes was minor; (2) The lakes of the DSB are terminal lakes, meaning that waters that reach the DSB are lost mainly by evaporation. A secondary process of water loss/gain is related to the long -term circulation of the lake's solution in/out the regional aquifers (e.g., Weber et al., 2018). (3) Due to the topography of the DSB, which is steep along the east-west margins, yet more moderate and open in the south-north margins the lakes of the DSB behave like "amplifier lake", meaning that the lakes' surface levels are sensitive to the freshwater inputs, and are used as good monitors for the hydro-climate conditions in the lakes' watershed. Moderate rises in lake levels are buffered, however, by enhanced evaporation in the rather shallow marginal areas (e.g. Bookman et al., 2004). (4) The watershed of the DSB is relatively large and extends from Mt. Hermon in the north with Mediterranean climate and high precipitation to the hyperarid Gulf of Aqaba in the south, that is part of the Sahara-Arabian deserts (Fig. 1). (5) The lakes of the DSB are unique by having a deep water column of several

hundred meters, even during extremely dry periods. This depth enable processes such as stratification and accumulation of large ionic repository that cannot occur in shallow hypersaline lakes (Fig. 2).

Since the closure of the Sedom lagoon the limnological and geochemical history of the lacustrine bodies in the DSB were controlled by the balance and interaction between the brine and freshwater from the lakes' watershed, evaporation process and the removal of Ca^{+2}, SO_4^{2-} and HCO_3^- from the brine through the precipitation of $CaCO_3$ and $CaSO_4$ minerals (Katz et al., 1977; Stein, et al., 1997; Gavrieli and Stein, 2006; Katz and Starinsky, 2009).

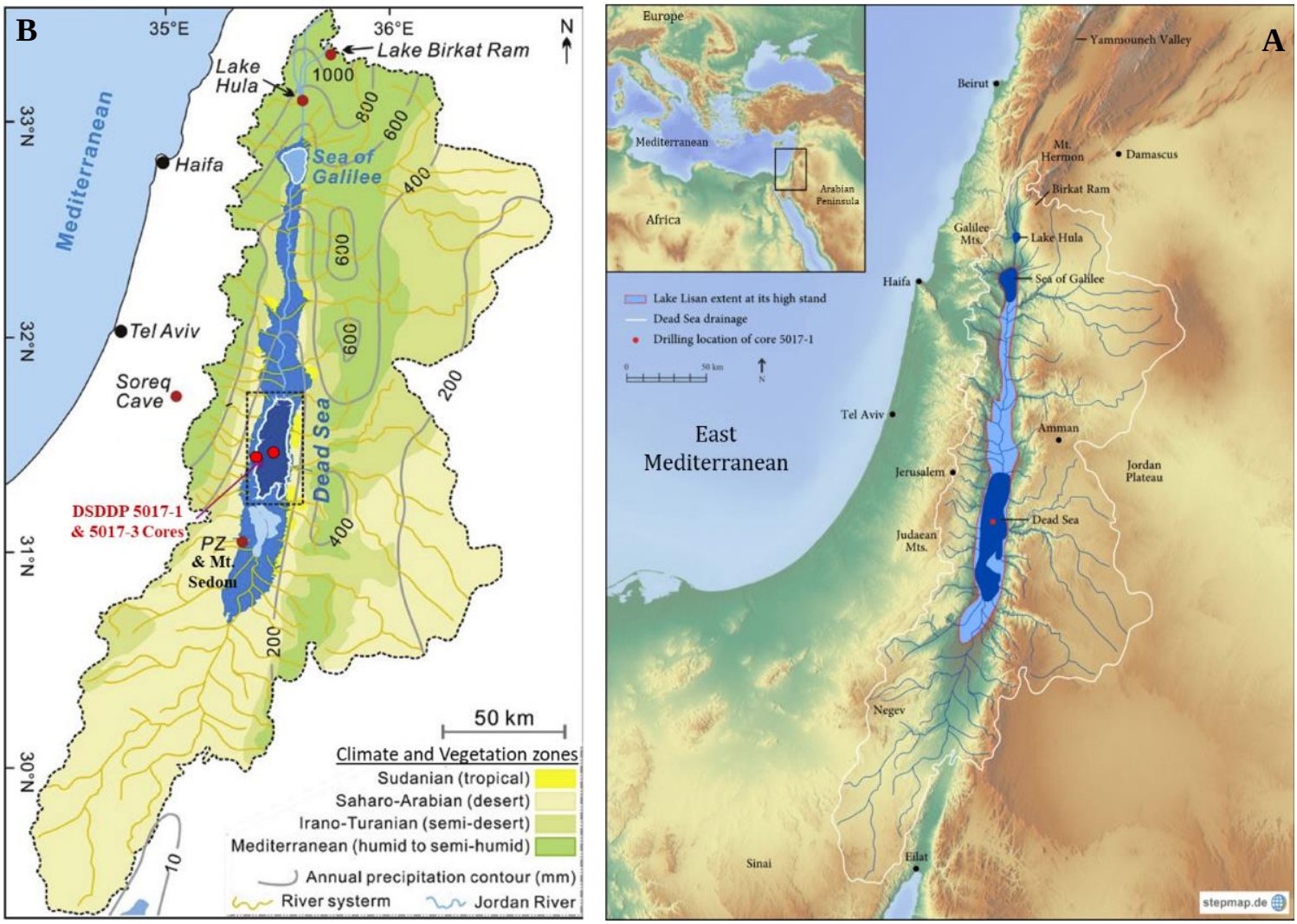

Figure 1: (A) Location of the Jorden Rift Valley and its lakes. Colors represent elevation. Presented on the map are: maximum extent of Lake Lisan, recent extent of the Dead Sea and Sea of Galilee, drainage basin of the Dead Sea and the location of the DSDDP 5017-1-A deep core.
(B) A closeup on the drainage basin of the Dead Sea showing: climate (and vegetation) zones in the area, modern annual precipitation contours, maximum extent of Lake Lisan and modern extent of the Dead Sea and Sea of Galilee, location of the DSDDP deep and shallow cores, Perazim Valley (PZ) and Mt. Sedom. (Figure from Yin Lu et al., 2020).

The geological configuration of the Jordan Rift Valley during the last several hundreds of thousands of years remained almost intact ("frozen landscape"), with small vertical movements that are associated with the seismic activity along the Dead Sea Transform and related faults (e.g., Marco et al., 1996; Kagan et al., 2018). Regional climate in the lakes' watershed are those that dictated the geochemical and limnological patterns (e.g., lakes' configuration, the circulation of the brine between the lake and marginal aquifers and lake level changes, e.g., Stein, (2014)). The variations in the regional hydroclimate that affected the lakes were dictated by global climate engines of the Ice Ages (e.g., Stein et al., 2010; Torfstein et al., 2015). In general, glacial periods were characterized with wet regional conditions in the Mediterranean climate zone that induced a positive water balance in the lake, lake level rise, spatial expansion, and dilution of the brine (e.g., the last glacial Lake Lisan). Interglacials were characterized with more arid climate conditions in the lake's watershed that induced negative water balance in the DSB, lake level drop, spatial shrinkage of the lake and concentration of the brine.

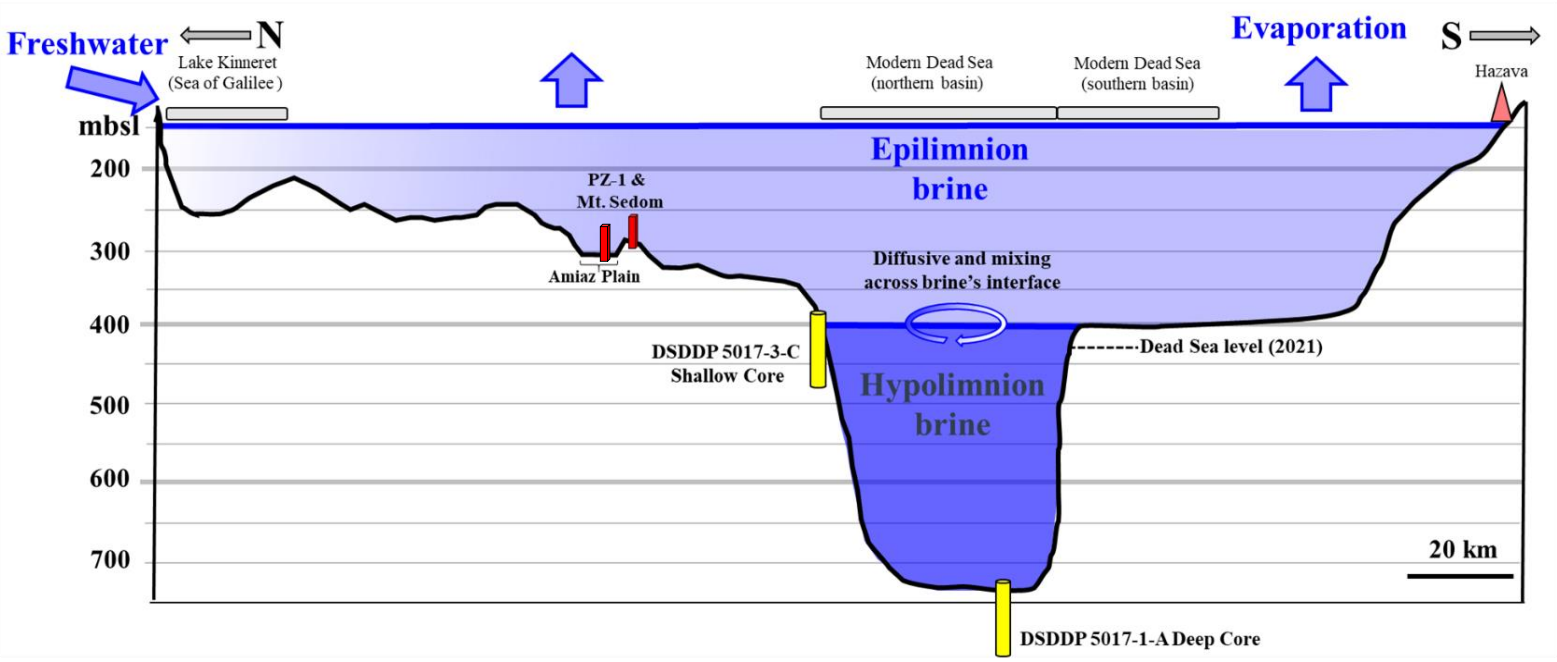

Figure-2: North-South schematic cross section of the Jordan Rift Valley and Lake Lisan. The lake is shown in its highest stand. Stratification in the lake is presented with a schematic elevation of the interface between the epilimnion to the hypolimnion. Locations of the deep and shallow DSDDP cores and marginal PZ-1 and Mt. Sedom White Hill are presented, illustrating the elevation of these sites in the lake. The locations of these sections is schematic. (Figure from Lazar et al. 2014).

Throughout these major climatic periods short/medium-term climatic events occurred that whether intensified, weakened or inverted the prevailing climate pattern. A medium-term hydro-climate interval characterized the time frame of MIS 3 (~50-30 ka) within the last glacial period (which encompassed the time intervals of MIS 4, 3 and 2, 70 to 14 ka). This period was characterized with an unstable, drier

climate compared to the previous and following wet and stable MIS 4 and 2. Short term climatic shifts during the glacial period are, for example, the Heinrich events that were periods of a few thousands of years with severe dry climate in the east Mediterranean. In general, climate shifts in the lake's hydrology coincide with global climate events, e.g., abrupt lake level drops that coincide with the Heinrich-events (Bartov et al., 2003; Stein et al., 2010; Torfstein et al., 2013).

The history of the DSB in terms of geology, climate, geochemistry, hydrology and limnology is recorded in the sediments of the Dead Sea Group, consisting of the Sedom, Amora, Samra, Lisan, and Zeelim Formations (Fig. 3 A. e.g., Zak, 1967; Stein, 2001; Waldmann et al., 2009). The formations comprise chronostratigraphic units that encompass the period of the Pliocene until recent Holocene.

Sedom Fm. was deposited within a marine evaporitic lagoon during the Pliocene. It is made up of some 77% salt rock, 7% of carbonates and sulfate minerals, and the rest being composed of clastics (Zak, 1967). The sediments of Sedom Fm., including its massive sections of halite (and additional salts) are exposed at the Mt. Sedom salt diapir and in several boreholes from the DSB area.

Amora Fm. includes the sediments that were deposited in the lake from the time of the disconnection of the Sedom lagoon ~ 3 Ma BP, to the last interglacial period. It is composed of evaporites (40% carbonates, 19% sulfates, and 8% halite) and clayey to silty and sandy clastics. Some sections of this formation are consecutive sequences of alternating laminae of primary aragonite and silty detritus, termed ***aad*** facies (Machlus et al., 2000), others are sequences compose of laminated silty detritus material termed ***ld*** facies (Haliva-Cohen et al., 2012). Layers of massive gypsum, several mm-cm thick, exist irregularly along the formation. A thick halite bed of 6 m appears approximately at the center of the section in the marginal Arubotaim cave sections. In the deep basin massive halite layers of several cm-meters exist along the transition between Amora to Samra formations. The Amora Fm. is partly exposed (past ~800 ka) in the eastern uplifted flanks of Mount Sedom (e.g., the Arubotaim section described by Zak, 1974 and Torfstein, 2008). Ages of around 720 and 135 ky were attributed to the exposed basis and top of the Amora Fm. by Torfstein et al., (2008), who related it to the MIS-19 until MIS-6 time frame. This time period, and especially its latest part between ~194-135 ka BP, is associated with the penultimate glacial period (MIS 6) and its intense wet conditions in the Levant area.

Samra Fm. is overlying the Amora Fm. and elapses over the last interglacial period (140-70 ka, MIS 5 e-a. Waldmann et al., 2007; Waldmann et al., 2009). The lithology of this formation displays graded sedimentation cycles (coarse grit → sand and silt → marl and chalk) in the marginal sections around the modern Dead Sea, while in the center of the basin it is composed of massive sections of halite, detrital

marl and some aad sections that appear in the upper part of the formation. A detailed description of this formation, as seen in the margins of the modern Dead Sea, was presented by Waldmann (2002).

Lisan Fm. lies above the Samra Fm. The sediments of this formation deposited from **Lake Lisan** which occupied the DSB during the last glacial period (70-14 ka BP, MIS 4-2) (Haase-Schramm et al., 2004). Above the Lisan Fm. an intermediate section was defined as Fazael Formation. It covers the post-glacial period (14-11 ka) (Palchan et al., 2018).

Zeelim Fm. lies at the top of the Dead Sea Group. It deposited during the Holocene. This formation is marked in the margins of the Dead Sea by a few meters thick massive halite layer at its base, where the top of the salt unit was dated to about 10.2 ka BP (Yechieli et al., 1993; Migowski et al., 2004; Migowski et al., 2006). In the depocenter of the basin this formation contains thicker units of halite (Neugebauer et al., 2014). Units of aragonite–detritus laminae, sometimes with gypsum, or beds composed only of pure detritus laminae, follow upward, containing in places sand and silt layers with gypsum crusts.

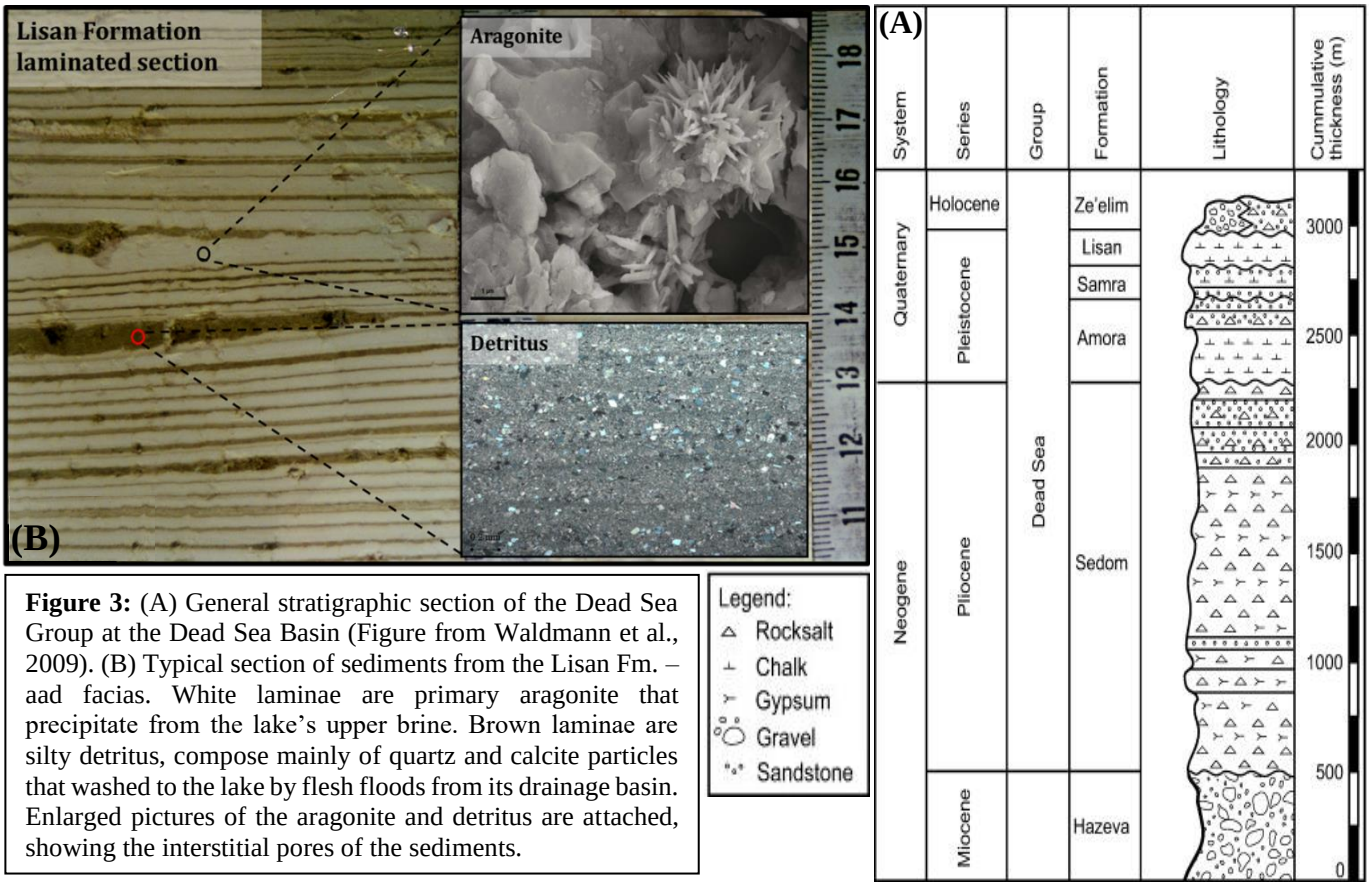

Figure 3: (A) General stratigraphic section of the Dead Sea Group at the Dead Sea Basin (Figure from Waldmann et al., 2009). (B) Typical section of sediments from the Lisan Fm. – aad facias. White laminae are primary aragonite that precipitate from the lake's upper brine. Brown laminae are silty detritus, compose mainly of quartz and calcite particles that washed to the lake by flesh floods from its drainage basin. Enlarged pictures of the aragonite and detritus are attached, showing the interstitial pores of the sediments.

This thesis focuses on the evolution the Dead Sea Ca-chloride brine during the last glacial period when Lake Lisan occupied the basin and deposited the sediments comprising the Lisan Fm.

Lake Lisan reached its highest level of ~170 m below mean sea level (m bmsl) during the LGM (~28-24 ka BP) expanding then from Lake Kinneret in the north to Hazeva in the south (Fig. 1 & 2)
(Neev and Emery 1967; Begin et al. 1974; Bartov et al., 2002; Hazan et al., 2005).

For most of its time Lake Lisan was characterized by stratified configuration where a hypersaline and dense brine (the hypolimnion) was overlain by less saline and dense waters (the epilimnion) (Fig. 2. Stein et al., 1997). The brine of the hypolimnion (as the modern Dead Sea brine) had a Ca-chloride composition. The limnological stratification of Lake Lisan was maintained by inputs of freshwater to the epilimnion and brine to the hypolimnion. The fresh water supplied ions such as: HCO_3^- and SO_4^{2-} to the lake (Stein et al., 1997; Lazar et al., 2014). These ions enabled the precipitation of primary aragonite and gypsum from the lake's water. In addition, the winter floods transported to the lake fine detritus material that comprises mainly calcite and quartz grains that were washed from the surface cover of the watershed (Haliva-Cohen et al., 2012). The surface cover material in turn comprises desert dust blown from the northern Sahara (and Arabian) deserts (Haliva-Cohen et al., 2012; Palchan et al., 2018). The Lisan Fm. was divided by Machlus et al., (2000) into three stratigraphic members. The Lower and Upper Members, corresponding to Marine Isotope Stages (MIS) 4 and 2, respectively (70-50 and 30-14 ka BP respectively), comprise mainly sequences of alternating laminae of primary aragonite and silty detritus (*aad* facies. Fig. 3 B). The Middle Member of the Lisan Formation (corresponding to MIS 3, 50-30 ka BP) comprises mainly sequences of laminated silty detritus material (*ld* facies) (Haliva-Cohen et al., 2012), and some sequences of *aad*. Gypsum layers appear irregularly along the three members of the formation.

The chronology of the Lisan Fm. was achieved by radiocarbon and U-Th dating of organic debris and primary aragonite (e.g. Haase-Schramm et al., 2004; Stein et al., 2006; van der plicht et al., 2004; Torfstein et al., 2013; Kitagawa et al., 2017, Goldstein et al. 2020). The dating indicates that the formation lies between 70 and 14 ka, corresponding to MIS 4, 3, and 2 (Stein, 2001; Haase-Schramm et al., 2004).

In the lake's depocenter the section with characteristic lithology of the Lisan Fm. is bracketed between massive halite sections of several meters in its top and bottom. This section actually covers the period of ~100-11 ka BP that is longer than the defined time frame of the Lisan Fm.

1.2. Interstitial soluble salts in the sediments

As sediments accumulate on a lake's floor they incorporate the brine solution within their pores (Katz and Kolodny, 1989). Diffusion and compaction may potentially "smooth" the original chemical profiles,

yet if the permeability of the sediments is low and the sedimentation rate is high the influence of this interruption is weakened so every layer conserve within its pores the original brine of the lake since the time of deposition. When the sediments desiccate (e.g., upon exposure), the interstitial brines evaporate and precipitate soluble salts in the sediments' pores. The more porous and the higher the hydraulic conductivity of the sediments are, the desiccation of the interstitial brine will occur faster upon exposure. The soluble salts that crystallize within the pores are a relic of the lake's brine and hence contain information on the chemical composition of the original brine (Katz and Kolodny, 1989). Schematic illustration of this process is given in Figure 4.

While sediments that deposited on the high margins of the DSB'S lakes are exposed for thousands of years due to the lake level decline that occurred since Lisan times, the sediments that were deposited in the central, deep part of the lakes were never exposed and thus contain the original pore fluids (Lazar et al., 2014; Levy et al., 2017, 2018). The low permeability of the sediments and the high sedimentation rates efficiently hampered the migration of pore fluids from their initial hosting layers (Levy et al., 2018).

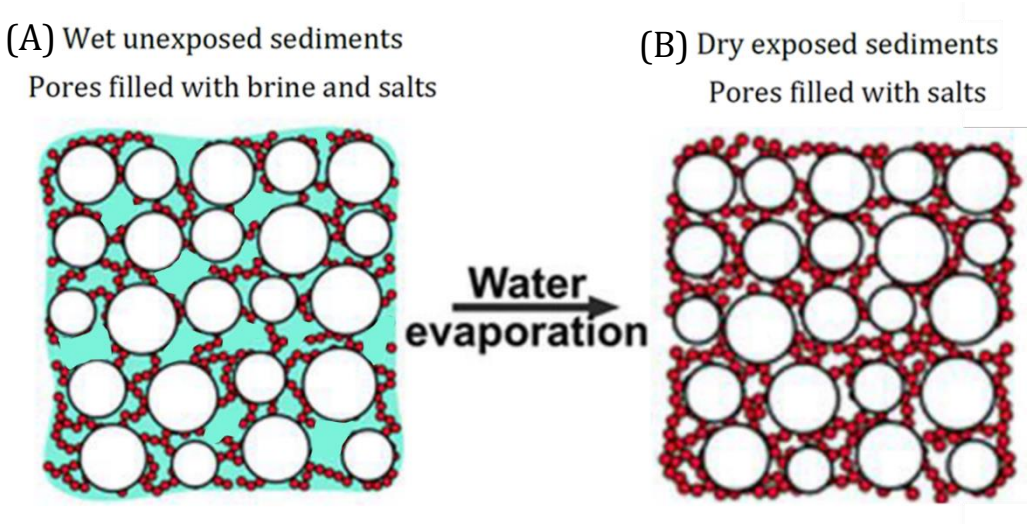

Figure 4: Schematic illustration of interstitial soluble salts. (A) Unexposed sediments (white circles). The pores are filled with brine and some soluble salts that crystallized from the brine (small red circles). (B) Exposed sediments. The interstitial brine dried out and soluble salts crystallized in the pores.

1.3 Geochemistry of soluble salts in the Lisan's marginal sediments

Several geochemical studies measured the chemical and isotopic composition of the marginal exposures of the Lisan Fm. in order to understand the chemical evolution of the lake (e.g., Katz et al., 1977; Katz and Kolodny, 1989; Stein et al., 1997; Haase-Schramm et al., 2004; Kolodny et al., 2005; Torfstein et al., 2008).

One approach was to learn on the chemistry of the lake's brine by measuring the chemical composition of pure aragonite laminae.

Katz et al., (1977) showed that the $\frac{Sr}{Ca}$ ratio in aragonite laminae from several Lisan sections (PZ-1, Masada, Deir Shaman) gradually declines along the formation and yielded (equivalent) values in the range $0.5 \cdot 10^{-2}$ - $1 \cdot 10^{-2}$ (Fig. 5 A). The $\frac{Sr}{Ca}$ ratio in the aragonite was suggested to reflect the ratio in the brine because the distribution coefficient of Sr in aragonite, $((Sr)_{aragonite}/(Sr)_{brine})$ is 1 (Katz et al., 1977; Kinsman and Holland, 1969). Thus, the $\frac{Sr}{Ca}$ decline reflects the evolution of Lake Lisan brine which began with a composition similar to that of modern Dead Sea (high $\frac{Sr}{Ca}$ ratio of ~0.01), and gradually diluted with low $\frac{Sr}{Ca}$ freshwater. This hypothesis was supported by Stein et al., (1997), who described a similar decline in the $\frac{Sr}{Ca}$ ratio of the Lisan Fm. aragonite along the PZ1 section at Perazim Valley and attributed the change to enhance introduction of freshwater with low $\frac{Sr}{Ca}$ ratio (~0.004) to the lake and its mixing with the Ca-chloride brine (with ~0.01). The mixing of the freshwater with the brine was corroborated by $^{87}Sr/^{86}Sr$ isotope ratios that were measured in the aragonites from the studied PZ-1 and freshwaters (e.g., north Jordan River water and Ca-chloride brine waters).

The profile of the $\frac{Na}{Ca}$ ratio in the aragonite laminae of Lisan Fm. is rather noisy (Fig. 5 B). It was suggested that this ratio is a salinity proxy of the short-lived brine of the uppermost layer (e.g., Katz et al., 1977; Machlus, 1996).

Machlus, (1996) investigated the chemical properties of the aragonite laminae along the PZ-1 section in Perazim Valley. She also found a gradual decline in the $\frac{Sr}{Ca}$ ratio along the Lisan Fm. while other elemental ratios, such as $\frac{Na}{Ca}$, showed frequent oscillations along the section, without a clear secular trend (Fig. 5 A & B). These scatters support the conclusion mentioned above about the $\frac{Na}{Ca}$ ratio and attest the model of aragonite precipitation in the upper short-lived brine of the lake.

Additional approach investigated the chemistry of the lake's brine in a more direct method by extracting and isolating the interstitial soluble salts from the sediments through rinses of the sediments with deionized water that were followed by leaches to separate between the sediments to the water-dissolved soluble salts.

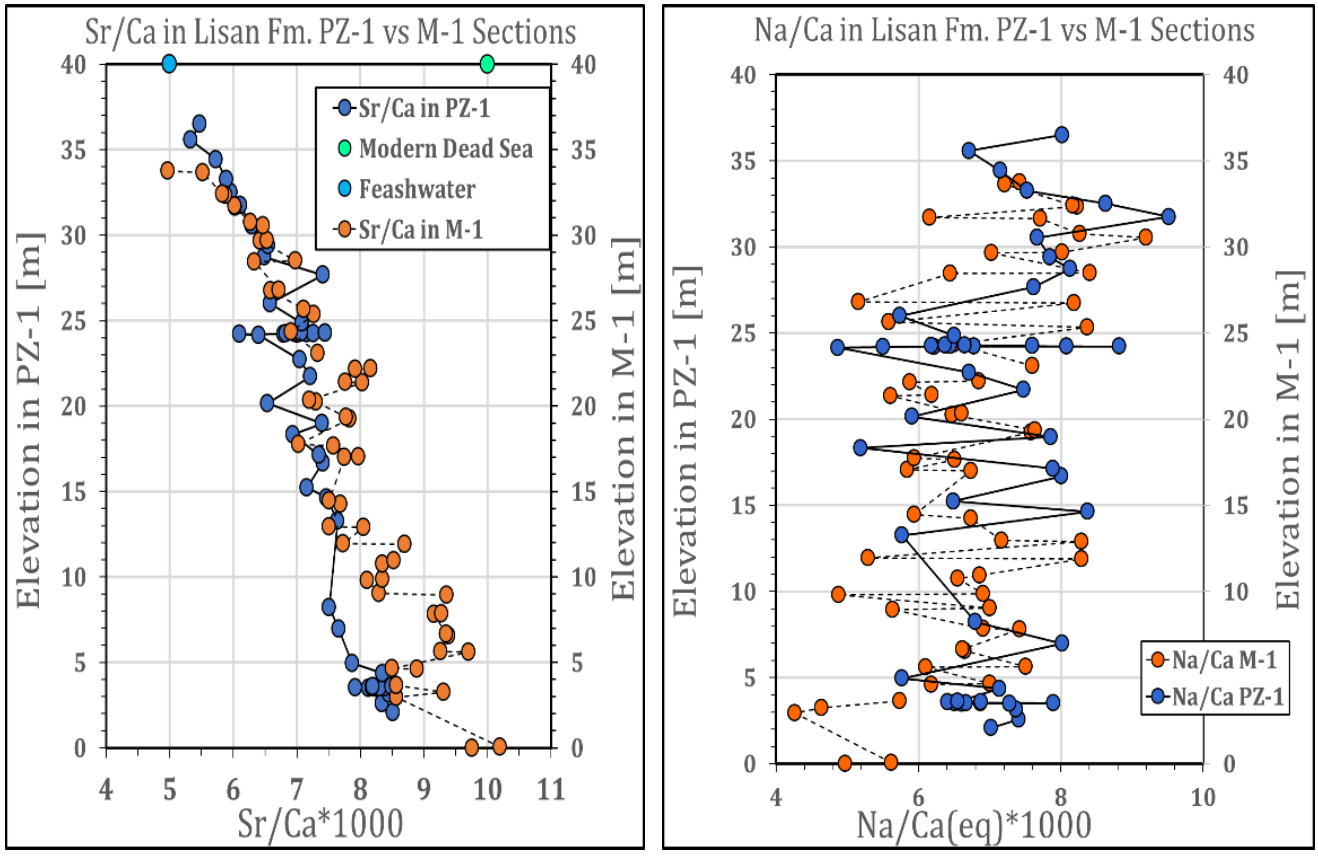

Figure 5: Values of (A) $\frac{Sr}{Ca}$ and (B) $\frac{Na}{Ca}$ in clean aragonite laminae (dissolved in acid) of the Lisan Fm. in two marginal outcrops – Masada (achieved by Katz et al., 1977) and Perazim Valley PZ-1 (achieved by Manchus, 1996). Note that each outcrop is presented with its own Y-axis of elevations.
The profiles from both sections are synchronized and show a gradual decline along the Lisan period in the $\frac{Sr}{Ca}$ and noisy behavior but within confined range in the $\frac{Na}{Ca}$.

Katz et al., (1989) found that the total soluble salts content ($mg_{(salts)}/g_{(sediment)}$) in the Lisan Fm. is 2 to 2.5 times higher in the lower part than in the upper part of the formation. This observation corroborates the idea of gradual dilution during Lisan time (Katz et al., 1977). Most elemental ratios are similar to those in the modern Dead Sea in the lower Lisan Fm., and upward the section thay vary according to various processes that occurred in Lake Lisan and associated aquifers, e.g. halite dissolution, dolomitization, etc. Values of $\frac{Na}{Cl}$ for example, rise with time in the detrital layers only, indicating the preferable crystallization of halite in these layers (after their exposure and desiccation) due to their higher porosity (Fig. 6 A). The $\frac{Mg}{Cl}$ ratios in the Lisan sediments decline along the section (Figs. 6 B), similar to additional ratios such as $\frac{Mg}{Ca}$. This decline was suggested to indicate that a diagenetic dolomitization of the aragonite took place after exposure, causing a loss of Mg and a gain of Ca and Sr relative to Cl in the brine. While

processes such as the growth of halite crystals and dolomitization commenced with the exposure and desiccation of the marginal sediments, the progress of these processes was ceased due to the advanced dry out of the sediments' interstitial brine. Such processes may be still operative in the recently exposed sections of the formation.

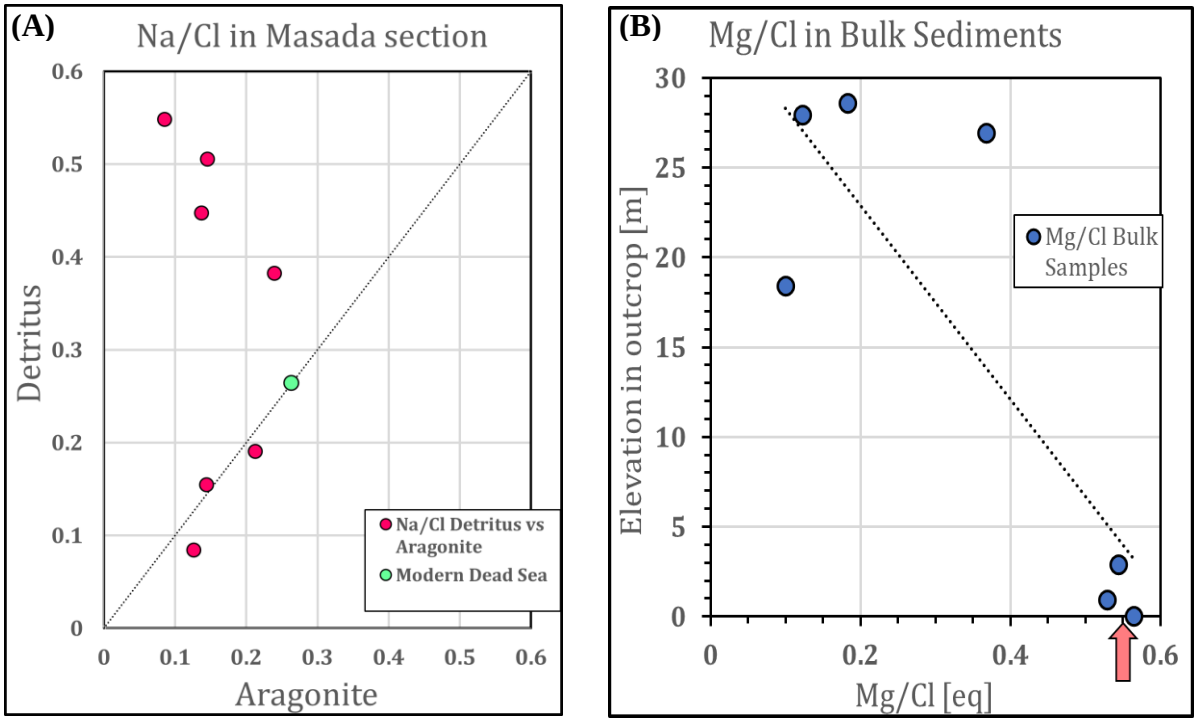

Figure 6: (A) Values of $\frac{Na}{Cl}$ in detritus against these values in aragonite in samples from Masada section. $\frac{Na}{Cl}$ rise with time in the detrital layers only. The $\frac{Na}{Cl}$ value in the bottom of the section is similar to the Dead Sea value.
(B) Values of $\frac{\mathrm{Mg}}{\mathrm{Cl}}$ in bulk sediments (aragonite + detritus) along Masada section. Red arrow shows the $\frac{\mathrm{Mg}}{\mathrm{Cl}}$ value in the Dead Sea. Both graphs from Katz & Kolodny, 1989.

Stein et al., (1997) proposed a mixing model for Lake Lisan between the lower and upper brines. The presence of primary aragonite in the section implies that the $\frac{Mg}{Ca}$ ratio in the precipitating solution was larger than 2 and that $\frac{Ca}{HCO_3}$ ratios were above 1. Since these ratios in all of the freshwater tributaries are lower a contribution of high $\frac{Mg}{Ca}$ water and Ca ions from the lower brine was required. The mixing of the lower and upper layers is also consistent with the $\frac{^{87}Sr}{^{86}Sr}$ ratios in the aragonite and the soluble salts that supposed to represent the two layers.

Gypsum solubility is higher than that of aragonite (Katz et al., 1981). The lithology of the Lisan Fm. shows that aragonite usually precipitated from the lake while gypsum remained dissolved. In such

conditions Ca^{2+} is removed from the upper layer by aragonite precipitation while SO_4^{2-} is accumulated after entering the lake with freshwater. The existence of gypsum layers in the Lisan Fm. imply on episodes in which the conditions changed. These conditions are related to drier periods when the supply of freshwater to the lake was reduced leading to overturn of the lake. Ca^{2+} from the deep Ca-chloride brine mixed with the SO_4^{2-} of the upper layer, gypsum saturation achieved, and precipitated (Stein et al., 1997). Similar mechanism was also suggested later and elaborated by Torfstein et al., (2005) and Torfstein et al., (2008).

The temporal decline in the $\frac{Sr}{Ca}$ ratio in the aragonites of the PZ-1 and Masada sections was related to the abovementioned mixing of freshwater (with low $\frac{Sr}{Ca}$ ratio) and brine (with high $\frac{Sr}{Ca}$ ratio) (Katz et al., 1977; Stein et al. 1997). Machlus (1996) argued that the drop in the $\frac{Sr}{Ca}$ along the Lisan Fm. (in the PZ-1 section) was too fast when considering freshwater incomes and aragonite precipitation as processes that lead to a drop in the $\frac{Sr}{Ca}$ ratio and mixing with the hypolimnion as a process that led to a rise in the ratio. Machlus proposed that brine solutions that discharged by saline springs buffered the $\frac{Sr}{Ca}$ ratio and reduced its rate of decline. The flow of these springs was dictated by the hydrostatic pressure of the lake, determined by its level. Therefore, their flow was high during low stand periods and their influence on the $\frac{Sr}{Ca}$ ratio as well, stabilizing it or even causing to rise. During high stand periods the pressure of the water column inhibit or even stopped their flow and thus a sharp decline in the $\frac{Sr}{Ca}$ ratio could occur. Later works dealt with the influence of the saline springs on Lake Lisan brine e.g., Weber et al., (2021) that demonstrate the significance of the discharge of sulfate-rich Ca chloride brines of Ein Qedem saline springs on the chemistry of the lake's brine. Several effects of the saline springs and their times of discharge to Lake Lisan is discussed below.

1.4. The Dead Sea Deep Drilling Project (DSDDP)

The above-mentioned works on the chemistry of the Lisan's marginal sediments, and additional works, led to the understanding that the marginal outcrops represent a partial record of the lake and since they undergo erosion and diagenetic processes their chemical information may not be pristine. It was clear that only the deep basin can provide a continuous and full sedimentation record with its original characteristics. The Dead Sea Deep Drilling Project (DSDDP), held by the ICDP, took place during the winter of 2010-2011. Within the framework of this international project several cores were drilled in the Dead Sea northern deep basin (730 mbsl and ~300 m below lake level), close to the deepest point of the

basin, along with cores that extracted from the shallow shore of the Dead Sea (water depth of 2.5 m) (Fig. 1 & 2 and Neugebauer et al., 2014). The longest profile (5017-1-A) was drilled in the depocenter of the lake, it is 455 m long, with 89.13% recovery (Neugebauer et al., 2014) (Fig. 7 B). The record covers the upper part of Amora Fm. (MIS 8-6), the last interglacial Samra Fm. (MIS 5), the last glacial Lisan Fm. (MIS 4-2) and the Holocene Ze'elim Fm. (MIS 1) (Neugebauer et al., 2014). It is therefore, include two entire glacial-interglacial cycles that span along the last 220 ka (Stein et al., 2011; Neugebauer et al., 2014; Torfstein et al., 2015; Goldstein et al., 2020). The main sedimentary facies of glacial periods (Amora & Lisan Fm.) and interglacial periods (Samra & Zeelim Fm.) in the sediments of the DSDDP drilled cores are illustrated in Figure 7 A. The deep core provides a continuous record of the Lisan Fm. that extend along ~110 m (compare to ~40 m in the above-mentioned marginal sections).

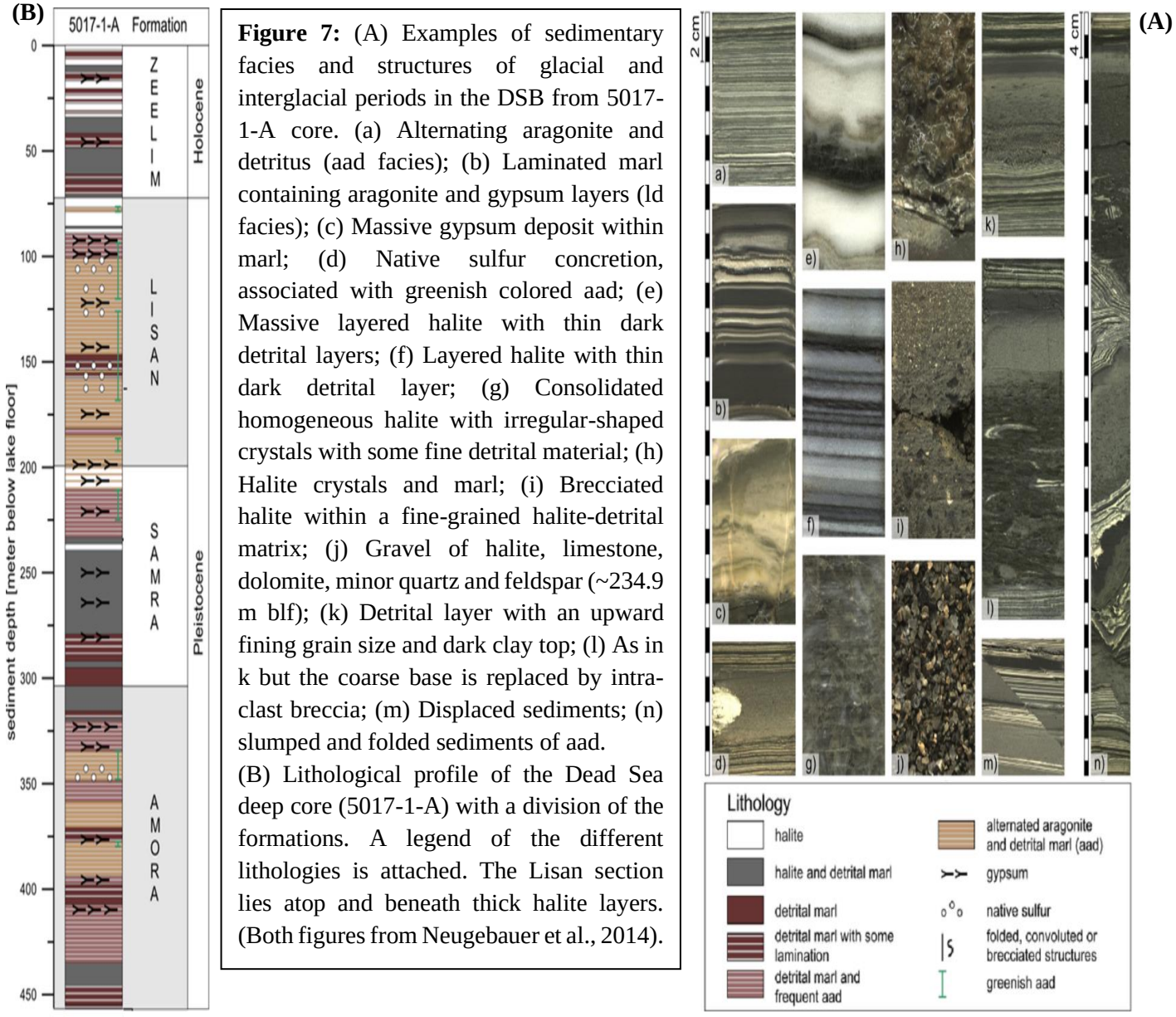

Figure 7: (A) Examples of sedimentary facies and structures of glacial and interglacial periods in the DSB from 5017-1-A core. (a) Alternating aragonite and detritus (aad facies); (b) Laminated marl containing aragonite and gypsum layers (ld facies); (c) Massive gypsum deposit within marl; (d) Native sulfur concretion, associated with greenish colored aad; (e) Massive layered halite with thin dark detrital layers; (f) Layered halite with thin dark detrital layer; (g) Consolidated homogeneous halite with irregular-shaped crystals with some fine detrital material; (h) Halite crystals and marl; (i) Brecciated halite within a fine-grained halite-detrital matrix; (j) Gravel of halite, limestone, dolomite, minor quartz and feldspar (~234.9 m blf); (k) Detrital layer with an upward fining grain size and dark clay top; (l) As in k but the coarse base is replaced by intra-clast breccia; (m) Displaced sediments; (n) slumped and folded sediments of aad.
(B) Lithological profile of the Dead Sea deep core (5017-1-A) with a division of the formations. A legend of the different lithologies is attached. The Lisan section lies atop and beneath thick halite layers. (Both figures from Neugebauer et al., 2014).

The sediments were exposed to the atmosphere for the first time during their extraction and since then they are kept in the core repository in Bremen, Germany in optimal conditions for the preservation of the sediments and brines. Therefore, they are well preserved and did not experience any significant erosion, desiccation or surface processes. Pore fluids exist in the interstitial voids, together with the soluble salts, and they are attribute to be a direct remnant of the deepest brine of the lake (low hypolimnion).

As opposed to the deep core, the exposed sections of the high margins (e.g., PZ-1, Masada) and the DSDDP shallow cores can represent the epilimnion or the hypolimnion, depends on the elevation of the section, the configuration of the lake in the time of deposition and local tectonic that worked since then.

1.5. Works on the pore fluids of the DSDDP deep core

Several works investigated the chemistry of the pore fluids that extracted from the DSDDP deep core sediments for their great scientific potential as pristine original brine of the lake's hypolimnion.

Lazar et al., (2014) conducted the first direct chemical measurements of the DSB lakes' deep brine (hypolimnion), as achieved from the pore fluids compositions. The chloride record of the deep core, as a proxy for brine's salinity, reveals the variations of salinity in the deep lake throughout the last two glacial-interglacial cycles (Fig. 8 A). It shows that the salinity has decreased during glacial periods and reached down to at least 70% of the modern Dead Sea value during the last glacial and particularly during MIS2 (~31–17 ka). Such conditions are referred to wet periods and are characterized by deposition of aragonite, which may be accompanied by mild gypsum precipitation. During drier episodes along glacials enhanced mixing result in increased gypsum precipitation. Interglacials on the other hand, are characterized with salinity increase as seen during the last interglacial (MIS 5) and the Holocene.

Levy et al., (2017) showed that Mg^{2+} and Br^{-} are conservative ions in the lake, meaning that they do not participate in any salt precipitation from the brine and hence their inventory in the lake remains constant. Therefore, a general long-term decline in the concentrations of these ions occurred during glacial periods due to the lake dilution, while during interglacials the concentration of these ions in the brine increased (Fig. 8 B-b). Levy et al., (2018) showed that pore fluids values of $\frac{Na}{Cl}$ rose during glacial periods as a result of halite dissolution that occurred by the lake's diluted brine. During interglacials the $\frac{Na}{Cl}$ dropped due to halite precipitation that took place in the lake after the brine was concentrated and reached halite saturation. Concentrations of conservative ions such as Mg and Br exhibit a mirror pattern relative to the $\frac{Na}{Cl}$ (Fig. 8).

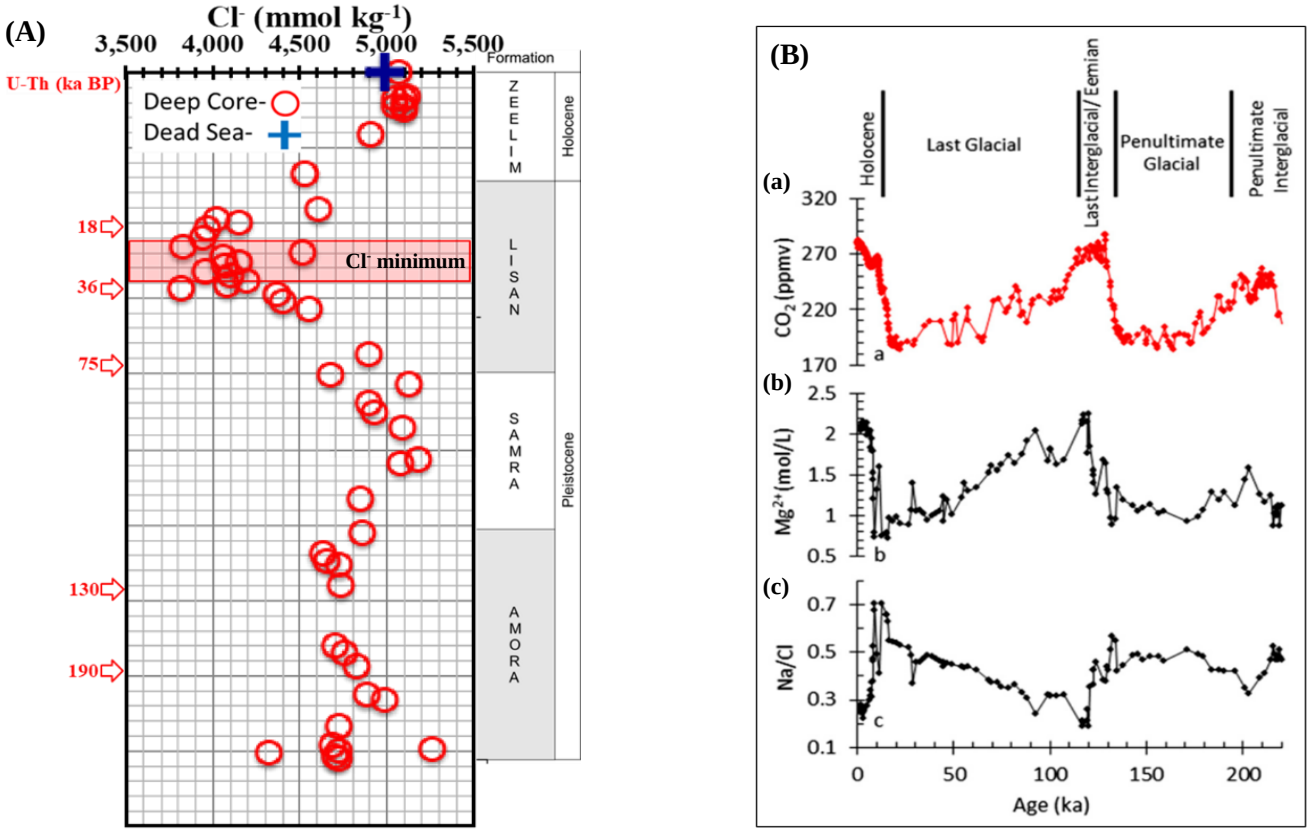

Figure 8: (A) Cl^- concentrations in the pore fluids of the Dead Sea deep core (5017-1-A). Blue cross represents the Cl^- concentration in the modern Dead Sea. Some U-Th ages are attached to the left in red arrows. A prominent decrease from the mean values, which is followed by an increase back to the modern Dead Sea values is observed during the Lisan period. (Figure taken from Lazar et al. 2014). (B) $\frac{Na}{Cl}$ ratios (c) and Mg^{2+} concentrations (b) as measured in pore fluids of the Dead Sea deep core (5017-1-A). Above them (a) attached the CO_2 record from Antarctic ice cores (Lüthi et al., 2008) and the division to glacial and interglacial periods. A high positive correlation is seen between the CO_2 record to the Mg^{2+} profile, and as good though negative correlation is seen with the $\frac{Na}{Cl}$ ratios. (Figure taken from Levi et al., 2018).

Several millennial-scale periods are evident as well in which Mg^{2+} and Br^- increase and $\frac{Na}{Cl}$ ratio decrease, together with halite precipitation. Levi et al., (2017) also showed that the Mg^{2+}, Br^- and $\frac{Na}{Cl}$ trends of the pore fluids from the DSB correlate well with CO_2 composition record from Antarctic ice cores and global SST record, showing similar glacial-interglacial patterns (Fig. 8 B-a). Levi et al., (2018) first suggested that the main source for halite dissolution in the lake, which can be observed by the pore fluids $\frac{Na}{Cl}$ ratio, is the salt diapir of Mt. Sedom that its most significant emergence occurred during the last glacial period, at the bottom of Lake Lisan. Later on, Levy et al., (2019) showed that significant amounts of chlorid, sodium and sulfate ions were replenished into the lake due to dissolution of halite and anhydrite from the Mt. Sedom salt diapir. The dissolution was facilitated by diluted and cool epilimnic waters. Given the increase in solution density a subsequent gravity driven flow transferred the solution deeper into the

hypolimnion. Following this mixing, the hypolimnion volume was increased and it replenished with chloride, sodium and sulfate and became supersaturated to gypsum. Other solutes, such as bromide and magnesium, were simultaneously diluted.

Pore fluids indeed provide new and reliable insights on the evolution of the lake; however, its data was achieved mostly from core catchers (the edges of each core section). Therefore, its record is relatively sparse with medium to low resolution. In addition, pore fluids exist only in unexposed sections and therefore this method cannot be applied in the marginal sediments.

2. Research objectives

The main objectives of this study are:

1. Verify the validity of the soluble salts data as representative of the lake's brine composition (as was originally suggested by Katz and Kolodny, 1989). This process also intend to reveal the reliable ions for brine reconstruction and those who require corrections before they are being used. This is achieved by comparison of the soluble salts and pore fluids data of the DSDDP deep core from the same stratigraphic horizons.
2. The **main goal** of this work is to use the soluble salts data to establish a high-resolution record of the temporal and spatial changes in the chemical properties of the deep and shallow brines of the last glacial Lake Lisan (and additional lakes of the DSB). This goal is achieved by using the most reliable ions for brine reconstruction. The comparison between ratios of such ions in the deep, intermediate, and marginal depositional environments of the lake will provide the temporal and spatial reconstruction of the lake's geochemical history.
3. Apply the reconstructed changes in lake's chemistry for establishing limnological and hydro-climate history of Lake Lisan and its watershed.

3. Significance

This work will be the first to study the soluble salts chemistry in the DSDDP deep and shallow cores and by that the first to have a continuous high-resolution reconstruction of the lake's brines chemistry.

The conclusions of this work have implications on the hydrological and geochemical conditions that prevailed in the watershed of the DSB during the examined periods (mainly the last glacial) and will allow to investigate the relation of the regional hydroclimate regime to global climate events.

Knowing the chemistry of the brines in high resolution and its variations through time can contribute to the understanding of climate changes in the levant and in general to global trends. In an era when climate changes became a known problem, even among the general public, it seems that thoroughly understanding of the climate patterns and mechanisms are essential for the proper understanding of the system and for the evaluation of upcoming risks.

4. Methods

4.1. Samples Collection

Samples for this work were collected from several sites where the Lisan Fm. is exposed or recovered by drilling (sampling sites are marked in Fig. 1). Each of these sampling sites represents a unique sedimentological environment in Lake Lisan, thus providing information on the composition of different water-bodies, e.g., the hypolimnion, the epilimnion and marginal areas (see Fig. 2).

4.1.1. Sampling the DSDDP cores

The DSDDP 5017-1-A core provides information on the deepest environment in the lake. The Lisan Fm. interval in this core was sampled in high resolution. The DSDDP- 5017-3-C core was drilled at shallow waters (~ 2.5 m) off Ein Gedi Spa shore and was sampled in low resolution. The brine solution recovered from the pore fluids of the 5017-1-A core provide information on the hypolimnion of the lake while the 5017-3-C core provides information on the hypolimnion or the epilimnion of Lake Lisan, according to the configuration of the lake during the time of deposition.

Sampling of these cores was done during two sampling sessions. The first session was in the GFZ Institute in Potsdam, Germany where a subsection of the Lisan Fm. from the 5017-1-A core was temporarily stored. The second session was in the Marum core repository in Bremen, Germany, where the DSDDP cores are permanently stored. In the GFZ, Potsdam sixty five samples were collected almost continuously along a short section of the Lisan Fm. at the depth interval of 104-115 m in 5017-1-A core. This interval was dated to 17.8 to 30.1 ka BP (Goldstein et al., 2020), and it correlates with the Cl^- low concentration peak that marks the lake's most advanced dilution of the last glacial period (Lazar et al., 2014). In Marum, additional 47 samples were taken above and below the interval sampled in Potsdam. Altogether, the sampling spans from the MIS 5/4 boundary at 200 m depth in the core to the MIS 2/1 boundary at 85 m depth. Both boundaries are marked by the appearance of massive halite units.

Additional, 28 samples were taken from the 5017-3-C core (termed here the "shallow core"). The deepest sample that was taken from this core is from 298.39 meters below lakes floor and the shallowest sample is from 58.51 meters below lake's floor. The sampled section of this core covers the period of ~145-11 ka BP (MIS 6-2) and include the upper part of Amora Formation (MIS 6), the last interglacial Samra formation (MIS 5), the Lisan Formation (MIS 4-2) and the onset of the transition to the Holocene (see chapter-8 for the chronology method of the 5017-3-C core). This core was sampled much more sparsely than the core 5017-1-A.

4.1.2. Sampling the exposed marginal terraces of the Lisan Fm.

Sampling the exposed marginal terraces of the Lisan Fm. allows getting data on the composition of the lake's epilimnion (see Fig. 2).

Perazim valley PZ-1 section. Thirty-seven samples were collected in aluminum canisters from the Upper Member ('the White Cliff') of the Lisan Fm. at the PZ-1 section in Perazim Valley, between the elevations of 3004.5 to 3343.5 cm above the base of the section (see similar samples in aluminum canisters from 5017-1-A core in Fig. 10). For detailed description of PZ-1 section and its U-series derived age-depth model see Haase-Schramm et al., (2004). These samples are spanning the time interval of 26.5-21.7 ka BP, when the lake level was at its highest stand. The samples are part of a complete sequence of the outcrop that was sampled several years ago by Amitai Katz and Mordechai Stein. These sections lie between -40 to 1400 cm and 1820 to 2737 cm above the base of the section, corresponding to the time intervals of 60.4-51.3 ka BP and 43.1-30.2 ka BP. Altogether the data of the soluble salts from this outcrop covers the majority of its total 40 meters. These samples were processed and analyzed in a previous work and will first publish here, while the section that used in this work add another important part to the processed segment. The top of the PZ-1 section (~ 40 m high) is located ~275 m below mean sea level (bmsl). Therefore, the soluble salts of these sections represent the composition of the epilimnion unless the interface with the hypolimnion reached very shallow depth in the lake during some periods.

The Mt. Sedom "White Hill" is an outcrop of the Lisan Fm. at top of the Mount Sedom salt diapir (e.g., Zak, 1967). The section comprises a few meters of aragonite and silty detritus laminae of the aad facies, that overlain by a pebble layer of a few meters, which is overlain by additional interval of aad (Fig. 9 A). Intermittent gypsum layers appear along the section. Seven samples were collected from the White Hill section for soluble salts analyses (Fig. 9 A&B). This section was dated by U-Th within the scope of this work. Following the dating method that described by Haase-Schramm et al., (2004), clean aragonite laminae were separate from the samples and sent for U-Th dating in the Geological Survey of Israel. The obtained U-Th ages (see Table 1), reveal that the Lisan Fm. in Mt. Sedom White Hill section of this work

covers the time interval of 36.6 to 24.5 ka BP. These ages are consistent with previous ages determined by Weinberger et al., (2007) on a separate section of the White Hill. Today, the top of the White Hill is at ~200 m bmsl but since it is located on an active salt diapir its accurate position during the time of deposition has to be considered. This issue will be addressed later in the discussion.

Table 1: U-Th dating data of Lisan carbonates from Mt. Sedom White Hill outcrop.
All ages are single sample (SS) ages with correction of the detrital contamination.

Sample Name	Position in outcrop	Lithology	Concentrations		Activity ratios:		SS Age (ka BP) Detritus Corrected	±Error (ka)
			$U_{(ppm)}$	$Th_{(ppm)}$	$\left(\frac{^{230}Th}{^{238}U}\right)$	$\left(\frac{^{234}Th}{^{238}U}\right)$		
GL 10-1-2	See Figure-10	Aragonite	0.3280	0.0096	0.4200	1.4603	36.6	~2
GL 10-1-1		Aragonite	0.3350	0.0127	0.3790	1.3282	36.1	~2
GL 10-2-2		Aragonite	0.2951	0.0088	0.3856	1.5049	32.0	~2
GL 10-2-1		Aragonite	0.3657	0.0128	0.2811	1.4633	31.5	~2
GL 10-3-2		Aragonite	0.2264	0.0052	0.1851	1.4734	27.5	~2
GL 10-3-1		Aragonite	0.4101	0.0165	0.3355	1.4817	27.0	~2
GL 10-4		Aragonite	0.3506	0.0084	0.3006	1.4700	24.5	~2

Details of detrital correction				
Sample Name	Assumed $\left(\frac{^{232}Th}{^{238}U}\right)$ detrital (atomic)	Derived detrital ^{238}U (μmol)	Assuming secular equilibrium:	
			Derived detrital ^{234}U (μmol)	Derived detrital ^{230}Th (μmol)
GL 10-1-2	1	$2.8933 \cdot 10^{-5}$	$1.5898 \cdot 10^{-9}$	$4.8814 \cdot 10^{-10}$
GL 10-1-1	1	$4.9527 \cdot 10^{-5}$	$2.7213 \cdot 10^{-9}$	$8.3558 \cdot 10^{-10}$
GL 10-2-2	1	$2.280 \cdot 10^{-5}$	$1.253 \cdot 10^{-9}$	$3.847 \cdot 10^{-10}$
GL 10-2-1	1	$3.4210 \cdot 10^{-5}$	$1.880 \cdot 10^{-9}$	$5.771 \cdot 10^{-10}$
GL 10-3-2	1	$5.846 \cdot 10^{-5}$	$3.212 \cdot 10^{-9}$	$9.862 \cdot 10^{-10}$
GL 10-3-1	1	$6.4303 \cdot 10^{-5}$	$3.5332 \cdot 10^{-9}$	$1.0848 \cdot 10^{-9}$
GL 10-4	1	$3.2740 \cdot 10^{-5}$	$1.7990 \cdot 10^{-9}$	$5.5235 \cdot 10^{-10}$

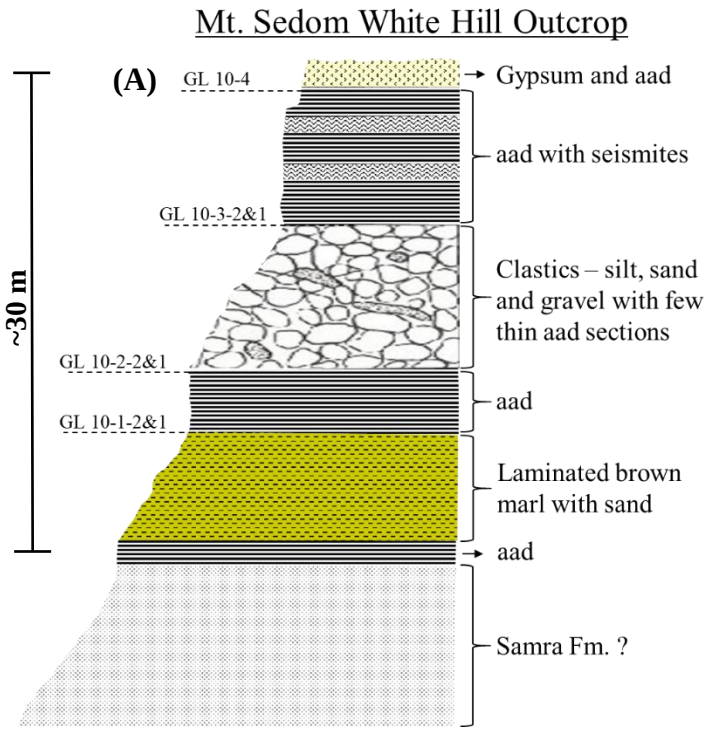

Figure 9: (A) Generalized section of Mt. Sedom White Hill outcrop that was sampled in the work. Locations of samples are marked on the section.
(B) An example for sample that was taken from Mt. Sedom White Hill section. The lamination of the aragonite and detritus is seen clearly.

4.2. Cores and outcrops' sampled sections

Samples of the DSDDP cores and the marginal outcrops were taken from undisturbed sections of the laminated *aad* facies. The sequences of the *aad* facies represent periods of limnological stability in the lake when laminae of silty detritus and primary aragonite were deposited annually.

In addition to the *aad* sequences samples were also taken from sequences that contain gypsum layers, sulfur concretions, thick layers of aragonite or detritus, or particles bigger than the common silt, as part of the general *aad* sequence. All of these lithologies indicate on changes in the composition of the brine and hence, can be reflected by variations in the soluble salts' composition. These changes could be part of a short or long-term processes that occurred in the lake and identifying them is essential for achieving a high-resolution reconstruction of the lake's brines chemistry and lake's paleo-limnology.

In several cases, the sampled section's lithology did not allow the sampling of an "ideal sample". These samples comprise distorted *aad* sequences, such as slumps or mixed layers (see Kagan et al., 2018). The composition of the soluble salts in each of these samples may or may not represent the brine's composition at the time the sample is dated for. Therefore, their results require extra attention and caution.

4.3 Sampling Method

Cores sampling: The removal of the samples from the cores done with specific tools that enable the extraction of undisturbed rectangle samples ±1 cm deep. The tools were washed in DW and dried with clean lab paper between each sample. The samples were placed in rectangle aluminum canisters that are 2.5 cm wide and 11 cm long, and accordingly, the maximum sample size is 10x2x1 cm (Fig 10). The majority of the samples are indeed at their maximum size. Smaller samples were taken where full sampling was not possible or in cases when there was no interest in a full-size sample. Each sample was wrapped in plastic wrap and stored in a cooler until its delivery to the Hebrew University, where they were stored in 5°C refrigerator inside sealed boxes.

Outcrops sampling: The Mt. Sedom White Hill samples were cut out of the exposed wall by a sharp knife and a spatula. A block approximately the size of 20x15x10 cm was cut off the outcrop for each sample. These blocks were placed inside plastic bags with zippers to keep their preservation and avoid desiccation or moisture adsorption (Fig. 9 B).

In the lab, the surface of the sample was removed, and two smaller samples were cut from each block, with acid clean, sharp knife, approximately the size of the cores' samples – 10x2x1 cm.

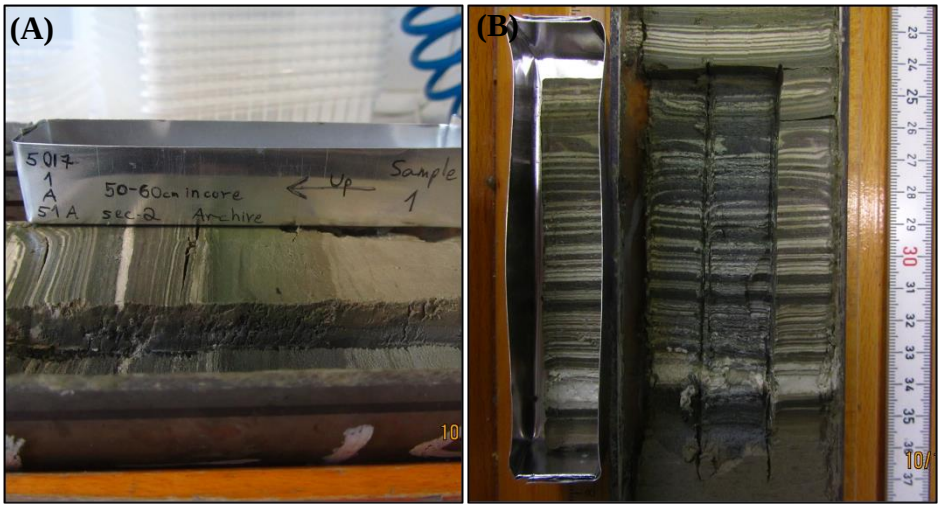

Figure 10: Representative sample taken from the 5017-1-A deep core, similar to the rest of the deep and shallow cores samples. The sample is shown next to the core it was sampled from. (A) Side view. The details of every sample are written on the side of the aluminum canisters, as seen here. (B) Top view. Laminated sections in the core and in the sample are clearly seen.

4.4. Multiple washes experiment

A dissolution experiment was performed in order to set the procedure for the extraction of the soluble salts. The main question of this experiment was: what procedure will be ideal for extracting brine remnants and dissolving the soluble salts entirely out of the sediments while dissolving minimum to none of the original minerals that precipitate in the lake, such as aragonite and gypsum? The experiment was conducted in the geochemical lab of the Geological Survey of Israel.

Dissolution experiment: Nine samples were selected for this experiment. They represent all major depositional environments and lithological units that are studied in this work. Five samples were selected from the deep core, and additional four samples were selected from the PZ-1 section, representing the marginal outcrops' sediments. Out of these samples, four are of the *aad* facies. One is half *aad*, half thick aragonite layer. Two are of the *aad* facies with a thick aragonite layer. One sample comprises only aragonite. One sample is of the *aad* facies with sulfur concretion, and one sample comprises a detrital layer with only few aragonite laminae (*the ld* facie). In the case of the DSDDP cores' sediments the whole samples were used, including salts that dried from the samples and crystalized on the canisters. The PZ-1 samples were cut into halves lengthwise and one halve was used for analyses.

The sediments were transferred into a mortar and thoroughly mixed and disaggregate with a pestle until reaching a uniform, homogenous mixture. The mixed sediment was then transformed into a 250 ml bottle and weighted (notice that the weight of the sediments was not uniform between samples). Two hundred and fifty ml (g) of DDW (resistivity of $\geq 18 \frac{megohm}{cm}$) were added to the bottle by washing the sediments' remnants off the mortar and other working tools that contact the sediments. The bottles were then weighted and thoroughly shook by hand for several minutes until all chunks of the sediment were disaggregated, and the mixture reached homogeneity. The bottles left on the table for 20-30 min of

interaction between the water and the sediments. Afterward, the water with some suspending particles was pumped with a syringe and filtered through a filter paper with a pore size of 0.45 μm to achieve separation between the sediment and the water that dissolved the soluble salts.

Filtering was done by using a syringe filter or a vacuum filtering device with a Whatman filtering paper. The water with soluble salts was transferred into a clean new bottle, and sediments that remained on the filter paper collected back into the sediments bottle.

The remained sediments in the bottle were weighed before and after the addition of additional 200 ml of DDW. Again, the bottles were shaken by hand, and this time were left for about an hour of water-sediment interaction. At the end of the hour, the water was separated from the sediments, implementing the same filtering technique as in the previous wash, and transferred into a new bottle. The third and fourth washes were done in the same way as the second wash. The fifth wash was left overnight on a shaking table (200 rpm, ~12.5 hours). On the following day, bottles were removed from the shaking table and left static for several hours until the majority of suspending particles sank. Once deposition was complete the solution was filtered. The time of water-sediment interaction reached to 15-20 hours.

When dealing with the deep core samples, as washes proceed, sediments tend to stay longer in suspension, and it became more challenging to filter the samples. When sediment sinking did not proceed enough, the water and suspended sediment transferred into 50 ml tubes and inserted into a centrifuge (15 min, 5000 rpm). Centrifugation was typically required in the fourth and fifth wash and in few samples already in the third wash.

All the tools and bottles used in this experiment and further on in the sample's processing were cleaned by two meticulous washes with DW and a third wash with DDW and then dried on a clean lab paper and beneath another layer of lab paper. Bottles were left to soak with the DDW for at least a night and then left to dry. The mortar, pestle, spatula, and other tools that interact with the sediments were washed in DW and then soaked in diluted HNO_3 1:4 (~4N/16.2%) for about 15 minutes before being washed as the other tools.

4.5. Procedure for extraction of soluble salts from the sediments

In light of the results received from the multiple washes experiment, a procedure was developed that maximizes the dissolution of the soluble salts from the sediments while minimizing the dissolution of minerals that originally precipitate in the lake, mainly aragonite and gypsum. Two procedures were applied:

The first procedure: At first, 30 samples were selected from the deep core, spreading along the Lisan section. A slice, $\pm 3\ mm$ wide, was cut lengthwise from each sample in a way that represents the whole sample. The sliced material was adequately mixed in a mortar with a pestle to achieve bulk samples that transferred into 50 ml falcon tubes. One gram of each bulk sample weighed in a new 50 ml tube. In the clean lab in the Institute of Earth Science, Hebrew University each sample went through 3 washes, first and second with 30 ml of DDW and third with 20 ml of DDW. The water with the sediments were thoroughly mixed and disaggregated manually and, on a shaker, and then left on a rotating device for few more minutes to enable dissolution. The mixed samples were centrifuged for 25 minutes (maximum speed), and then the water carefully poured into a $125\ ml$ bottle (all three washes in the same bottle) while the sediments were left in the initial tube.

Finally, the water was filtered using a syringe filter with pore size of 0.45 μm to ensure complete separation between the sediments and the water containing the soluble salts (samples' filtering was dune several months after samples preparation). Samples of this group are called ***Bulk samples***.

The second procedure: The sediments stored inside the fridge dried out since their wrapping and storing boxes were not sealed enough. It led to the crystallization of the soluble salts on the sediments and the canisters. Due to that there was a need to process and analyze the whole sediment filling the canister otherwise some soluble salts could have lost. This procedure was carried out in the geochemical lab in the Geological Survey of Israel. The salts were collected and scratched from the canisters and transferred to the mortar. The sediments and their salts were mixed and disaggregated in the mortar, with a pastel until receiving homogenous bulk sediment, then transferred into a 250 ml bottle. The amount of sediment was weighted before the tools used to mix and transfer the sediment were washed with DDW into the bottle to collect remnants of sediments and salts. The bottles were then filled with DDW to its threshold unless the sample size was small (~2.5X2X1cm). Very small samples (~1.5X1.5X1 cm) were transferred into 125 ml bottles filled to their threshold. When full, the bottles were weighed again to receive the amount of DDW that interact with the sediment. The bottles were manually shaken for several minutes to receive a homogenous mixture that enabled a comprehensive interaction between the water and the sediments. To allow some time for dissolution, the bottles were left on the table for 20-30 minutes. During this time, salts could have dissolved, and suspending particles partly sank. 50 ml of water + suspending particles pumped from the top of the solution with a syringe and filtered to a 50 ml tube through a syringe filter with a pore size of 0.45 μm. This portion of water + soluble salts is called ***Short samples***.

The bottles with the remaining portion of the solution left on a shaking table during the night (200 rpm, ~12.5 hours). On the following day, bottles were removed from the shaking table and left static for several hours until the majority of suspending particles sank. The solution was pumped from the bottles, with minimum sediments as possible, using a syringe and filtered through a syringe filter with pore size of 0.45 μm or a vacuum filtering device and Whatman filtering paper with the same pore size. Total time of water-sediment interaction after the short portions were pumped is ~15-20 hours. Solutions were transferred into a clean 125 ml bottle. This portion of water + soluble salts is called ***Long sample*s**.

Schematic illustration of the second (main) procedure is presented in Fig-11.

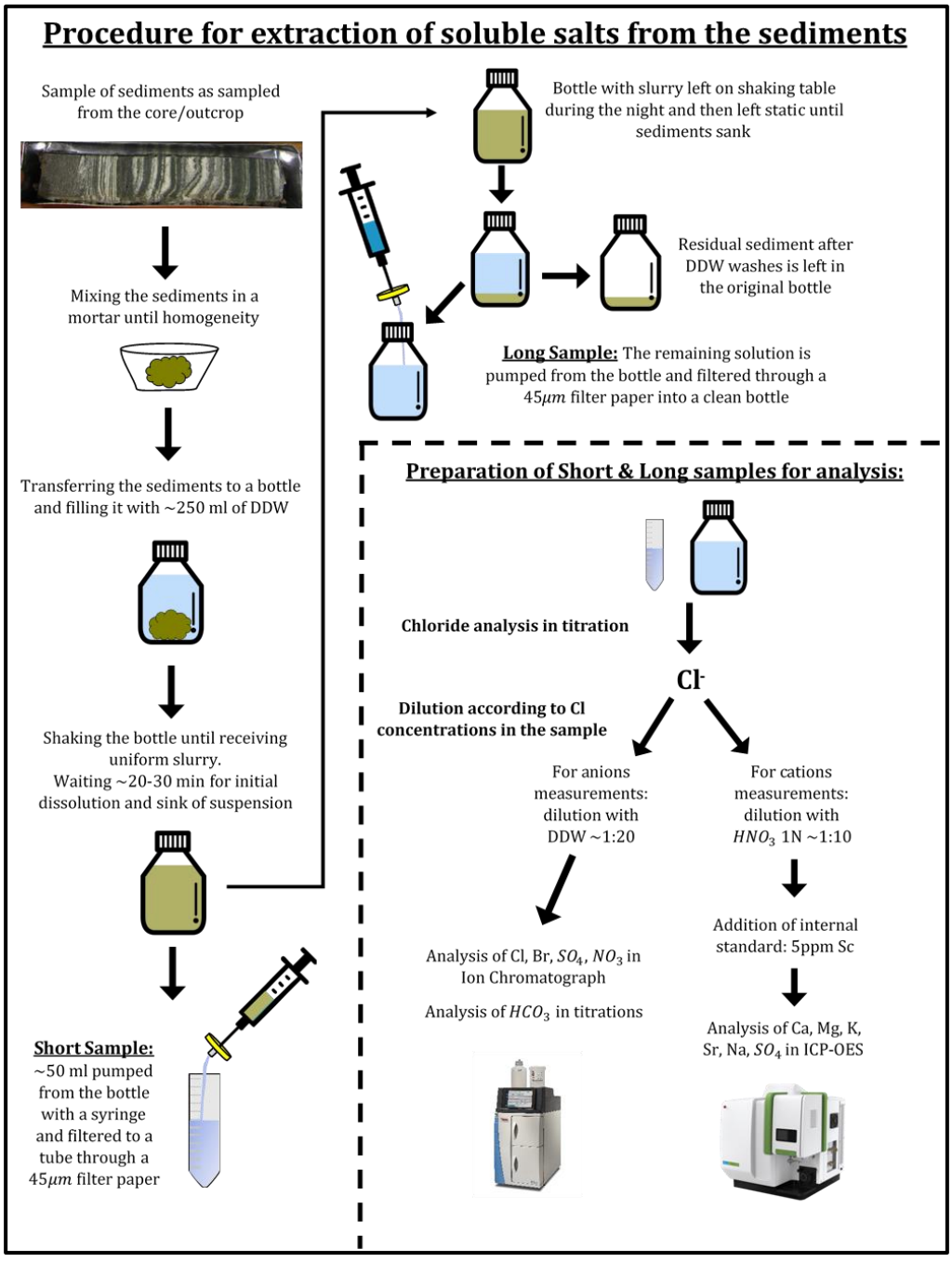

Figure 11: Schematic illustration of the main method that was used in this work for extraction of soluble salts from the sediments.

During the preparation of each core/outcrop group of samples, 2-3 blanks were prepared as well. In the deep core case, where the samples number is high and their preparation was divided into several batches, 2-3 blanks were prepared for each group of ~30 samples. Blank samples went through the same procedure as regular samples, from storing canisters to analyses, although without the sediment.

4.6. Preparations for chemical analyses and chemical analyses

The salts that are dissolved in the brines or crystallized out of them comprise, mainly, the major ions in the solution, i.e., the most abundant cations and anions that are found in the highest concentrations.

In light of that, the chemical analysis of each sample was focused on the major elements in the solutions: Na^+, K^+, Ca^{2+}, Mg^{2+}, Sr^{2+}, SiO_2, Ba^{2+}, Cl^-, Br^-, NO_3^-, SO_4^{2-} and for several groups of samples F^-, PO_4^{3-}, Fe, and HCO_3^- (Alkalinity) were measured as well.

All samples were measured in the geochemical department in the Geological Survey of Israel. Cations (Na^+, K^+, Ca^{2+}, Mg^{2+}, Sr^{2+}, SiO_2, Ba^{2+}, Fe) and SO_4 were measured with Perkin Elmer Optima 5300 V ICP-OES. Anions (Cl^-, Br^-, NO_3^-, SO_4^{2-}) were measured with Dionex ICS-2000 Ion Chromatograph. Chloride was also measured in titration (Metrohm 702 SM Titrino). HCO_3 was measured in titrations mostly in the Geological Survey of Israel (Manual titrator: Metrohm 775 Dosimat. Automate: Metrohm 785 DMT-Titrino) with several test measurements done in the Institute of Earth Science, Hebrew University (Radiometer TIM865 titration manager).

Samples were usually first measured for Cl in titration, without dilution, or diluted up to 10 times with DDW. According to the Cl concentrations in the titrations, the samples were diluted and prepared for analyses (Fig. 11). For Ion Chromatography, samples were diluted with DDW, 1:20, or more, in high Cl samples. For ICP-OES samples were diluted with HNO_3 1N, 1:10, or more, in high Cl samples. After acid addition, 5ppm of Scandium were added, to be used as internal standard during measurements. For every 10 ml of the diluted samples 0.2 ml of 250 ppm scandium solution was added.

Blanks were prepared in the same method but were diluted only by half in order to include the influence of the dilution process in their preparation but, at the same time, reduce their concentrations as minimum as possible.

The accuracy of Cl titrations was checked with tap water and at least three repetitions of NaCl or KCl 1000 ppm Cl standard before and after each ~25 samples in every measurement session. The acceptable error range was considered to be 1%. Bromide concentrations that received from ion chromatograph were reduced from each Cl measurement since the Cl electrode dose not differentiate between them.

Calibration of the ion chromatograph was done with four multi-element standards composed of Merck single elements standards (STD 1-4). They contain each of the measured anions and together create a calibration curve for each element. Accuracy was checked after calibration, along measurements - after every 10-15 samples, and at the end of the measurements, using the four standards of calibration, additional standard fit for anions measurements in ion chromatography (Mercury SDT II) and, in several cases, Mercury single element standard of Br. DDW samples were used as blanks to account for instrumental background signal and to verify that the DDW are indeed clean and dose not contribute any amount of elements along the procedure.

Calibration of the ICP-OES was done with a blank (HNO_3 1N + 5ppm Sc) and three multi-element standards that were composed of *Merck* or *High-Purity Standards* single elements standards. Each standard consists of several of the measured elements, and altogether they create a calibration curve for each element. Accuracy was checked after calibration, along measurements - after every 15-20 samples, and at the end of the measurements, using, USGS standards for major elements, blanks, and additional multi-elements standard (RW) composed of the *Merck* or *High-Purity Standards*. Since the second half of the measurements, six deep core samples were chosen to serve as additional external standards. These samples help identify a drift along measurements and reduce the use in the scarce USGS majors standards. The 5ppm Scandium added to all the standards, samples, and blanks used as an internal standard and provide an estimation for each specific measurement's accuracy.

The method used in the measurements is built in particular for the analysis of major elements and suits the range of concentrations in the different types of samples of this work.

In the case of sulfate and sodium two wave lengths were measured in each measurement of the ICP-OES (SO_4 (measured as S) 181.984 & 180.677 and Na 589.582 & 588.992). In each measurement the option with the better result was chosen among the two, in terms of standards fit, precision, and concentrations relative to the blanks.

Accuracy and stability of the manual and automatic alkalinity titrators was confirmed by measuring a 215 ± 10 ppm HCO_3^- Merck standard of alkalinity several times before, along and at the end of measurements.

Precision of the measurements of the different devices (ICP-OES, Ion chromatograph and Cl titrations) were estimated by calculating the standard deviation of the repetitive measurements of standards and repetitive measurements of samples. An average value of the standard deviation received for each standard and per each measurement for the group of samples that re-measured. The combined values

were than received by calculating the weighted average of all the repetitive measurements performed, considering the number of repetitions done for each standard or group of samples.

This method produces a proximation for the precision of the analysis of each element, expressed by σ, and the standard deviation on this value (since it is an average by itself).

5. Quality of the measurements and required corrections

5.1. Accuracy, precision, and blanks

In the Cl titrations, concentrations of the NaCl or KCl 1000 ppm Cl standards were received within the 1% error range, with a constant deviation of the concentrations upward. Average deviations were used to correct the samples' results, each group of measurements with its deviation correction factor. Standard deviation (σ) of the chloride titrations was usually low (less than 5 $\frac{mg}{L}$) but in several cases got high (up to 15-45 $\frac{mg}{L}$, in samples with high concentrations of Cl). In any case the percentage of the standard deviation from the sample's average value is usually less than 1% and rarely reach to 2-3% (Table 2).

Table 7: Weighted average of the standard deviation of the chloride values measured in titrations and its percentage out of the average chloride values. The standard deviation on these values is presented below since these values are average by themselves.

Chloride titrations	Std Dev	%Std Dev of Average
Weighted Average:	4.45	0.61
Std Dev:	3.06	0.31

Precision of the Ion Chromatograph measurements was estimated from the repetitive measurements of standards that used along the measurements. Standard deviations (σ) in each standard were low and rarely exceed 2 $\frac{mg}{L}$. In the case of Cl and Br, results of standards measurements that were beyond the σ range were rejected in order to improve their standard deviation values. It was done for these two elements since they are essential further in the discussion. The estimated standard deviation values for each anion are presented in Table 3. Estimated standard deviation values did not exceed 6‰ of the minimum concentration of Cl in the samples, 4.5% of Br, 3% of SO_4 and 3% of NO_3.

The accuracy of several major standards that used in the Ion-Chromatograph measurements is presented in figure 12.

Table 15: Weighted average of the standard deviation of the anion values measured in Ion Chromatograph. The standard deviation on these values is presented below since these values are average by themselves. (Cl & Br values are after results rejection of σ outliers)

Standard Deviation of Ion Chromatograph Measurements					
Element:	**Cl**	**Br**	**NO3**	**SO4**	**F**
Weighted Average:	0.62	0.15	1.26	1.11	0.15
Std Dev of Weighted Average:	0.63	0.20	0.76	1.08	0.12

DDW blanks were absent of any element except of NO_3^- that exist in several measurements and could get up to ~2.5 $\frac{mg}{L}$. When NO_3^- was found in the samples as well a correction was done, although usually it was not the case.

Procedural blanks show no contamination of anions along the procedure except for minimal Cl that did not exceed 1% of the lowest concentrations in the samples. In few measurements Cl in the blanks did reached up to 2-4.5% of the minimum value in the samples. In addition, in the blanks of the outcrops' samples NO_3 was high and reached at maximum to ~8.5% of the minimum values in the samples. This surplus of chloride and nitrate was subtracted from the relevant samples.

Accuracy of the ICP-OES measurements was estimated by comparing the values of the standards that measured along measurements to their known values. Accuracy was found to be within 95% fit for all elements, except for K which was 85-90%, with reproducibility in all measurements. A correction was carried out for K according to the accuracy in each measurement. The accuracy of several major standards that used in the ICP-OES measurements is presented in figure 12.

Precision of the ICP-OES measurements was estimated from the repetitive measurements of standards that used along the measurements and repetitive measurements of samples. In the case of Na results of standards measurements that were beyond the σ range were rejected in order to improve its standard deviation value. It was done for this element since it is essential further in the discussion. The weighted average values of the standard deviation for each cation (together with the deviation on these numbers) are presented in table-4. Estimated standard deviation values does not exceed 1% of the minimum values of all elements measured in the samples, except of sulfate that in several batches could reach up to ~6% of the minimum value.

Table 19: Weighted average of the standard deviation of the cations and sulfate as measured in ICP-OES. The standard deviation on these values is presented below since these values are average by themselves. (Na values are after results rejection of σ outliers)

Standard Deviation of ICP-OES Measurements										
Element:	**SO4**	**SO4-1**	**Mg**	**Ca**	**Sr**	**Na**	**Na-1**	**K**	**Ba**	**SiO2**
Weighted Average:	1.19	1.64	0.18	0.56	0.0025	0.60	0.93	0.18	0.0026	0.21
Std Dev of Weighted Average:	1.07	1.98	0.12	0.35	0.0019	0.53	0.50	0.10	0.0024	0.18

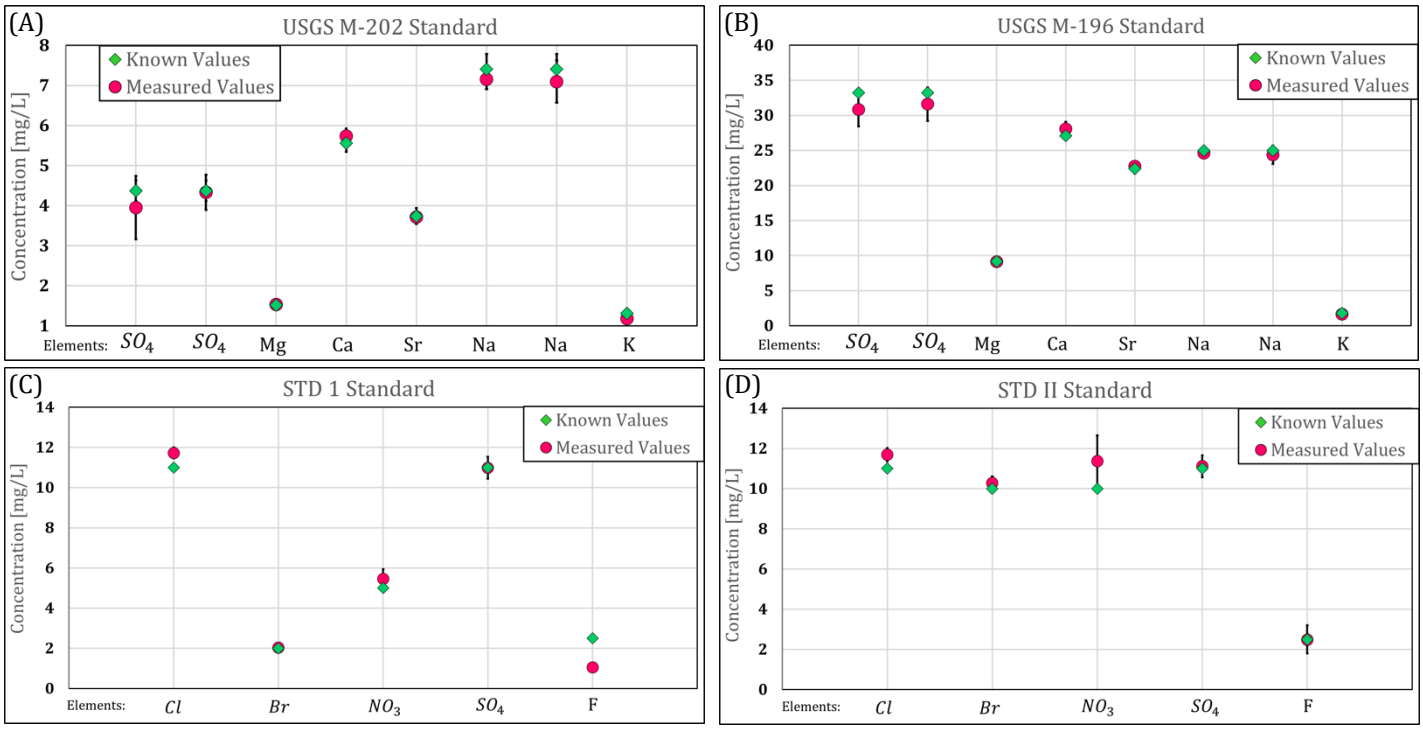

Figure 12: Accuracy of several USGS standards that used the most in ICP-OES measurements and Multi-element standards that used in Ion Chromatograph measurements. Measured and known values are presented, including standard deviation. When standard deviation lines are not seen it is due to their short range that lies behind the symbol. (A) USGS M-202. Used in ICP-OES. (B) USGS M-196. Used in ICP-OES. (C) STD 1. Used in Ion Chromatograph. (D) STD II. Used in Ion Chromatograph.

The deep core samples that used as standards along the measurements show no significant drift along measurements. The accuracy of the internal 5 ppm Scandium standards was not uniform. The Scandium values could be accurate and stable along measurement (up to $\pm$10% deviation), accurate at the beginning with a drift along measurement or inaccurate all along the measurement. Deviations were typically upward with maximum scandium concentrations of ~8 ppm. Nevertheless, measurements with inaccurate scandium could still be accurate for the major elements due to internal automatic correction that is part of the program.

Major elements' concentrations in the external blanks, that used to check the accuracy of the device together with the standards, were insignificant and did not overcome 5‰ of the concentrations measured in the samples.

Concentrations in the procedural blanks were typically higher than the external blanks. At maximum blanks reached to ~6% of the minimum concentration of SO_4 in the samples of the same batch, and up to 4% for the rest of the elements. On average, blanks' concentrations reached to 1.2% in SO_4 and up to 0.8% in the rest of the elements. Either way, concentrations of all elements in the procedural blanks were within or slightly higher than the standard deviation of the measurements.

Concentrations of the Merck HCO_3^- 215±10 ppm standard of the alkalinity titrations were within the range of error. The estimated precision of the measurements comes from the long-term experience with this titrators and is evaluated to be at maximum 5%.

Concentrations of SiO_2, Ba^{2+}, Fe, F^-, PO_4^{3-} in all measurements are very low to insignificant and therefore they will not be discussed.

In the majority of the samples positive and negative ions were balanced with a charge balance $\leq \pm 2.5\%$. Few samples, with results that seems to be correct, are presented with charge balance $\leq \pm 5\%$. The charge balance of each sample is found in the supplementary.

In this work the main investigation of the results will perform on ion ratios rather than concentrations of individual elements. Therefore, it is essential to calculate the error of the discussed ion ratios. Error of a ratio between two elements was calculated by the following equation:

$$\delta\frac{X}{Y} = \frac{X}{Y}\cdot\sqrt{\left(\left(\frac{\delta X}{X}\right)^2 + \left(\frac{\delta Y}{Y}\right)^2\right)}$$

Where X and Y are the concentrations of each element as received from the measurements in $\frac{mg}{L}$. δX and δY are the standard deviation calculated for each element.

The ranges of the standard deviations that are presented on the graphs in this work incorporate the standard deviation themselves (without the ± error range of the standard deviation).

In all the graphs of this work that present ion ratios the standard deviation error bars of the ratio are displayed on each data point. If the bars are not seen it is due to their short range that is smaller than the data point itself.

The only graphs that do not include the standard deviation bars are graphs of ratios that include SO_4. This is since this anion was measured both with the ICP-OES and with the Ion Chromatograph. The standard deviation that obtained for SO_4 ratios is different when using the SO_4 standard deviation and concentrations that received from the two devices. Therefore, it is required to check for each sample whether its SO_4 value was taken from the ICP-OES or from the Ion Chromatograph results in order to obtain the true standard deviation of these ratios, a task that was not accomplished in this work.

Nevertheless, as will be seen in the results and discussion of these ratios they present a very distinct behavior and the conclusions that come out of them rely on their general behavior and not on specific trends and variations.

5.2. Correction for results of the multiple washes experiment

The results of the multiple wash experiment, as all other results, were received in $\frac{mg}{L}/ppm$. A calculation was applied on the results in order to convert the concentrations' units to $\frac{mmol}{g}$. In the case of the multiple washes experiment additional calculation was required on the results of the 2-5 washes. In these washes the solution in the bottles was not pure DDW, as in the first wash, but rather a mixture of the DDW that added in the specific wash and remnant water from the previous wash that already interact with the sediments and hence contain some amount of dissolved ions. This calculation subtracts from each wash the amount of elements that comes from the remnant water (carry over) and therefore leaves only the amount of elements that dissolved in the specific wash. After conducting this subtraction, it will be possible to track the dissolution process of each element along the five washes. The subtraction calculation is detailed below:

$M_{k,i} - Mass\ of\ ion\ k\ afer\ wash\ i \qquad\qquad i = 1,2,3,4,5$

$M_{k,C.O.,i} - Mass\ of\ ion\ k\ in\ carry\ over\ after\ wash\ i$

$C_{k\ measured\ i} - Concentration\ of\ ion\ k\ as\ measured\ after\ wash\ i$

$G_{total\ i} - Weight\ of\ sediment + water\ at\ wash\ i$

$G_{sed} - Weight\ of\ sediment$

$G_{measured,i} - Weight\ of\ water\ taken\ for\ analysis\ after\ wash\ i$

1) $M_{k,i} = C_{k\ measured\ i} \cdot (G_{total\ i} - G_{sed}) - M_{k,C.O.,i}$

2) $M_{k,C.O.,i} = C_{k\ measured\ i-1} \cdot (G_{total\ i-1} - G_{sed} - G_{measured,i-1})$

Substitute (2) into (1)

$M_{k,i} = C_{k\ measured\ i} \cdot (G_{total\ i} - G_{sed}) - C_{k\ measured\ i-1} \cdot (G_{total\ i-1} - G_{sed} - G_{measured,i-1})$

$M_{k,i} = C_{k\ measured\ i} \cdot G_{total\ i} - C_{k\ measured\ i=1} \cdot G_{total\ i=1} + G_{sed} \cdot (C_{k\ measured\ i=1} - C_{k\ measured\ i}) + C_{k\ measured\ i=1} \cdot G_{measured,i=1}$

When i=1 → $C_{k\ measured\ i-1} = 0$

The results of this work and the discussion regarding them are divided into 3 chapters. In each chapter, the relevant results for its discussion will be presented.

6. Assessment of the validity of the soluble salts method and tracing each element's dissolution path

This chapter focuses on the assessment of the soluble salts method validity. This is addressed by examining the data achieved by the multiple washes experiment and by comparing the soluble salt data of the deep core with pore fluids results from the same core. The results of the multiple washes experiment provide insights on how each element dissolves in the DDW washes of the soluble salts method and reveal whether it comes only from soluble salts dissolution or additionally from dissolution of the primary minerals that originally precipitate from the lake such as gypsum and aragonite. The comparison between the soluble salts to the pore fluids results of the deep core provide the first opportunity to check the accuracy of the soluble salts data with an independent source of data since both of them supposed to supply the same information – the chemistry of the lake's deep hypolimnion.

6.1. Results

6.1.1. Results of the multiple washes experiment

The multiple washes experiment reveals the following patters:

The elements, Cl, Na, Mg, Br (Fig.13 A-D) and NO_3 (Fig. 29 Chapter-3) dissolve almost exclusively in the first wash and the remnant dissolve in the second wash. In washes 3-5 the concentrations of the elements are zero or insignificant. K as well dissolved in the same pattern but with slightly higher concentrations in the third wash (Fig 13 E).

The elements Ca, SO_4 and Sr display a different pattern of dissolution.

Sulfate dissolution (Fig. 13 F) in the first wash of PZ-1 samples is not high and is just slightly above the rates of dissolution in the 2-4 washes. In the fifth wash on the other hand, the sulfate dissolution in these samples peaks high, above all deep core samples in the first wash, except one, and clearly above the deep core samples of the fifth wash. The deep core samples show an opposite pattern, with high amounts of sulfate dissolved in the first wash, similar amounts in the 2-4 washes as those of the PZ-1 samples, and lower amounts than the PZ-1 samples in the fifth wash.

The concentrations of Ca in the first wash are the highest with greater amounts of calcium in PZ-1 samples than in the deep core samples (Fig. 13 H). In washes 2-4 the Ca concentrations are low and stable (above the zero reading) or decline gradually with PZ-1 more or less converge with the deep core

concentrations or stay a little higher. In the fifth wash PZ-1 samples peak up again to ~30% of the first wash while the deep core samples show just a mild rise. The strontium dissolution pattern is similar to the calcium, but with concentrations ~2 orders of magnitude lower (Fig. 13 G).

The complete results of the multiple washes experiment are attached in the supplementary data.

6.1.2 Data of the DSDDP- 5017-1-A deep core

The most detailed and comprehensive set of data in this study comes from the DSDDP 5017-1-A deep core. The complete table of results is found in the supplementary.

All the results here are presented in concentrations units of milli mol per gram of sediment. The results of the deep core samples are divided into three groups – Bulk, Short, and Long samples. Subtracting from the long samples the amount of residual dissolved ions left from the dissolution period of the short samples, similar to the calculation done on the multiple washes' samples, could not apply in this case due to a lack of weighing of the bottles after the short samples were pumped. By applying this subtraction on the 5017-3-C shallow core and on the marginal samples I can conclude that this operation does not have a remarkable influence on the results of this work (graphs with this correction can be seen in the supplementary data).

In light of this, the definitions of the short and long dissolutions, for all samples, will be the following: (1) The results of the short dissolutions show all the ions that dissolved from the sediments since the time of interaction with the DDW until the short portions were pumped from the bottles (20 to maximum 50 minutes); (2) The results of the long dissolutions show all the ions that dissolved from the sediments since the time of the initial interaction with the DDW until the water were pumped completely, in the following morning, for the long portion. Considering these definitions, the bulk samples represent an intermediate dissolution between the short and the long dissolutions.

The depth-age model used to convert the depth of the deep core samples – soluble salts and Elan Levi's pore fluids samples, to a chronologic age follows Goldstein et al., (2020).

The deepest sample comes from the depth of 199.1 meters below lake floor (mblf) and dated to 98.5 ka BP. The shallowest sample taken from the deep core is 85.7 mblf, and dated to 11.1 ka BP.

Figure 14 (A-F) shows six representative ion ratios that were retrieved from the deep core soluble salts data, plot against pore fluids data from the same section of the core. These graphs will be described here and will be analyzed in detail in the discussion of this chapter and the followings.

Figure 13: Results of the multiple washes experiment. PZ-1 (triangles) and deep core samples (circles) are presented together for each element along the 5 washes. Concentrations in milli mol/g. Previous page: (A) Cl^- (B) Na^+ (C) Mg^{2+} (D) Br^-. This page: (E) K^+ (F) SO_4^{2-} (G) Sr^{2+} (H) Ca^{2+}. Results of NO_3^- in chapter-3 Figure 29.

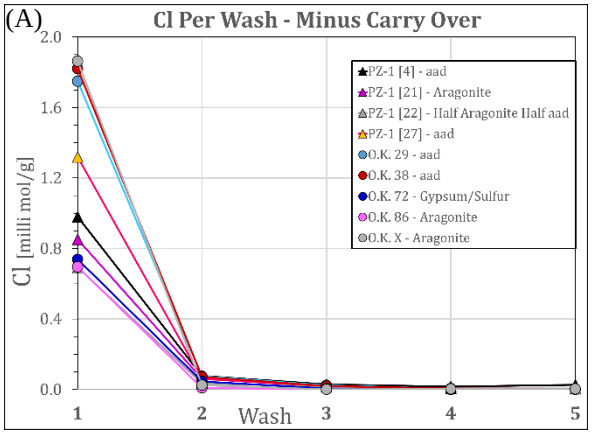

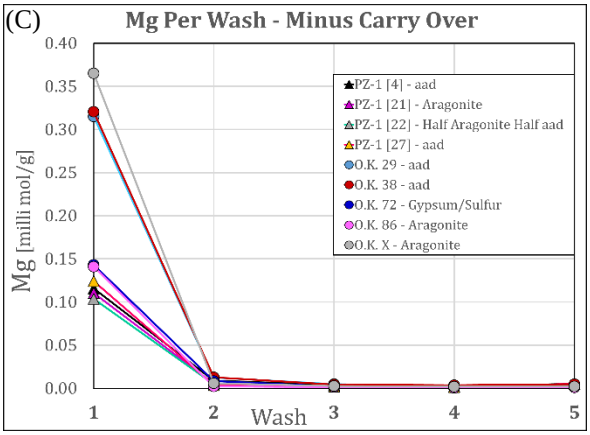

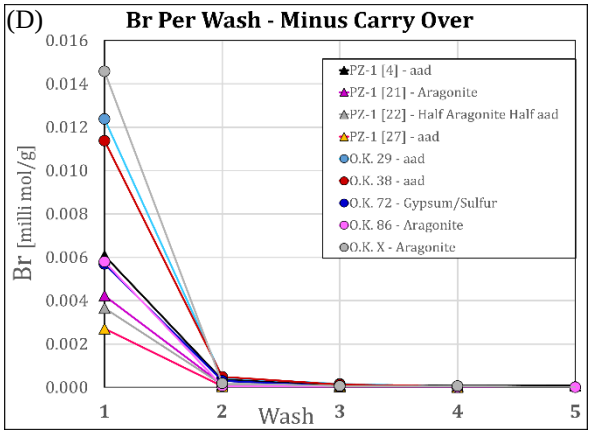

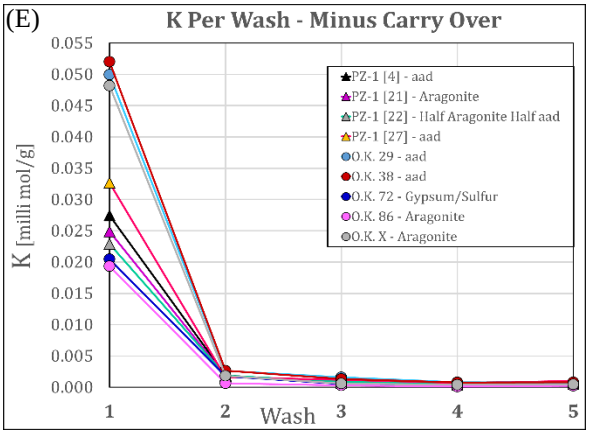

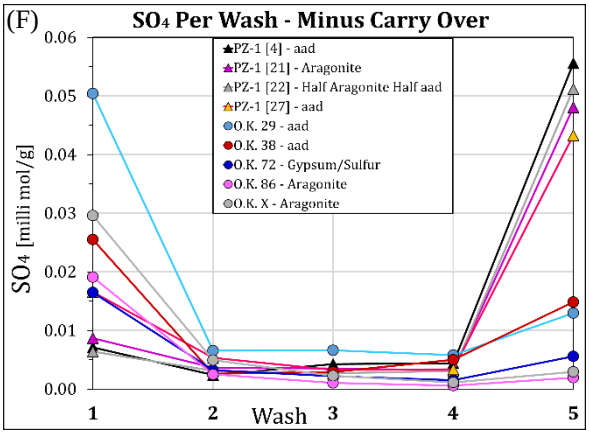

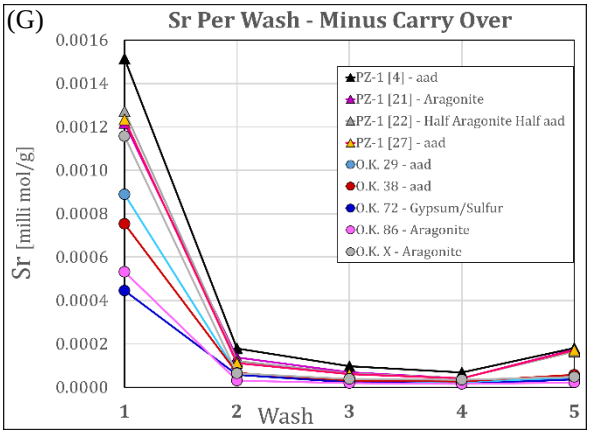

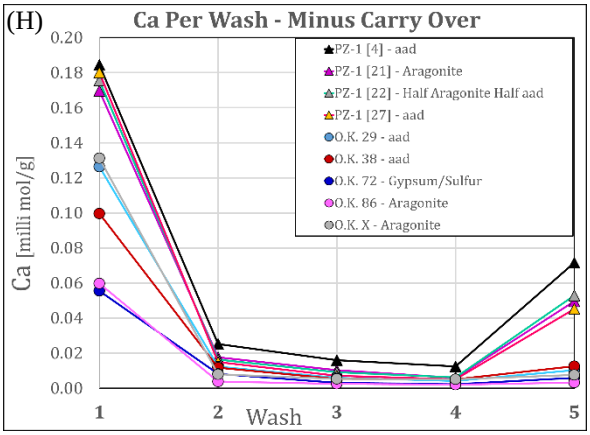

These representative ion ratios reveal three types of ratios. The first type represented here by the $\frac{Na}{Cl}$ (Fig. 14 A) and $\frac{Mg}{Cl}$ (Fig. 14 B) ratios, are ratios that show high correlation to the pore fluids data and there is no significant difference between their short and long results. These ratios are combinations of elements from the first group that shows high solubility in the multiple washes experiment. The second type, represented here by the $\frac{Sr}{Cl}$ (Fig. 14 C) and $\frac{K}{Na}$ (Fig. 14 D), are ratios that display close correlation to the pore fluids, with a similar pattern, but with a constant shift of the soluble salts results higher/lower than the pore fluids results. The short and long ratios of this type are similar as well. These ratios are combinations of ions, one from the first group of the highly soluble ions, such as Cl or Na, and the second from ions that showed an intermediate behavior, with a mild additional dissolution after the second wash, such as K or Sr. The third type, represented here by $\frac{SO_4}{Cl}$ (Fig. 14 E) and $\frac{Sr}{Ca}$ (Fig.14 F), are ratios with low to no-correlation with the pore fluids data and distinct differences between the short and long samples. These ratios include one ion from the group that showed mild dissolution in the 2-4 washes and additional distinct dissolution in the fifth wash, such as the SO_4 and Ca while the second ion is from the highly soluble group. Even more evident are ratios with both ions from the second group, such as $\frac{Sr}{Ca}$ or $\frac{SO_4}{Ca}$.

In Figure 14 (A), both the pore fluids and the soluble salts reveal that 100 ka BP the $\frac{Na}{Cl}$ ratio was as low as 0.3. From there this ratio rose gradually and steadily in a rate of ~0.02 per ten thousand years, without significant fluctuations, until ~35 ka BP. At ~35 to 31.7 ka BP a sharp drop in the ratio (from ~0.47 to ~0.36) is shown by the pore fluids data which is not fully supported by the soluble salts due to a lack of samples in this section. This drop is followed by a rapid rise to a value of ~0.52 at ~30 ka BP. In the next period of ~30-17 ka BP the pore fluids display again a gradual rise, similar to the rise before the sharp drop. The soluble salts data, which is much more detailed here, reveal that the $\frac{Na}{Cl}$ ratio was more dynamic and fluctuated several times between ~0.5 to 0.6. At ~17 ka BP an abrupt rise occurred that last ~5000 years and reached, at its maximum to a $\frac{Na}{Cl}$ value of 0.7-0.72, 12 thousand years ago. This maximum does not last long. Shortly after reaching to its peak the $\frac{Na}{Cl}$ ratio steeply dropped and got down to a value of ~0.48-0.41 at ~11.1 ka BP.

Figure 14 (B) shows that compare to the $\frac{Na}{Cl}$, the $\frac{Mg}{Cl}$ ratio changed along this period of time in a mirror pattern. This ratio variate between its highest values of 0.54, 98.5 ka BP, to its minimum of ~0.18, 12 ka BP, and ends with a sharp rise up to ~0.43-0.47, 11.1 ka BP. A mild difference between the $\frac{Mg}{Cl}$ and $\frac{Na}{Cl}$

that worth mentioning is the stabilization of the $\frac{Mg}{Cl}$ values between ~65 ka BP to 36 ka BP, both in the pore fluids and in the soluble salts data.

In figure 14 (C) the $\frac{Sr}{Cl}$ ratio is presented. The pore fluids value of this ratio at 100 ka BP was ~0.0014. Later on, this ratio moderately variate between ~0.0011 to 0.0015 until ~50 ka BP. Then, it dropped and reached to a value of 0.0006 at 46.1 ka BP and after another similar rise and drop stabilized on low values of 0.0005-0.0008. The final point of the relatively stable low values of the $\frac{Sr}{Cl}$ is at 12 ka BP, with a 0.0005 ratio. This last low value is followed by a rise to a ratio of 0.001. The soluble salts data on the other hand present a picture that is similar in several aspects but also has some distinct differences. The oldest value, at 98.5 ka BP, is also the highest and stands on ~0.0037. The following period, until ~60 ka BP, is characterized with scattered (and sparse) values of ~0.0016 and exceptional higher values of ~0.0022 at ~72 ka BP. At ~55 ka BP until ~45 ka BP the data are scattered although clearly show that several samples in this period have higher values that gets up to ~0.0026, compare to ~0.0018 of the lower samples. Since then, the soluble salts values gradually decline in a rate of ~0.0002 for every ten thousand years. The $\frac{Sr}{Cl}$ values of the soluble salts are steadily higher than the pore fluids values with a common gap of ~0.0001-0.0002. Since ~55 ka BP until the top of this section the gap between the two data sets is reduced. At ~18.2 ka BP the first short samples coincide with the pore fluids samples, and at 12 ka BP the soluble salts data matches the pore fluids data. Another distinct feature of the $\frac{Sr}{Cl}$ results is that the majority of the short samples have lower values than the long and bulk samples.

In the $\frac{K}{Na}$ ratio, presented in figure 14 (D), the results of the pore fluids are highly similar in their pattern to the $\frac{Mg}{Cl}$ pattern, with the same trends and variations. The highest value in the pore fluids data is 0.013, at 100 ka BP. Intermediate value is ~0.05, and the lowest value is ~0.029, at 12 ka BP. The soluble salts' results of the $\frac{K}{Na}$ show some similarities to the soluble salts results of the $\frac{Sr}{Cl}$. The maximum value is, as well, in the oldest sample, 98.5 ka BP, and stands on ~0.14. From there upward there is a period with sparse data, focused around ~0.11 but with scatter. The samples of ~72 ka BP are as well with values of ~0.11 but when compared to the pore fluids data, the gap between the data sets is much more significant and suggests that these values are elevated. Around ~50 ka BP the soluble salts values seem a bit higher than their proximity (~0.075-0.09). From this climax the values decline gradually, with short term exceptions, until they coincide with the pore fluids data at ~18-12 ka BP. This synchronization occurs during a clear period of $\frac{K}{Na}$ decline that reachs its minimum at ~12 ka BP with values of ~0.03-0.035.

Following this decline, the $\frac{K}{Na}$ peaked and reached almost to 0.08 at 11.1 ka BP. When compared to the $\frac{Sr}{Cl}$ graph, the $\frac{K}{Na}$ soluble salts results are closer in their values to the pore fluids data and seems more stable and consistent. It fit the pore fluids trends better and has no clear tendency between the short, long, and bulk samples.

Figure 14 (E) exhibit the $\frac{SO_4}{Cl}$ ratio. In the case of this ratio the highest results of the soluble salts are two orders of magnitude higher than the pore fluids highest results. Therefore, the pore fluids data seems to be zero. When observed with the two data sources, the main feature of this graph is the approximately constant values of the soluble salts that span above the pore fluids data (mean values of ~0.04 in the short, ~0.06 in the long and ~0.08 in the bulk samples). Several times along the section the soluble salts data peak, for relatively short periods, high above their constant values. The most prominent rise occurred between ~55-46 ka BP and reached to a maximum value of 1.1. Additional similar peaks are seen around 98, 72, 22.5 and 11.5 ka BP. The short values are constantly lower than the long values and usually lower than the bulk values. The highest $\frac{SO_4}{Cl}$ value of the pore fluids is 0.0134, at 18.5 ka BP, and the lowest is 0.0017, at 84.1 ka BP. The $\frac{SO_4}{Cl}$ data of the pore fluids is more sparse than other data sets due to lack in SO_4 measurements.

The $\frac{Sr}{Ca}$ ratio is presented in figure 14 (F). The values of this ratio are multiplied by 1000, in all of the $\frac{Sr}{Ca}$ graphs, in order to ease the interpretation and the correlation to previous works that presented this ratio in the context of the Lisan brines. In this case there is also a need to describe the pore fluids in separate from the soluble salts data due to the differences between them. The pore fluids data begins with a $\frac{Sr}{Ca}$ value of ~11.3, 100 ka BP. From there the values moderately fluctuate until ~55 ka BP, with a mean value of ~10.4. From 55 to 46 ka BP a large drop occurred (from ~11.28 to 5.15), and after another similar fluctuation the $\frac{Sr}{Ca}$ stabilized on lower values of ~7.5-5.8 until 17 ka BP. At 17 ka BP the $\frac{Sr}{Ca}$ values rose rapidly and reached to 10.7 at 11.1 ka BP. The soluble salts $\frac{Sr}{Ca}$ data is a bit scattered, but its secular trend is still noticeable. At least five distinct negative peaks are noticed along the section, all of them coincide with the positive peaks of the $\frac{SO_4}{Cl}$ soluble salts' data, at ~98-95, 72, 55-46, 22.5 and 12-11.5 ka BP. The values of these negative peaks reach as low as ~1.5-6. The short values are almost constantly higher than the long values. Bulk values are in between them, except for the negative peaks' episodes. Beside the data points of the negative peaks, along the period of 98.5 to 55 ka BP the data is sparse. Several data points, mostly short and bulk data, coincide with the pore fluids trend. Since 55 ka BP until

the top of the section at 11 ka BP, and apart from the negative peaks, the majority of the short and bulk values are higher than the pore fluids values or coincide with them. Highest values reach to 10-12, and lowest to ~6. The simultaneous long samples show lower values that has a lower gap relative to the pore fluids data or coincide with it (highest values ~10, lowest ~4.2-5). Several scattered samples show lower values than the general trend. The major trends of the pore fluids data in this section can be observed also in the soluble salts' samples.

The presented ion ratios demonstrate the major three types of ratios, that are the result of different combinations of elements. The dissolution properties of each element dictate the behavior of the ratio. The implications of these observations will be analyzed and discussed in this chapter and the followings.

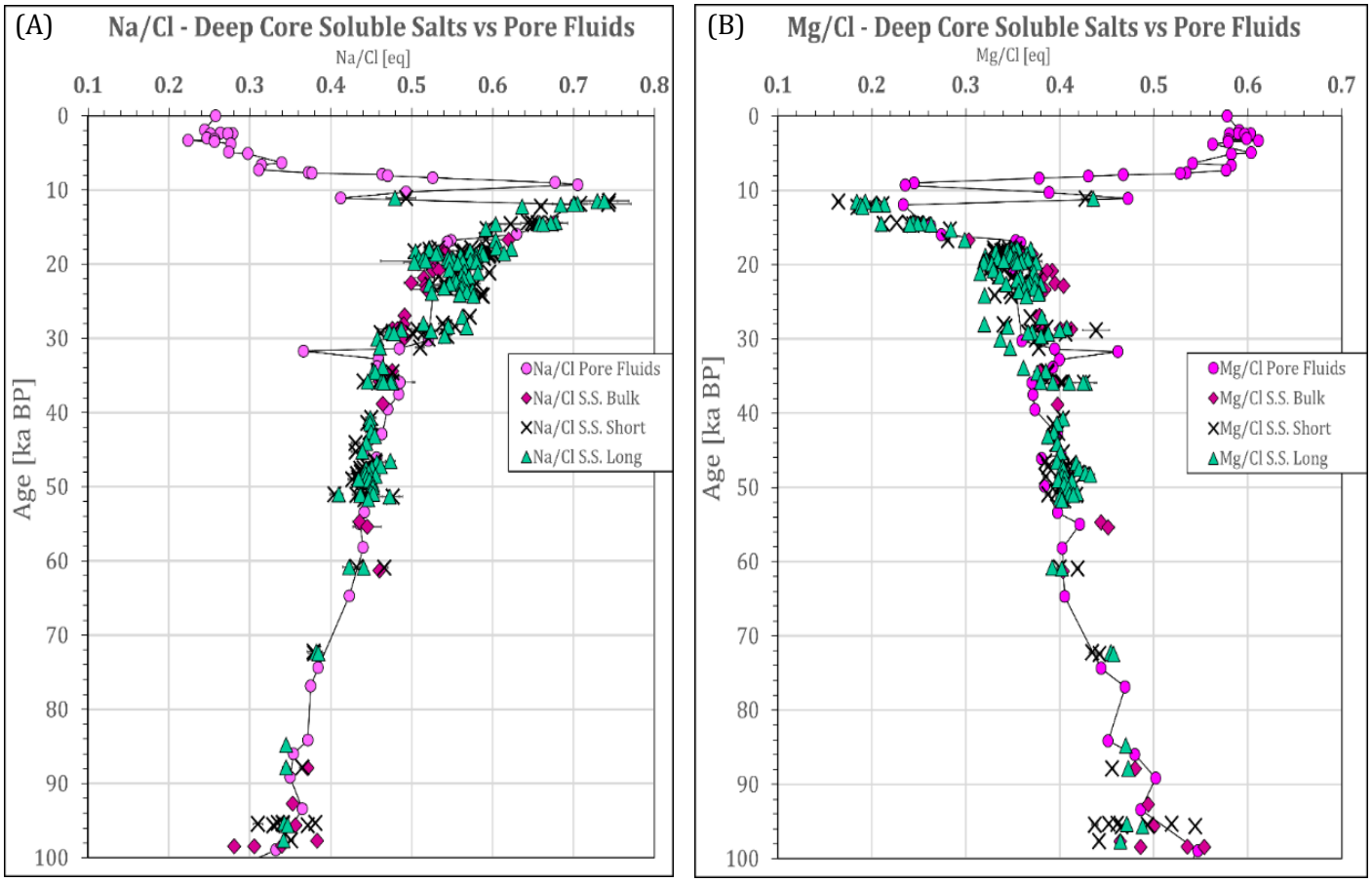

Figure 14: Representative elemental ratios of results that received from 5017-1-A deep core. All ratios are in equivalent. Short, long, and bulk samples are presented against the coeval pore fluids values from the same core, received in Elan Levy's works. (A) $\frac{Na}{Cl}$ & (B) $\frac{Mg}{Cl}$ show the behavior of ratios that compose of highly soluble elements. (C) $\frac{Sr}{Cl}$ & (D) $\frac{K}{Na}$ show the behavior of ratios that include one element that mildly dissolved after the first wash. (E) $\frac{SO_4}{Cl}$ & (F) $\frac{Sr}{Ca}$ show the behavior of ratios with one or two elements that distinctly dissolved after the first wash, mostly in the fifth wash.

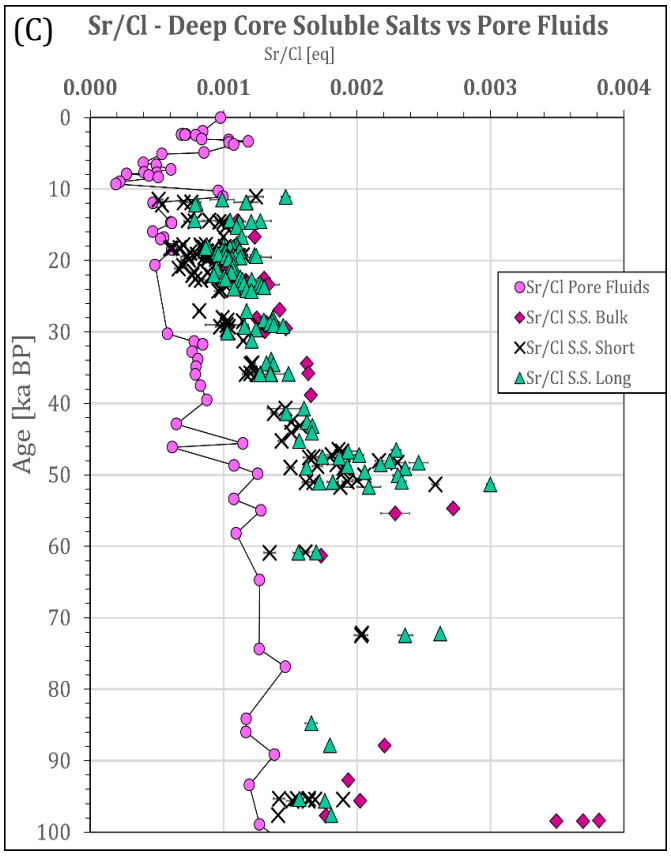
(C)
Sr/Cl - Deep Core Soluble Salts vs Pore Fluids
Sr/Cl [eq]
0.000
0.001
0.002
0.003
0.004
Age [ka BP]
0
10
20
30
40
50
60
70
80
90
100
Sr/Cl Pore Fluids
Sr/Cl S.S. Bulk
Sr/Cl S.S. Short
Sr/Cl S.S. Long

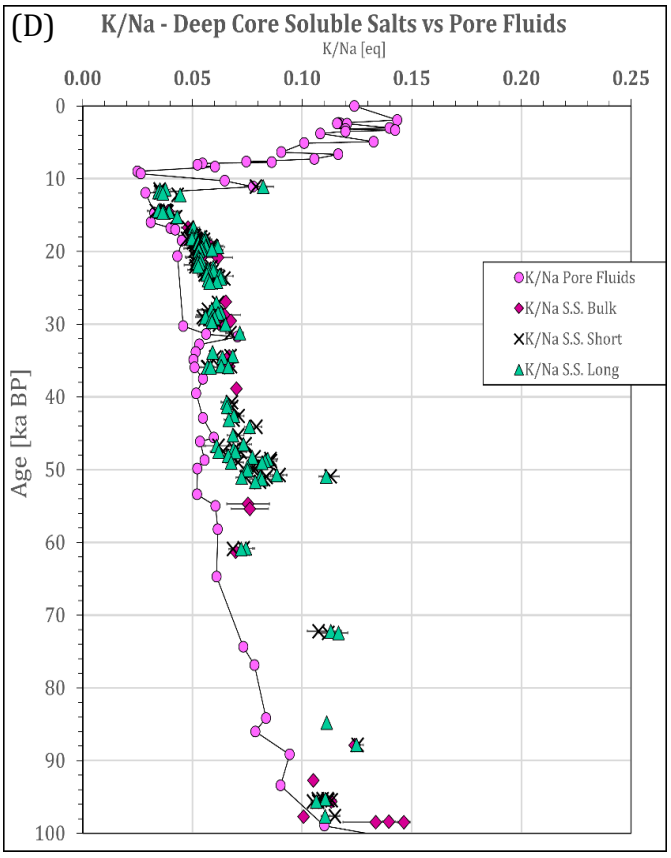
(D)
K/Na - Deep Core Soluble Salts vs Pore Fluids
K/Na [eq]
0.00
0.05
0.10
0.15
0.20
0.25
Age [ka BP]
0
10
20
30
40
50
60
70
80
90
100
K/Na Pore Fluids
K/Na S.S. Bulk
K/Na S.S. Short
K/Na S.S. Long

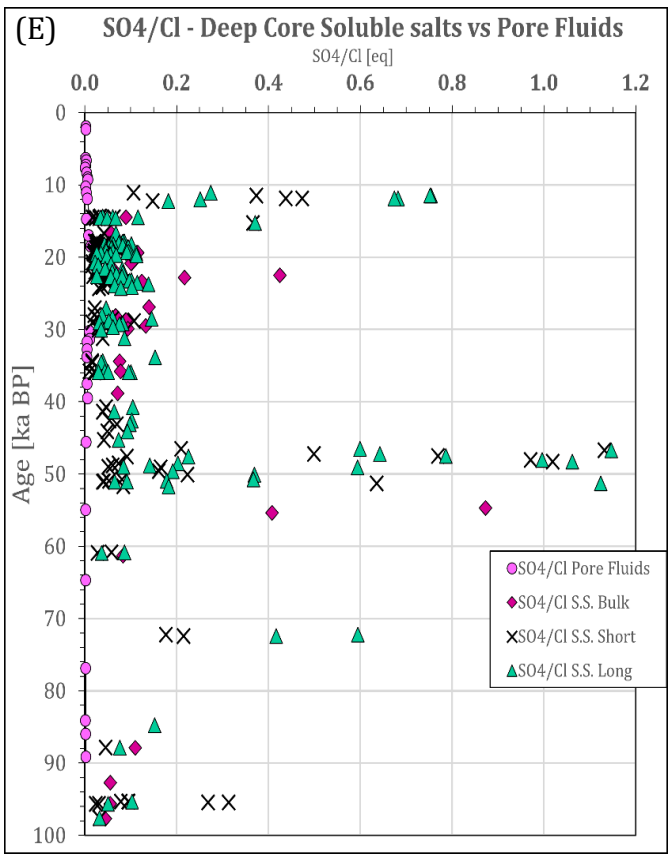
(E)
SO4/Cl - Deep Core Soluble salts vs Pore Fluids
SO4/Cl [eq]
0.0
0.2
0.4
0.6
0.8
1.0
1.2
Age [ka BP]
0
10
20
30
40
50
60
70
80
90
100
SO4/Cl Pore Fluids
SO4/Cl S.S. Bulk
SO4/Cl S.S. Short
SO4/Cl S.S. Long

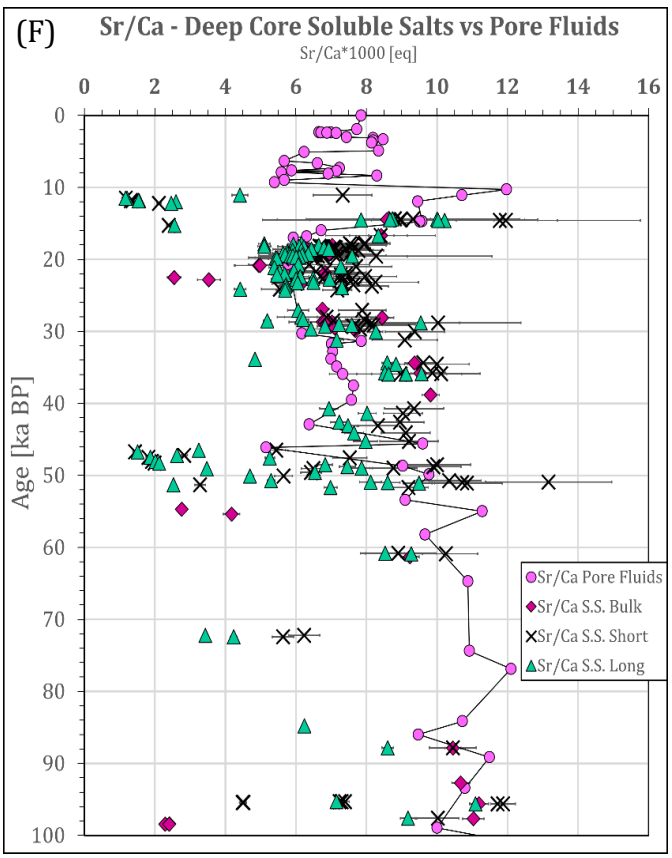
(F)
Sr/Ca - Deep Core Soluble Salts vs Pore Fluids
Sr/Ca*1000 [eq]
0
2
4
6
8
10
12
14
16
Age [ka BP]
0
10
20
30
40
50
60
70
80
90
100
Sr/Ca Pore Fluids
Sr/Ca S.S. Bulk
Sr/Ca S.S. Short
Sr/Ca S.S. Long

6.2. Discussion

6.2.1. Division of the major elements by their dissolution pattern

The two types of elements dissolution observed in the results of the multiple washes experiment divide the major elements into two groups. *The first group of elements* include the Na, Mg, Br, Cl, NO_3 and at first glance, the K as well. Generally, these elements dose not participate in salts precipitation from the lake, especially not during the last glacial. Although, in some cases, they do take part in salts precipitation. These cases include halite precipitation during interglacials, before the onset of the last glacial lake's freshening and at the shift to the Holocene, or as a secondary process, as a consequence of advanced brine desiccation due to diagenetic processes, natural sediments exposure or drilling. In the second case, more advanced salts can form such as carnallite ($KMgCl_3 \cdot 6(H_2O)$), bischofite ($MgCl_2 \cdot 6(H_2O)$), magnesium bromide ($MgBr_2 \cdot 6H_2O$), calcium chloride ($CaCl_2(H_2O)_x$, $x=0,1,2,4,6$) and more (Krumgalz et al., 2002). These salts develop in the interstitial voids of the sediments and not as a sedimentary bed, as would have happen when a salt precipitate from the lake. In addition, these salts are highly to extremely soluble and hence dissolve quickly and easily when interact with freshwater. The elements of this group considered as conservative elements since they do not take part in salts precipitation occurred in the lake and hence their concentration in the brine depends on dilution or concentration processes that take place in the lake (Na and Cl do participate in halite precipitation and dissolution). The quick and terminate dissolution of these elements in the first and second wash suggest that these elements originate from dissolution of highly soluble salts, as those mentioned. The lake apparently did not reach saturation levels of these salts at the periods represented by the samples of this work. This can be concluded from their absence as layers in the sediments, the sediments record of the Dead Sea and its precursors, XRF data of the deep core, several XRD measurements and previous works that present the conservative behavior of these elements in the lake's brine (Levi et al., 2017, 2018, 2019, Lazar et al., 2014). In the scope of Elan Levi's works the degree of saturation of several salts in pore fluids that extracted from the deep core sediments were calculated. These examinations revealed that these fluids that represent the deepest brine of the lake did not reached saturation of the advanced salts, while maximum saturation of halite was found. It can be concluded that the source of these elements is dissolution of interstitial salts crystals that have developed in the sediments as a secondary process, later to the sedimentation and pore fluids extraction from the sediments. These salts could have crystalized from the interstitial brine due to a natural diagenetic process or after the sediments were naturally exposed to the atmosphere, in the case of the marginal terraces, or artificially, in the case of the DSDDP cores. Another source for these elements can be the remnants of the brine itself that washed from the

interstitial voids of the sediments during the process of the procedure. In light of that, the elements of this group seem to reliably represent the composition of the interstitial brine, which they originated from, and hence also the composition of the local brine of the lake. A robust approval for this conclusion is the good accordance between the pore fluids and soluble salts data of the ion ratios from this group, such as $\frac{Na}{Cl}, \frac{Mg}{Cl}, \frac{Br}{Cl}$.

The second group of elements include the Ca, SO_4, and Sr. Ca and SO_4 are the main elements that constitute gypsum (and anhydrite). Ca and CO_3 (bicarbonate has a dissolution pattern of its own) are the main elements that compose aragonite (and other calcium-carbonate minerals). Strontium tends to replace calcium both in aragonite and gypsum crystals, though it is more common in aragonite (with distribution coefficient of 1 between the brine and the aragonite crystals. Katz et al., 1977). Aragonite and gypsum used to precipitate from the lake, and they are common salts in the Lisan Fm. and in the Dead Sea sediments in general. In addition, SO_4 and Sr (and bicarbonate) reach to the lake with freshwater. In light of that, the concentration of these ions relies on the precipitation-dissolution and dilution-concentration processes that occurred in the lake. Furthermore, since the aragonite and gypsum precipitated from the lake as solid salts, their solid laminae will be subjected to dissolution during the soluble salts procedure but will not be include in the extracted solutions of the pore fluids procedure. The gypsum and aragonite are much less soluble than the salts mentioned in the context of the first group. The aragonite, which is the first salt that precipitates from the lake, is the least soluble salt in the series (Browman and Hastings, 1937; Morse et al., 1980), and gypsum, which is an intermediate salt, has also an intermediate solubility (Katz et al., 1981). The dissolution pattern of the elements of this group in the multiple washes experiment (Fig. 13 F & H) suggests that the first wash may dissolve some gypsum, but the majority of the dissolved ions in this wash has originated from soluble salts dissolution and from remnants of Ca-chloride brine that washed from the sediments. Figure 15 A clearly shows a great surplus of Ca over SO_4 in the first wash while the values are far from fitting the 1:1 line that represents gypsum dissolution. Figure 15 B shows the same observation but for aragonite dissolution. The second wash shows a remnant of this pattern with much lower concentrations (with one sample peaks). This surplus of Ca in the first and second washes reinforces the idea that the first and second washes dissolve mostly soluble salts and remnants of Ca-chloride brine. Washes 2-4 in figure 13 F & H show that the dissolution of Ca and SO_4 remain stable above zero or moderately declined along these washes (Sr dissolution shows the same pattern). Figure 15 A reveals that the values of these washes do converge towards the 1:1 line of gypsum dissolution (with mild Ca surplus in wash 2), and hence suggest that gypsum dissolved in these washes in small amounts. In the fifth wash though, the concentrations of Ca and SO_4 rise in most

samples and fit well on the 1:1 line of gypsum dissolution. In this wash it is clear that an enhanced dissolution of gypsum occurred. Figure 15 B does not show a clear pattern of aragonite dissolution along the washes. Aragonite probably did dissolve in small amounts, at least in the advanced washes, but this graph shows that these dissolutions were not significant. It is important to emphasis that the distinct increase in the amounts of Ca, Sr and SO_4 dissolutions in the fifth wash are also due to the loner water-sediments interaction time of the fifth wash that last ~15-20 hours and included the shaking of the bottles on shaking table for 12 hours, compare to the ~1-1.5 hours and without shaking table of the 2-4 washes. The differences in the dissolutions of Ca and Sr compare to SO_4 between the PZ-1 and deep core samples suggest that SO_4 ions are more accessible in the deep core sediments than in the marginal terraces and dissolve easier from these sediments. The cause for this difference can be that the deep core sediments are not fully dry and therefore some amount of SO_4 is still present as dissolved ions in the interstitial brine instead of as solid crystals. The sediments of the marginal terraces on the other hand, have been exposed to the atmosphere thousands of years ago and the brine in their pores desiccated completely. The SO_4 ions from the brine of these sediments were crystalized as gypsum and hence they are less accessible for quick dissolution as the first wash. The fifth wash support this hypothesis with the higher rates of dissolution in the marginal terraces samples. This observation suggests that during the long water-sediment interaction of the fifth wash the gypsum crystals dissolved from the sediments of the marginal terraces.

Additional source for dissolved SO_4, that settle with the observations so far, is sulfur that oxidized and transformed into gypsum. Sulfur, in its primary form is scattered along the deep core sediments, and its concretions can be easily identified due to their distinct yellow color. These concretions were formed under the anoxic conditions in the deep brine, where sulfur could not precipitate as gypsum (Torfstein et al., 2005, 2008). After the exposure of the marginal sediments to the atmosphere, some portion of the primary sulfur was transformed into gypsum, given the available oxygen in the air. This process could occur in the DSDDP cores as well, but in much restrict extent due to their recent exposure and meticulous preservation conditions. Sulfur is insoluble in water and therefor as long as it exists in the sediments, as in the deep core sediments, it will not release SO_4 into the solution. After some portion of it transformed into gypsum, as in the marginal terraces' sediments, this gypsum can potentially dissolve and release SO_4 and Ca into the dissolving solution. The higher concentrations of SO_4 that observed in PZ-1 samples, compare to the deep core samples can also be explained by this process.

The Ca and Sr dissolution patterns reveal that the amount of these elements that will dissolve in a short dissolution is greater in the marginal terraces than in the deep core.

It was shown before that the majority of these elements originate in the first wash from soluble salts dissolution and brine remnants.

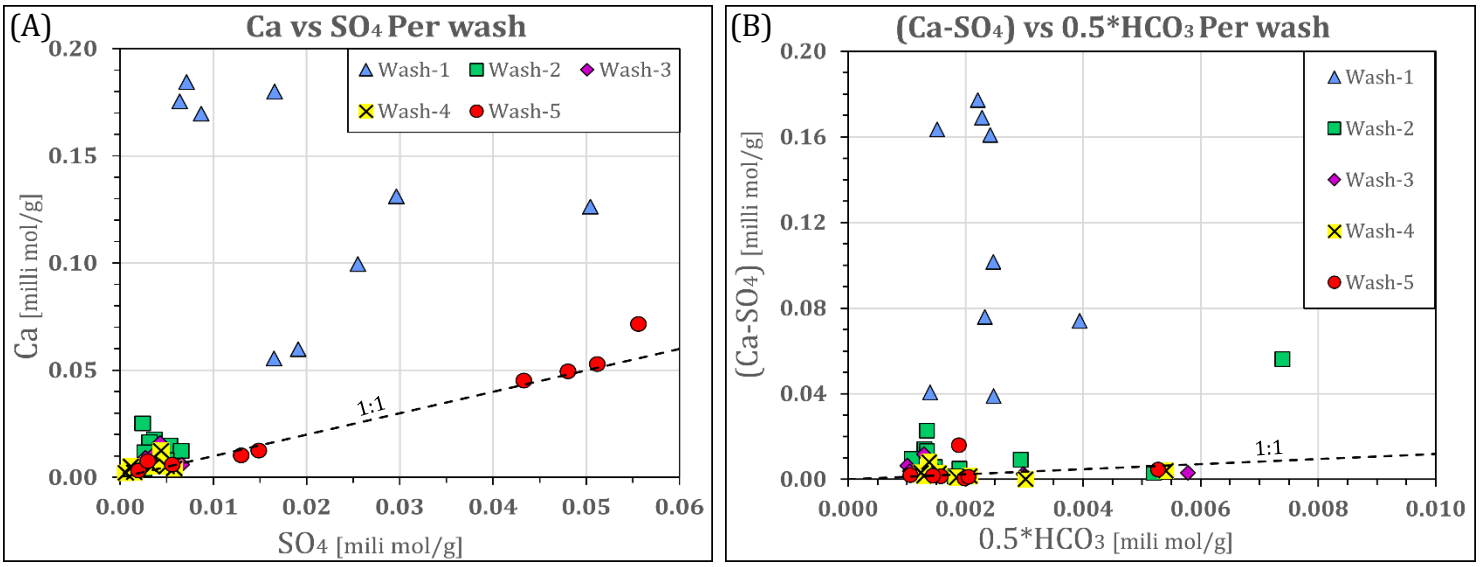

Figure 15: (A) Ca vs SO_4 concentrations (in mmol per gram of sediment) of each sample, divided into the 5 washes. The 1:1 dashed line represents gypsum dissolution. (B) Ca minus SO_4 vs 0.5*HCO_3 concentrations (in mmol per gram of sediment) of each sample, divided into the 5 washes. The 1:1 dashed line represents $CaCO_3$ dissolution.

6.2.2. Potassium and sulfate surplus

Potassium shows a mild dissolution in the third wash. This observation alone would not arouse suspicion. Yet, a surplus is observed in the soluble salts' K ratios with highly soluble elements such as $\frac{K}{Cl}$, $\frac{K}{Mg}$ and $\frac{K}{Na}$ in the deep core compare to the pore fluids. Together, these observations suggest that a mild enrichment of K occurred in the soluble salts' samples. The source of this enrichment is not certain but can by reasonably speculated.

One reason for the surplus of the K in the soluble salts data can be the existence of a potash soluble salt in the sediments, in its solid crystal form. Such crystals would miss by the pore fluids procedure since this method covers only the information that comes from the remnant of fluid brine; however, they will dissolve in the soluble salts procedure and will include in its results. It also has to exist in low concentrations since it was not identified so far in the sediment's sections of this work and since its influence in the dissolution procedure is not significant.

Two main potash salt candidates that may present as solid crystals in the sediments and donate K while dissolved are suggested here.

One candidate is the sulfate salt polyhalite ($K_2Ca_2Mg(SO_4)_4{\cdot}2(H_2O)$). The formation of this salt was suggested to occur as a secondary process (Li et al., 2020) and its dissolution was described to be

differential with the K and Mg ions dissolve first and more easily while the SO_4 and Ca components are less soluble and require additional advanced dissolution (Barbier, 2017; Yermiyahu, U., I. Zipori, C. Omer, 2019). Polyhalite was described to be part of the sulfate minerals that compose the Sedom Fm. and was observed in association with precipitation of anhydrite. In several cases, it is abundant enough to be identified by eye (García-Veigas et al., 2009; Charrach, 2018, 2020). However, polyhalite was never identified in the Lisan sediments, not even in small amounts. Eight XRD measurements done on the deep core samples, in the frame of this work, did not recognize polyhalite as part of the mineralogical assembly. It can still be that this salt exist in concentrations that are lower than the detection limit of the XRD. A careful conclusion will be that the polyhalite may present in the sediments and donate some K during the soluble salts' dissolutions, but it is very scarce and probably not the only source for the K surplus.

Another potash salt that could be the source for some K in the soluble salts' solutions is carnallite ($KMgCl_3 \cdot 6(H_2O)$). The precipitation of this salt from the Dead Sea brine was documented in experiments (Krumgalz et al., 2002) and it is well familiar from the evaporation ponds of the Dead Sea Works. This salt is the first to precipitate after halite, when the enrichment factor gets to ~2 relative to the modern Dead Sea and the water activity gets to ~0.5, at 25°C (in experimental conditions).

The salinity of Lake Lisan hypolimnion was suggested to be ~70% of the modern Dead Sea salinity (in terms of Cl concentrations. Lazar et al., 2014). It could be that diagenetic processes concentrate the pores brine, most likely by desiccation, until some carnallite crystalized in the interstitial pores. In this case it is required that the carnallite crystallization occurred before the drilling, or at least before the pore fluids were extracted from the sediments. Being known in the Dead Sea system and abundant in the evaporation ponds, make the carnallite a more reasonable candidate as a K source.

However, Levy et al., (2017) mentioned that pore fluids that were extracted from the deep core sediments were found to be undersaturated with respect to carnallite ($\Omega_{Carnallite} < 1$). This observation reduces the probability of carnallite to present as solid crystals in the sediments.

If indeed carnallite crystalized in the sediments' pores as a secondary process, the previous salts in the series should have to crystalize in the pores as well, mainly gypsum and halite.

When examining the results of the soluble salts and the pore fluids from the deep core a supportive observation is seen for the crystallization of such salts.

A similarity is seen between the values of K ratios with conservative elements, such as $\frac{K}{Na}, \frac{K}{Cl}, \frac{K}{Mg}$ to the values of SO_4 ratios with conservative elements, such as $\frac{SO_4}{Na}, \frac{SO_4}{Cl}, \frac{SO_4}{Mg}$ (Fig. 14). These ratios resemble in their consistent higher values in the soluble salts data compare to the pore fluids data. Furthermore, the

soluble salts' data shows several restrict periods, synchronized between the ratios, in which the data peaks into much higher values. The most prominent synchronized peaks along the section appear at ~72 ka BP, ~51 ka BP and ~11.5-14.5 ka BP. These peaks show values that are clearly higher than the pore fluids values, but also distinctively higher than the rest of the soluble salts data. The values of the soluble salts that are constantly higher than the pore fluids values, in both sets of ratios, support the presence of solid minerals of SO_4 and K in the sediments, that crystalized before the extraction of the pore fluids. The mineral that donates the great majority of the SO_4 during dissolutions is most likely gypsum.

Three types of gypsum appearances were described in the Lisan Fm. (Torfstein et al., 2005, 2008): massive or laminated gypsum, which gets up to several tenth' of cm thick, thin laminae of gypsum, several mm thick, and disseminated crystals of gypsum. Mechanisms for the presence of the disseminated crystals were suggested in several previous works (e.g., Stein et al., 1997; Torfstein et al., 2008), although it seems that the vast majority of them developed in the pores out of the drying interstitial brine. Gypsum laminae (thick or thin) present occasionally along the section, whereas the SO_4 ratios reveal a constant SO_4 surplus all along the section. It can be concluded that the source of the consistent gypsum excess is the disseminated gypsum crystals that were crystalized before the extraction of the pore fluids. Since K ratios show a similar pattern, its excess can be contributed to small amounts of disseminated potash mineral that as well crystalized in the sediments prior to the pore fluids extraction. The most reasonable mineral that donates the K is seems to be carnallite. Both gypsum and carnallite can present in small amounts but still have a notable influence on the SO_4 and K ratios since the concentrations of these ions in the Ca-chloride brines and in the soluble salts' solutions are low. Hence, every addition of these elements will reflect in their ratios, especially when the other element in the ratio is abundant in the brine, such as Cl, Mg, Na, and Ca.

The K surplus can be addressed by additional mechanism, which is the mild release of K from clays (that are a component in the detrital laminae) in the sediment-water interactions. This mechanism was addressed in several previous works (e.g., Feigenbaum and Shainberg, 1975; Jalali, 2006; Li et al., 2015) that showed how small amounts of non-exchangeable potassium can release from the interlayer sites in clays such as illite, smectite and kaolinite.

Several conditions along the soluble salts' procedure (solution composition, temperature) support K release from the clays in the samples. The time factor though, seems to be the restrict element for K adsorption from clays. These clays were precipitated from the lake and had plenty of time to interact with the brine and exchange the K from the interlayer sites (with sedimentation rates of ~0.5-1.5 mm per year the sediments were subjected to interactions with the brine at least for several years before they

were buried and isolated from the brine). In addition, the time of interaction between the water and the sediments in the soluble salts' procedure (~1hour to 1 day) is short relative to the periods of interaction that reported in the mentioned works (~10-20 days) and hence was not adequate for significant K adsorption from the clays.

Nevertheless, as a primary conclusion, it seems that K adsorption from clays occurred simultaneously with the dissolution of small amounts of carnallite (or other potash salt). Additional mechanism that was not suggested here may donate small amounts of K to the solution.

6.3. Summary

This chapter deals with the validation of the soluble salts method and gets into the details of the processes that occur during the extraction of the soluble salts by the water rinses. The main results and conclusions of this chapter are:

1. Na, Mg, Cl, Br and NO_3 dissolved mainly in the first wash of the multiple washes experiment, with a small remnant in the second wash and minor to zero dissolution in the following washes. Ratios of these elements (except NO_3) along the deep core section of the last glacial exhibit great correlation to coeval data of pore fluids from the same core. These observations suggest that these elements originate mainly from dissolution of interstitial soluble salts and washes of brine remnants from the pores. The ratios of these elements (in sediments that did not expose and desiccate) are reliable and can serve as accurate tools for reconstruction of brine chemistry in the lake.
2. Ca, Sr and SO_4 showed two main phases of dissolution, in the first and fifth washes, with mild dissolution in between. Ratios with one or two of these elements showed constant or disordered higher/lower values of soluble salts compare to pore fluids data of the deep core. These observations are attributed to some amount of primary gypsum dissolution in the rinses and milder dissolution of $CaCO_3$ (mostly aragonite) which added Ca, SO_4 and Sr ions to the solution that did not include in the method of the pore fluids. These ions can originate from minerals that precipitate originally from the lake or disseminated crystals that developed in the pores from the drying brine. Corrections are required on these ratios before they are used for reconstructions of brine chemistry in the lake (these corrections are discussed in chapter-3).
3. K dissolution pattern is similar to the highly soluble group, but its deep core data reveals a constant surplus of this ion in the rinses. This surplus is suggested to originate from dissolution of potash soluble salts that developed in the pores from the drying brine, most likely carnallite, and by adsorption of K from clays during the sediments-water interactions.

7. Spatial and temporal variations in the chemical compositions of Lake Lisan brines from highly soluble ions

In this chapter the data sets of the soluble salts from the deep, shallow and marginal elevations in the lake are compared along chronological lines. This comparison enables the investigation of each data set separately and provides insights on simultaneous processes that occurred in the various limnological setting: the epilimnion, hypolimnion and lake's marginal areas. This chapter uses only the data of the highly soluble group (Na, Mg, Br, Cl) which requires no corrections for potential dissolution of primary phases and thus reliably monitors the brine composition and its evolution.

7.1. Results

Results of the deep core that are required for the discussion of this chapter are presented in the previous chapter. These results include ratios of the highly soluble elements, such as $\frac{Na}{Cl}, \frac{Br}{Cl}, \frac{Mg}{Cl}$ ($\frac{Br}{Cl}$ results of the deep core are presented in this chapter in Fig. 20 C). Additional results of highly soluble elements are given here from the shallow core and the marginal terraces.

7.1.1. Data from the DSDDP 5017-3-C Shallow Core

The chronology of 5017-3-C core is based on stratigraphic correlation to 5017-1-A core, using lithological and geophysical properties (Coianiz et al., 2019). Using these lines of correlation as "anchor ages", I applied a linear interpolation constructing a depth-age model for this core (Fig. 16).

The deepest sample taken for the current study from the 5017-3-C core is from 298.39 meters below lakes floor and it is dated to ~143.4 ka BP. The shallowest sample taken from the shallow core is from 58.51 meters below core's top.

The age of this sample is largely relying on the defined age of the Lisan Fm. - Zeelim Fm. boundary, due to the linear interpolation method. The age for this transition at 5017-1-A core lies at 11.44$\pm$1.2 ka BP (Kitagawa et al., 2017). When this age is considered together with its error the linear interpolation method provide an age for the shallowest sample of 5017-3-C core (~11.1-11.3 ka BP) that shows a good fit with the data of the pore fluids from the deep core (Fig. 17 A-C).

According to this chronology, the time frame that covered by the samples of the 5017-3-C shallow core include the final spell of the penultimate glacial (Lake Amora period, MIS 6), the last interglacial (Lake Samra period, MIS 5), the last glacial (Lake Lisan period, MIS 4-2) and the transition to the Holocene.

Note that the chronology of the 5017-3-C shallow core that suggested here is general and should be taken with a grain of salt. It does not intend to provide accurate ages for the samples but rather time frames that will be sufficient for the correlation. It is likely that future dating of these sediments in radioactive methods will provide more accurate ages although I presume that the suggested chronology is quite accurate and sufficient for the use of this work.

Figure 17 A-C presents several representative ion ratios that received from the shallow core data. The data is compared with coeval pore fluids data from the deep core.

The $\frac{Na}{Cl}$ values of the short and long samples are identical or very close (Fig. 17 A). At ~143.4 ka BP the $\frac{Na}{Cl}$ ratio is well correlated with the deep core pore fluids value of ~0.47. This correlation prevails for several thousand years, until ~127 ka BP. During this period, the $\frac{Na}{Cl}$ ratio is relatively high and fluctuate between ~0.41-0.57. At 127 ka BP the $\frac{Na}{Cl}$ ratio is still high (~0.45), but a sharp decline has already begun in the pore fluids of the deep core, heading for a prominent minimum of ~0.19 at 119-116 ka BP. The shallow core's soluble salts however remain high, and even rose a bit to ~0.53 at 113.4 ka BP, at least until ~82.4 ka BP, as can be seen from the data. While the $\frac{Na}{Cl}$ of the pore fluids gradually rose back to higher values of ~0.46-0.52, the $\frac{Na}{Cl}$ values of the shallow core slightly declined to ~0.42-0.45 and shift to be lower than the deep core values. The sharp rise in the pore fluids' $\frac{Na}{Cl}$ that began ~20 ka ago is not supported by any shallow core sample. This rise reached to a peak of 0.7 at 12 ka BP and was followed by a very sharp, short term, drop to ~0.41 value, at ~11.1 ka BP. This drop is evident in the shallow core by three samples that show low values of ~0.28-0.3 at the equivalent time.

Figure 17 B is showing that the mirror pattern that seen in the $\frac{Mg}{Cl}$ ratio compare to the $\frac{Na}{Cl}$ values, in the deep core results, is seen in the shallow core data as well. Short and long samples also show close values as in the $\frac{Na}{Cl}$. High correlation is observed during the period of ~143.4-127 ka BP, while the $\frac{Mg}{Cl}$ values are relatively low (~0.34-0.42). Then the pore fluids values rise up to a value of 0.63 while the shallow core values stay low (~0.34-0.43). While the pore fluids values gradually declined back to ~0.4-0.35 the shallow core values mildly rose to ~0.45 and become higher than the pore fluids values. At ~11.1 ka BP three samples of the shallow core with values of ~0.56-0.59 fit to a sharp rise in the $\frac{Mg}{Cl}$ values that observed as well in the pore fluids, right after reaching to a negative peak of 0.23 at 12 ka BP.

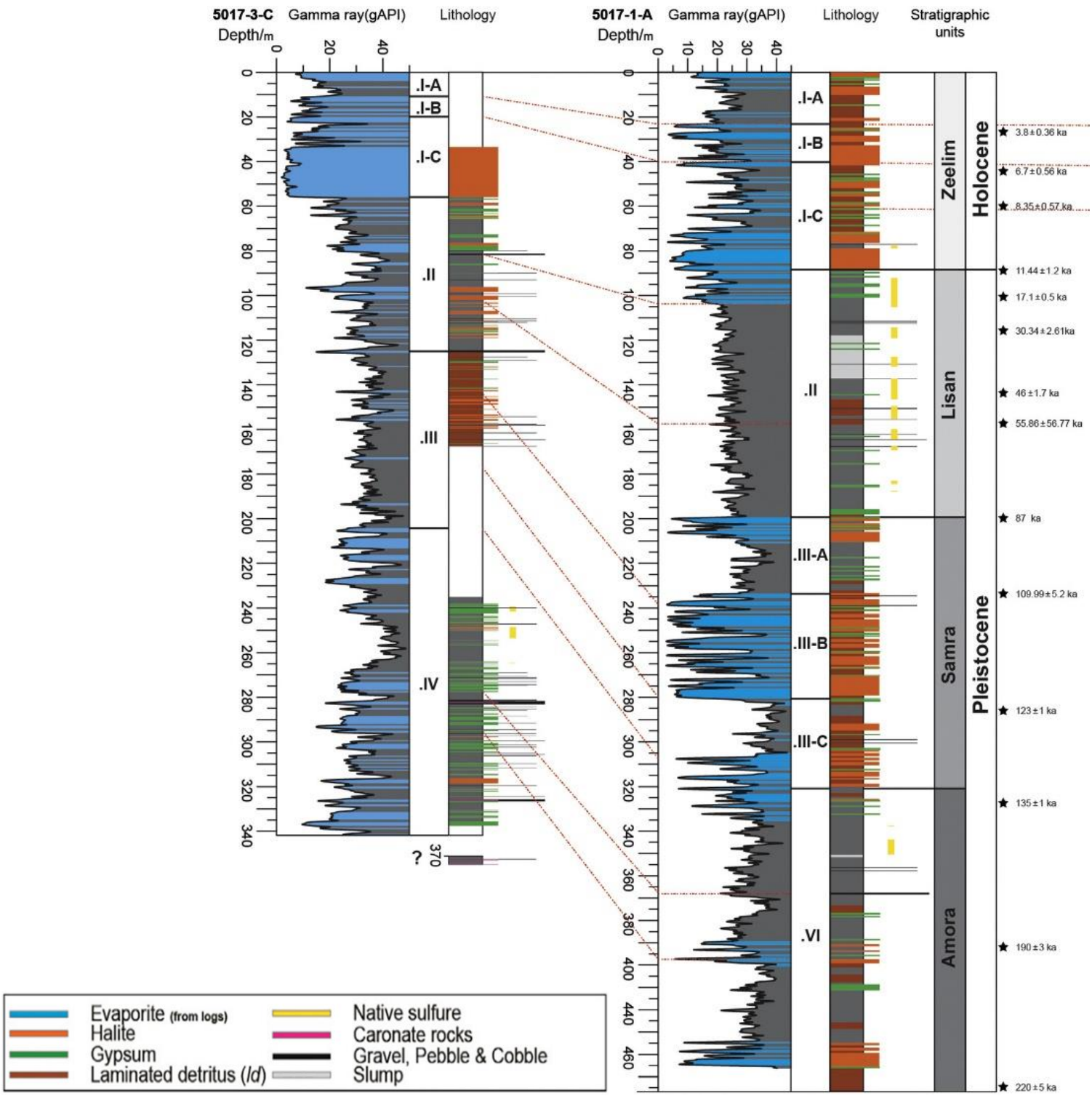

Figure 16: Correlation between 5017-1-A deep core to 5017-3-C shallow core conducted by Coianiz et al. 2019. The chronology is based on distinct lithologies and geophysical properties. Well correlated layers get their age from the chronology of the deep core and serve as anchor ages for the depth-are model of the shallow core.

Figure 17 C presents the $\frac{Br}{Cl}$ ratio. Note that the error bars here are more significant than previous ratios, due to the higher standard deviation of the Br (relative to its concentrations). This ratio dispalys a highly similar pattern as the $\frac{Mg}{Cl}$ although with values ranging between ~0.0046-0.0123, both in the pore fluids and the soluble salts and with a similar fit between them. Short and long values are correlated, within their range of error.

During ~145-127 ka BP the $\frac{Br}{Cl}$ values of the shallow core range between ~0.006-0.01 and show a good correlation with the pore fluids data. Later on, at ~117.3-113.8 ka BP the values of the shallow core remain the same (~0.006-0.009) while the pore fluids peaks high up to ~0.01-0.012.

After this high peak, between ~100-20 ka BP, the pore fluids gradually dropped back to values in the range of ~0.006-0.009 while the shallow core data slightly rose to values of ~0.008-0.009, that are higher than the pore fluids data. Between 20-12 ka BP the pore fluids values dropped to a negative peak of ~0.0055 which was followed by an immediate sharp rise to ~0.009 at ~11 ka BP. There are no shallow core samples from the period of the negative peak to support/refute it but the high rise of 11 ka BP correlates well with 3 shallow core samples with similar values.

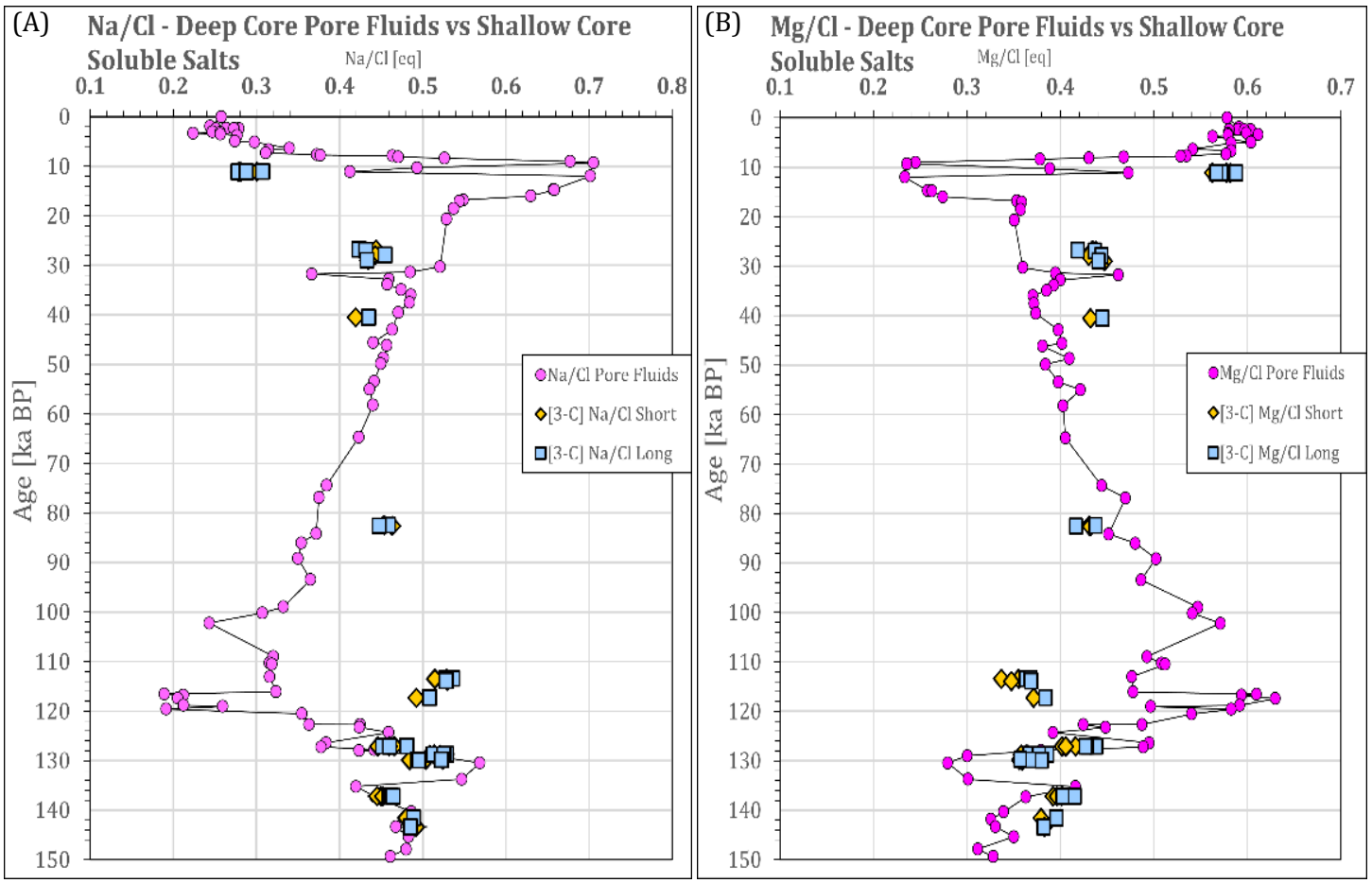

Figure 17: Ion ratios that received from the soluble salts data of the 5017-3-C shallow core. All ratios compose of elements from the highly soluble group. Results are plot together with coeval pore fluids data from the 5017-1-A deep core. Three representative ratios are presented: (A) $\frac{Na}{Cl}$, (B) $\frac{Mg}{Cl}$, (C) $\frac{Br}{Cl}$. All ratios are in equivalent.

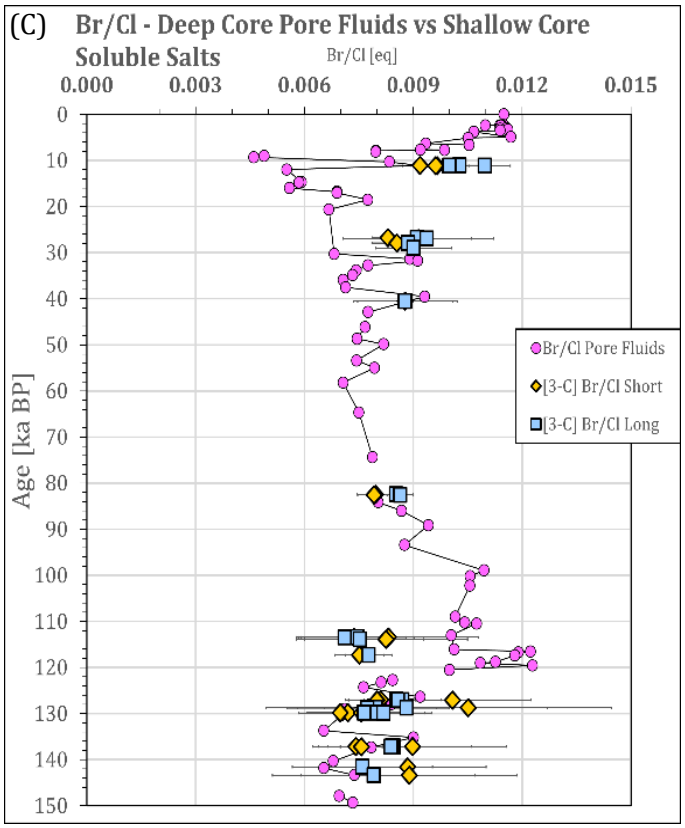

7.1.2. Marginal terraces results of PZ-1 and Mt. Sedom White Hill

The three data sections of PZ-1 roughly correlate with the timing of the three members that were defined for the Lisan Fm. by Machlus, (1996), But not precisely. According to the chronology of Haase-Schramm et al., (2004) the Lower Member of the Lisan Fm. correlates with MIS 4 and spans from ~70-58.7 ka BP while the lower section of samples spans from 60.4 to 51.3 ka BP and include the initial part of the Middle Member. The Middle Member correlates with MIS 3 and spans from ~58.7-31 ka BP while the middle section of samples spans from 43.1 to 30.2 ka BP. The Upper Member correlates with MIS 2 and spans from ~31-14 ka BP while the upper section of samples spans from 25.6 to 21.7 ka BP. Therefore, the three sections of samples from PZ-1 will be referred in this work as the lower, middle and upper sections rather than members.

The oldest sample achieved from Mt. Sedom White Hill section is ~36 ka old and the youngest is ~24 ka old, so this section covers a period that correlates with the upper half of the middle section up to the middle of the upper section.

Figure 18 A-C present soluble salts results of several ratios from PZ-1 and Mt. Sedom White Hill sections. The PZ-1 values are presented as moving averages between each two following samples. Two gaps between data points are observed in the graphs. The gap between the lower to the middle sections

reflect a real hiatus in PZ-1 section (first found by Haase-Schramm et al., 2004). The gap between the middle and the upper sections is due to a deficiency in samples along the section of 2740 to 3004.5 cm. Another section of the PZ-1 outcrop is missing at its top since the highest sample comes from 33.4 m while the complete outcrop is ~40 m tall.

Few short samples of the PZ-1 upper section show increased error range. This is due to exceptionally low concentrations of Br, Na and Mg in these samples.

Figure 18 (A) shows the $\frac{Na}{Cl}$ values that received from the PZ-1 and Mt. Sedom sections. The $\frac{Na}{Cl}$ short and long values in these sections are highly similar. When the Long values are not identical to the short values, they are slightly higher than them. All $\frac{Na}{Cl}$ values variate frequently along the section, rising and declining often, ranging within a large range of values from ~0.068 to 0.9.

In the lower section, 60.4-51.3 ka BP, the $\frac{Na}{Cl}$ values variate between 0.468 to 0.837. The data in this section is constantly higher than the deep and shallow data, it seems the most stable and with the steadiest development among the three sections. The middle section, 43.1 to 30.2 ka BP, is the noisiest with values that frequently variate in the largest range of 0.068 to 0.935. This section also show a mean value that is lower than the mean values of the lower and upper sections. The Mt. Sedom samples in this section fit well to the coeval samples of PZ-1. In the upper section, 26.5-21.7 ka BP, the PZ-1 data as well show short-term variations in the range of 0.337 to 0.8. Although here a general mean trend of rising values seems to occur along the period. Mt. Sedom samples in this section have values that are slightly higher or correlate with the highest values of PZ-1. The marginal data of the middle and upper sections variate below and above the deep and shallow cores coeval values.

Figure 18 (B) present the $\frac{Br}{Cl}$ values that received from the PZ-1 and Mt. Sedom sections. Short and long values of these sections fit or close to fit. In the PZ-1 samples the error range of the long samples is slightly smaller than the short samples and it is more consistent. The lowest $\frac{Br}{Cl}$ value of the PZ-1 samples is ~0.001 and the highest is ~0.011. The values of this ratio also tend to rise and drop frequently within their range. Similar to the $\frac{Mg}{Cl}$ soluble salts data of the deep and shallow cores, the $\frac{Br}{Cl}$ results of PZ-1 also reveal a general mirror pattern compare to the $\frac{Na}{Cl}$ ratios. The data of the lower section is as well the most stable and variate between ~0.004 to 0.0072. The middle section is the noisiest with frequent changes between ~0.0025 to 0.0105. The data of this section does not seem to rise up in the same proportion as it dropped in the $\frac{Na}{Cl}$ middle section but rather it rise more moderately, and its mean value mostly remain stable. The upper section is noisy but show a mean secular decrease from ~0.007 to 0.0015. Several Mt.

Sedom samples correlate with the coeval PZ-1 samples while the rest seem to have lower values that get down to zero in one sample. In the Mt. Sedom samples, the bromide content is very low and in most samples is below the error level or just slightly above it. It seems that such a low content of bromide could have distort the original $\frac{Br}{Cl}$ values of the soluble salts in these sediments.

Figure 18 C present the $\frac{Mg}{Cl}$ values that received from the PZ-1 and Mt. Sedom sections. It can be seen that the lower half of PZ-1 data is suspiciously low. Additional ratios with Mg in the numerator but different elements in the denominator show a similar behavior, constraining the Mg to be the cause for the low values. It could be that such low values represent the original values of the brine although it seems more as an artifact. Anyway, the discussion of this work will not deal with Mg results of the lower half of PZ-1. The upper half of the data, however, seems reliable. Short and long samples are almost identical in this ratio. The variations in the upper half of the data are often, in the range of 0.034 to 0.93. This section exhibits a similar behavior as the $\frac{Br}{Cl}$ data. PZ-1 values of the middle section (upper half) variate between 0.034-0.343 with several Mt. Sedom samples that correlate to it while other show higher values. PZ-1 values of the upper section variate in the range of 0.096 to 0.311 and show a mild decrease of the mean value from ~0.3 to 0.1. One data point of Mt. Sedom from this period correlate well with the PZ-1 data while several Mt. Sedom samples that precede the PZ-1 upper group show values that seem to be a bit lower.

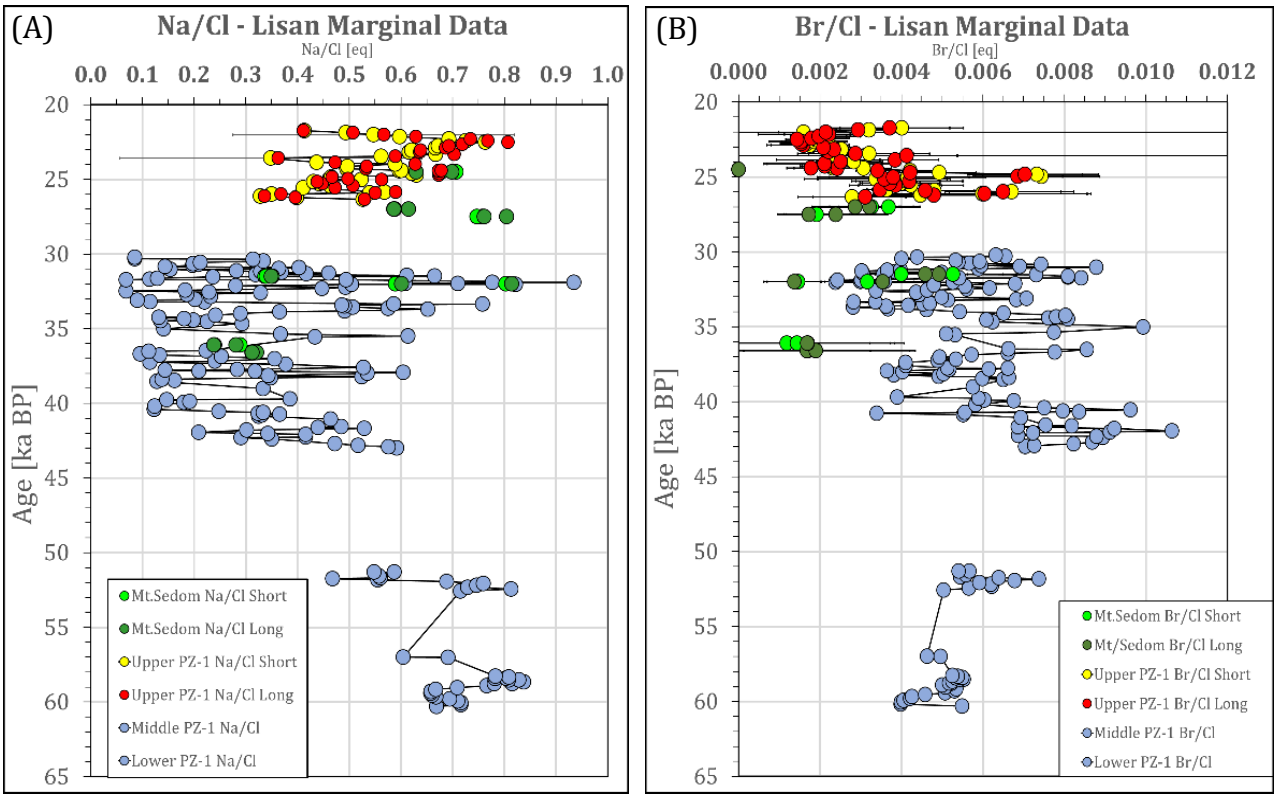

Figure 18: Ion ratios of highly soluble elements received from the soluble salts' data of PZ-1 and Mt. Sedom White Hill outcrops, plot against chronologic age. PZ-1 data combined results from this work and previous work of Amitai Katz and Mordechai Stein that published here for the first time. Short and long samples are displayed when samples are from this work. All ratios are in equivalent. Three ratios are presented: (A) $\frac{Na}{Cl}$, (B) $\frac{Br}{Cl}$, (C) $\frac{Mg}{Cl}$.

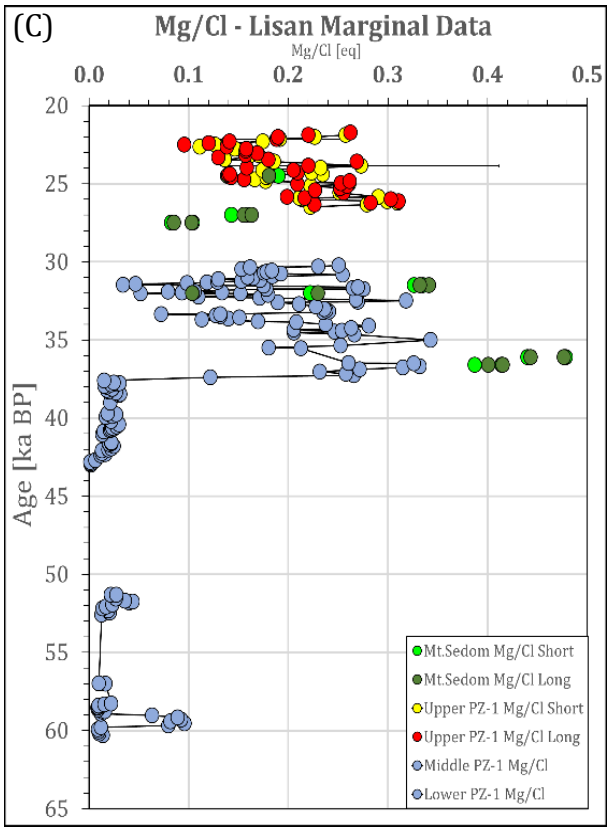

7.2. Discussion

7.2.1. Spatial and temporal variations in the chemical composition of Lake Lisan's brines

By comparing the chemical data of the deep, shallow and marginal sections a comprehensive spatial and vertical picture is obtained on the chemical evolution of the lake's brines (the deep, intermediate and marginal sectors of the lake. see Fig. 2).

First, a comparison between the data of the soluble salts from the deep core (5017-1-A) to the data of the pore fluids from the same core is established for the $\frac{Na}{Cl}$, $\frac{Br}{Cl}$ and $\frac{Mg}{Cl}$ ratios (Figure 14 A-C Chapter-1). This comparison reveals high correlation between the soluble salts and the pore fluids data. The trends of these three ratios are almost identical while the $\frac{Na}{Cl}$ ratio shows a mirror pattern compare to the $\frac{Br}{Cl}$ and $\frac{Mg}{Cl}$ ratios. Since the profiles of highly soluble ions in pore fluids and soluble salts from the deep core are similar the main conclusions that obtain from these profiles are similar as well. Nevertheless, there are several unique conclusions and advantages that the soluble salts data provide.

First, the high correlation of the $\frac{Na}{Cl}$, $\frac{Br}{Cl}$, $\frac{Mg}{Cl}$ data between the soluble salts to the pore fluids reinforce the validity of the soluble salts method and proves that it can be used on its own, at least when dealing with elements from the highly soluble group.

As explained before, Br and Mg are conservative elements in the lakes of the DSB since they did not participate in precipitation or dissolution of salts and their income or outcome from the lake by additional processes during the discussed period is too little to be considered. The Cl and Na on the other hand participates in halite precipitation and dissolution when it occurred. Therefore, under the condition of $\frac{Br}{Cl} / \frac{Mg}{Cl} / \frac{Na}{Cl} < 1$, the values of $\frac{Br}{Cl}$ and $\frac{Mg}{Cl}$ will drop when halite dissolution take place in the lake, due to the addition of Cl to the brine and the conservation of Br and Mg. Upon halite precipitation these ratios rise due to Cl loss from the brine while Br and Mg remain conserved. The $\frac{Na}{Cl}$ response is the opposite since both of the elements participate in halite precipitation/dissolution in a ratio of 1:1. When halite precipitation occurs both Na and Cl ions leave the brine and the $\frac{Na}{Cl}$ ratio of the brine drops. When halite dissolves the brine gain Na and Cl ions and the ratio rise. If the lake is diluted by freshwater but do not reach halite dissolution or concentrate but do not reach halite precipitation the values of these ratios supposed to remain stable unless additional process influence the system.

During the time interval of ~100 to 12 ka BP the soluble salts and pore fluids data of the $\frac{Na}{Cl}$ ratio show a persistent rise while the $\frac{Br}{Cl}$ and $\frac{Mg}{Cl}$ ratios show a persistent drop. These trends are interpreted as a consequence of halite dissolution.

Another advantage of the soluble salts data from the deep core is its higher resolution relative to the pore fluids. Sections with high-resolution of soluble salts data reveal additional patterns that are absent in the pore fluids data. The most prominent section spans along the highest-stand period of Lake Lisan and the following shift to the Holocene, from ~30 to ~11 ka BP. The pore fluids data along this section is very sparse and include about 7 samples, while the soluble salts data comprise several tens of samples that reveal additional details.

Since ~30 ka BP the pore fluids show an almost uniform $\frac{Na}{Cl}$ value of ~0.52 between the sparse data that moderately rise to ~0.54 until ~16 ka BP, while the soluble salts data exhibit several variations.

At ~28 ka BP the $\frac{Na}{Cl}$ ratio rises from ~0.52 to a peak of ~0.58 at 26-25 ka BP. This peak coincides well with the timing of the highest stand in the lake of ~ 170 m bmsl (Bartov et al., 2002; Torfstein et al., 2013). The significant lake level rise reflects enhanced inputs of freshwater to the lake and freshening of the brine. It most likely had a greater influence on the upper brine, although this data reveals that this dilution also had an impact on the more isolated hypolimnion which reflect in greater rates of dissolution.

After ~ 25 ka, the $\frac{Na}{Cl}$ ratio drops to ~0.52 and from there variate frequently until it rises again to a peak of ~0.58 at 22-21 ka BP. This noisy period coincide with the lake level drop from the highest peak of the

LGM (~160 to ~205 m bmsl) while the followed peak correlates with the last rise of the LGM in the lake (~205 to ~190 m bmsl). From there the soluble salts values oscillate between 0.5 to 0.6 until ~17.8 ka BP, while the pore fluids mildly rise to 0.54. During this period of oscillations, the lake shrank dramatically due to the cease of the glacial wet climate and onset of the shift to the drier Holocene.

It seems that rising $\frac{Na}{Cl}$ ratio and uniformity in the values retrieved from the soluble salts indicate on continuous dilution of the deep brine and continuous halite dissolution during time intervals of enhanced freshwater input to the lake and continuous freshening of the hypolimnion. Periods of lake level drop, on the other hand, are characterized with oscillating values and larger spread in the $\frac{Na}{Cl}$ ratio. In addition, it seems that the more significant the lake level drop is, the greater the oscillations of the $\frac{Na}{Cl}$ values, which could testify on the instability of the lake during these periods.

At ~17.5 ka BP, the deposition time of the "Upper Gypsum Unit" of the Lisan Fm. and H1, the $\frac{Na}{Cl}$ ratio in the soluble salts of the deep core rose up reaching its highest values (in the whole core) of 0.7-0.74, at ~11.9-11.5, just before the deposition of the "base of the Holocene salt unit". This rise in the $\frac{Na}{Cl}$ ratio is documented by ~4 sparse pore fluids samples and supported by ~14 soluble salts samples that show the same general rise but with additional details.

This $\frac{Na}{Cl}$ great rise occurred along a period of a general significant level drop, yet with prominent wet periods at the end of H1 (~16-14 ka BP) and the Younger Dryas (~12.9-11.7 ka BP) that led to lake level rise and brine dilution, as seen in the lake level curve (Fig. 29 & Torfstein et al., 2013).

The soluble salts data shows the stepwise increase in the $\frac{Na}{Cl}$ values that correlate these two wet periods rather than the continues rise that reflect by the sparse pore fluids data.

It is suggested here that in the shrank lake it was easier to change the values of elemental ratios due to the reduced volume and lower amount of ions that should have enter or exit the lake in order to influence the ratios. As long as the lake remained undersaturated to halite the lake's brines dissolved halite and any addition of ions had a greater influence on its ratios relative to periods of higher lake level. Machlus, (1996) suggested a similar mechanism regarding the $\frac{Sr}{Ca}$ rate of change in a stratified lake relative to a mixed lake). Due to that effect the $\frac{Na}{Cl}$ values of the deep brine could reach such a high value while actually the lake underwent through a period of reduced rain and halite dissolution ability. During this period, the final accumulation of the large repository of Na and Cl ions took place in the lake and once halite saturation reached this salt could have extensively precipitate in the lake for several thousands of years.

It is seen that the $\frac{Na}{Cl}$ maximum is represented by one data point of the pore fluids at 12 ka BP with a value of 0.7, while several data points of the soluble salts show a trend of rising values, from ~0.64 at 12.2 ka BP to ~0.74 at 11.5 ka BP. This maximum coincides well with the timing of the Younger Dryas (~12.9-11.7 ka BP) and support the rise that occurred in the lake level as a result of this event. The end of the Younger Dryas is followed by an extremely sharp and rapid decline in the $\frac{Na}{Cl}$ values. One data point of the pore fluids at 11.1 ka BP shows a value of 0.41 while a soluble salts data point from a coeval time shows a value of 0.48. It is worth emphasizing that this section (~85 m in the core) is part of the thick halite section at the top of the Lisan sediments and the transition to the Holocene. This sample of the soluble salts is an intermediate section of aad between two thick halite layers, and therefore it could be that these sediments contain some amount of halite crystals that dissolved during the procedure of the soluble salts, what led to a rise in its $\frac{Na}{Cl}$ value. The $\frac{Mg}{Cl}$ ratio support all the discussed insights that obtained from the $\frac{Na}{Cl}$ ratio with its remarkable mirror pattern and even reinforce them due to its lower range of error. The $\frac{Br}{Cl}$ show a similar pattern yet conclusions cannot obtain regard such short-term variations due to its increased error.

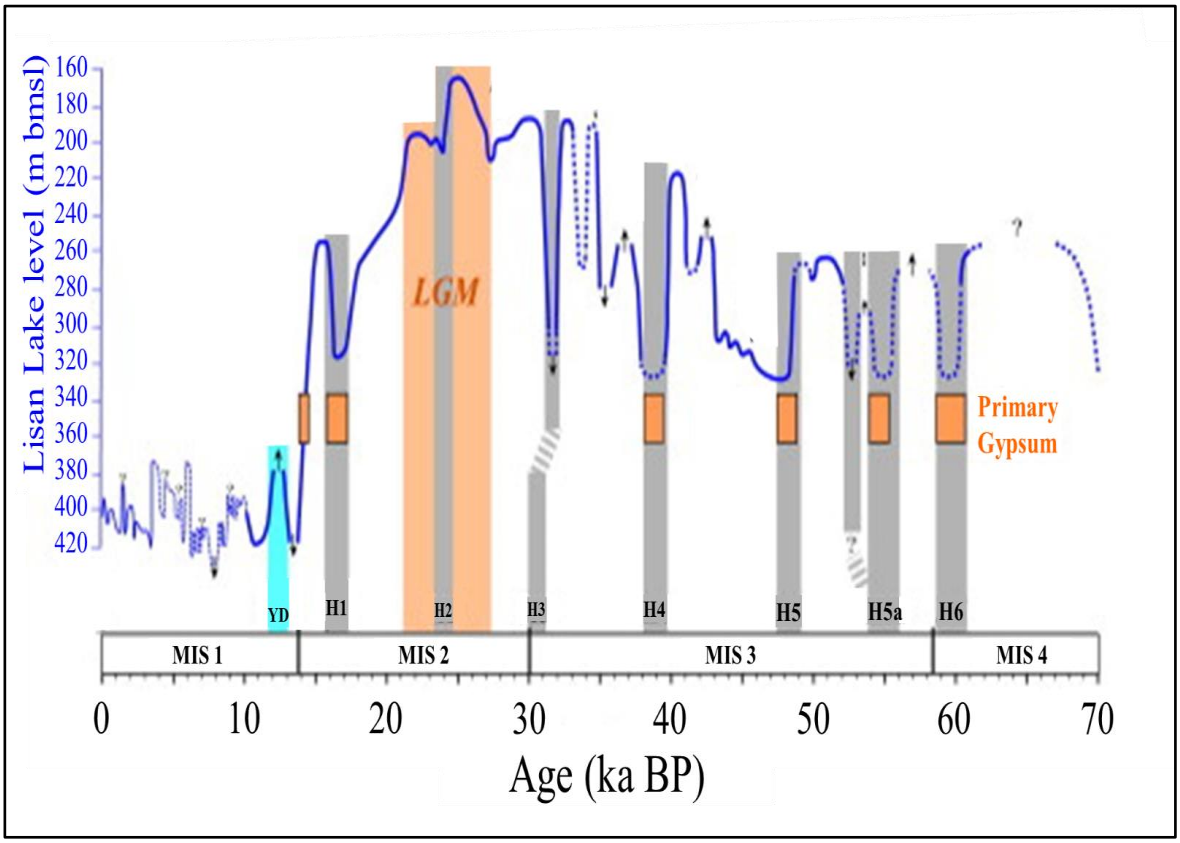

Figure 19: Lake Lisan level curve as reconstructed by Torfstein et al., (2013).

In a general view, the perseverance rise of the $\frac{Na}{Cl}$ and drop of the $\frac{Br}{Cl}$ and $\frac{Mg}{Cl}$ along the period of ~100-12 ka BP points on the gradual freshening of Lake Lisan during this period and the consistent halite dissolution that took place in the lake. The close examination of the soluble salts data reveal that this ratio also captures shorter events that are part of the general trend, such as the peaks of significant lake level rises, as the rise of the LGM and those who followed it during the transition to the Holocene.

When stand on its own, the $\frac{Na}{Cl}$ ratio can mislead and suggest that the freshening of the lake during the last glacial period was consistent and consecutive, that halite dissolution occurred at some rate, even if mildly, all along this period, and that the rate of the dissolution, and in accordance also the rate of freshening, increased after the end of H3 (~31 ka BP) and became even greater after the cease of H1, between ~17 to 11.5 ka BP. Although, when compared with an independent lake level a deficiency reveals. The reconstructed level of Lake Lisan (Fig. 19) is showing that the freshening of the lake along the last glacial period and its gradual rise until the climax of the LGM was punctuated with many significant level drops that mark drier periods with negative water balance in the lake, when the freshening of the lake was oppressed. This observation reveals that in a lake such Lake Lisan, that did not reach halite saturation but rather maximum saturation of gypsum, the $\frac{Na}{Cl}$ ratio, that controlled mainly by halite dissolution and precipitation, will not document dry periods with negative water balance as long as the lake did not reach halite saturation along them. In this case, during wet periods of lake level rise, when significant halite dissolution take place the $\frac{Na}{Cl}$ values will rise (under the condition of $\frac{Na}{Cl} < 1$). Although, during dryer periods when the lake level drops but did not reach halite precipitation the ability of the brine to dissolve halite will reduce and the $\frac{Na}{Cl}$ rise will become more moderate or even stabilize but will not drop. This clarification suggests that the only time that a significant precipitation of halite did occur in Lake Lisan was during the abrupt arid conditions of H3, as observed in the pore fluids data point from 31.7 ka BP. As a result of this event the lake level dropped from ~190 m bmsl to ~320 m bmsl during a period of ~1000 years. However, since halite is absent at this period in the sediments of the deep core this conclusion arises a new question; what happened to the precipitated halite that led to its absence? A reasonable explanation will be that in this case the halite precipitation period was very short (several hundred years) and was followed by a rapid return to the wettest conditions of the last glacial period. Consequently, the hypolimnion was diluted, became undersaturated to halite and dissolved the few halite that precipitate during H3.

7.2.2. Comparisons with the 5017-3-C Shallow core

By exhibiting each of the $\frac{Na}{Cl}$, $\frac{Br}{Cl}$ and $\frac{Mg}{Cl}$ data from the deep core together with its contemporaneous shallow core data on the same graph a comparison is achieved between the deepest brine of the lake to its brine of intermediate depth. This comparison is presented in Figures 17 & 20 A-C. The shallow core data, although sparse, has some data points from Samra and the upper part of Amora formations. By having such data sprawling conclusions can attain regard several processes that occurred in the lake that precede the Lisan Period.

Glacial MIS 6: The deepest samples from the shallow core are part of the Amora Fm. (~143.4-137 ka BP). They precipitate during MIS 6, which was characterized in glacial climate and wet conditions in the lake's watershed (Torfstein et al., 2009). Such conditions are testified here by the relatively high values of the pore fluids in the $\frac{Na}{Cl}$ ratio (~0.42-0.57) and low values in the $\frac{Br}{Cl}$ and $\frac{Mg}{Cl}$ (~0.0065-0.0092 and 0.2794-0.45 respectively). The shallow core data of this period correlates well both in its values and trends in all of the three ratios. The values of the pore fluids, that resemble the values and trends of the Lisan period, testify on a diluted lake that its deep brine dissolved halite in a similar scale as dissolved in Lake Lisan. Such dilution of the lake requires large amounts of incoming fresh water, that consequently led to a rise in the lake's level. Therefore, it is obligated that during the late MIS 6 the lake levels were relatively high, similar to the typical high levels of the Lisan. In addition, such a diluted high-level lake was also, most likely, stratified, having a highly diluted epilimnion atop a more saline, but still diluted, hypolimnion. The highly correlated values of the shallow core suggest that during this period the elevation in which the shallow core samples were precipitated was well below the epilimnion-hypolimnion interface, and that the samples of the two cores represent the same brine. The uppermost sediments that recovered from the shallow core are from a depth of ~34.57 m below lake's floor, ~460 m below mean sea level (Neugebauer et al., 2014). The samples of this core from the Amora formation (and the following samples from the onset of Samra formation) are from depths of ~200-300 m below lake's floor. Consequently, at the time of deposition the elevation of the shallow core site was ~660-760 m below mean sea level (neglecting sediments' subsidence and tectonic movements). In such depths, and during glacial period with wet climate it is highly reasonable that the brine and soluble salts in the shallow core's sediments of this time represent the deep hypolimnion.

Interglacial MIS 5: The next group of shallow core samples is from the beginning of the Samra Fm. (~129.8-127 ka BP). These samples correlate with the onset of the drop in the $\frac{Na}{Cl}$ and rise of the $\frac{Br}{Cl}$ and $\frac{Mg}{Cl}$ towards the low/high values of the MIS 5, last interglacial, and appear right after the highest $\frac{Na}{Cl}$/lowest

$\frac{Br}{Cl}, \frac{Mg}{Cl}$ values of MIS 6. The high correlation of these samples to the pore fluids' values and trend suggests that despite shifting to the dryer climate of the interglacial and the initiation of halite precipitating that was required also a lake level descend, during this period the lake was probably still stratified and the hypolimnion ceiling kept above the elevation of the shallow core samples.

During this period a dramatic change was already initiated in the lake. The $\frac{Na}{Cl}$ dropped and $\frac{Br}{Cl}, \frac{Mg}{Cl}$ ascended sharply and rapidly towards the lowest/highest values of the last interglacial. This drop/rise resembles the drop/rise from the beginning of the Holocene, occurred after the ratios reached their highest/lowest peaks of the last glacial period. As occurred during the large shift to the Holocene, the significant shift of the last interglacial was probably accompanied with a remarkable level decline of several hundred meters and a notable shrinkage of the lake's brines. The next group of the shallow core samples consist of a sample from 117.3 ka BP and 3 close samples from ~113.4-113.9 ka BP. The older sample correlates in its age with the MIS 5e's lowest/highest peak along the entire core but its value is much higher/lower than the deep core pore fluids value (0.5 vs 0.2 in $\frac{Na}{Cl}$, 0.0078 vs 0.0122 in $\frac{Br}{Cl}$, 0.384 vs 0.63 in $\frac{Mg}{Cl}$). The next 3 shallow core samples correlate with a MIS 5d's rise/fall in the deep core pore fluids values, and their values remain similar to their preceding sample. This data group of the shallow core and the coeval deep core pore fluids testify on a lake with different characteristics than those observed during the late MIS 6. At first, the lake level apparently dropped dramatically during MIS 5 but these samples suggest that its level remained above the level of the shallow core samples (which was lower than current elevation of the shallow core). The difference between the values of the shallow core to those of the pore fluids from the deep core suggest that each data source shows the chemical composition of a different brine. While the pore fluids show the values of a concentrated deep hypolimnion that precipitate halite, the shallow core samples show the values of an undersaturated epilimnion. The similarities between the values of the shallow core samples of this period to those of the late MIS 6 and beginning of MIS 5, suggest that the epilimnion remained undersaturated to halite but did not dissolve large amounts of the salt but rather remained relatively constant. Another scenario takes in account a mild error on the ages of the shallow core samples from ~117 and 113 ka BP. In this case the ages of these samples will shift to be ~800 years younger. After this shift all of the samples from this group correlate with the MIS 5d's rise in the $\frac{Na}{Cl}$ and drop in the $\frac{Br}{Cl}$ and $\frac{Mg}{Cl}$ values that observed in the deep core pore fluids (the rise/drop between the samples of 116.5 to 116.1 ka BP).

A lake configuration of a concentrated hypolimnion that extensively precipitates halite while simultaneously the epilimnion is undersaturated or mildly precipitates halite is known and familiar from

the modern Dead Sea (Sirota, 2016; Sirota et al., 2017, 2018). These works performed a comprehensive study on the halite precipitation mechanism in the modern Dead Sea. Several observations and conclusions from these works support the assumption that halite used to precipitate in Samra Lake in a pattern that highly resembles the halite precipitation in the modern Dead Sea. Sirota, (2016) revealed the annual cycles of halite precipitation in the Dead Sea. It was shown that during the cold winter months the mixed water column reaches thermal saturation due to its cooling and halite precipitates throughout the entire water column. In the summer, on the other hand, a thermocline develops in the lake and the heating of the epilimnion lowers its saturation levels until reaching undersaturation with respect to halite. The hypolimnion stays cool and hence its saturation remains year-round. Therefore, halite precipitates in the deep lake (~25 m and deeper) throughout the year whereas, in the shallow lake it precipitates only during winter and dissolves during summer. Sirota et al., (2017) described the characteristics of the halite that precipitates under the conditions of the Dead Sea or similar, in terms of crystals size, roughness of the interface between layers and the variations of the precipitation along the annual cycle and across the spatial and vertical water column. Kiro et al., (2016) described in detail the characteristics of the thick sequences of halite in the deep core of the DSDDP, which were precipitated along the three interglacials that present in the core, during periods of hyperaridity in the lake's watershed. These characteristics were found to highly correlate, in several core sections from the last interglacial, with the modern halite characteristics that were described by Sirota et al., (2017) in the deep lake. Sirota et al., (2018) described a model for halite accumulation in hypersaline deep basins based on in situ observations of halite precipitation that occurs today in the Dead Sea. The process, called halite focusing, is a limno-sedimentological model for halite accumulation. This model accounts for a halite-saturated hypersaline basin under negative water balance and a stratified water column. According to this model and the observations from the Dead Sea, halite dissolves in the undersaturated epilimnion and the dissolved Na^+ and Cl^- ions transfer down to the hypolimnion by double-diffusive fluxes, resulting in an undersaturated epilimnion and continuous supersaturated hypolimnion with respect to halite. This process leads to the focusing of halite in the hypolimnion and to a large amplification of its accretion in the depocenter, at the expense of dissolution from the shallow basin margins.

The presence of thick halite sequences in the last interglacial deep core sediments while its coeval sections in the shallow core utterly absent of halite support the occurrence of halite focusing during the hyperarid periods of the last interglacial. Altogether, the observations from the MIS 5 sections in the deep and shallow cores support the suggestion that the limnological configuration and halite precipitation processes in Lake Samra were highly resemble to those observed today in the Dead Sea. This conclusion

explains how the hypolimnion that precipitates halite during the MIS 5 held low $\frac{Na}{Cl}$ values (~0.2-0.3) and high $\frac{Br}{Cl}, \frac{Mg}{Cl}$ values (~0.012-0.01 and ~0.63-0.47 respectively) while simultaneously the undersaturated epilimnion dissolved halite or remained stable and accommodate higher values of $\frac{Na}{Cl}$ (~0.45-0.5) and lower values of $\frac{Br}{Cl}, \frac{Mg}{Cl}$ (~0.007-0.008 and 0.34-0.38 respectively). The values from ~117-113 ka BP may suggest that during the extreme arid spell of the halite precipitation in the deep lake, between ~122-116.5 ka BP, the lake level remained above the elevation of the shallow core samples, and it remained stratified, with halite focusing taking place in the lake. If halite did precipitate in small amounts in the epilimnion during this period it dissolved later due to lake's dilution. This scenario is not unreasonable considering that the Dead Sea remained stratified until 1978, deep into the Holocene and its severe arid conditions, and having the shallow core located in an elevation that is relatively low (current core's top~430 m bmsl, ~490-730 m bmsl at time of deposition). However, it is more reasonable to embrace the approach of shifting the ages of this group ~800 years younger. In this case the lake level probably dropped below the elevation of the shallow core samples during the massive halite precipitation of the late MIS 5e (~122-116.5 ka BP). This assumption is supported by the dominance of halite over a section of ~45 m with thin interspersed silt and gypsum which is capped by a pebbles section of ~40 cm, and since it is considered to be the most extreme arid spell known in the DSB (Torfstein et al., 2015; Kiro et al., 2017). This level drop led to a hiatus in the area of the shallow core during this period. As a response to the resumed wetness in the lake's watershed that occurred at the onset of MIS 5d, 5c and 5b (~116-93 ka BP) the lake was diluted, its level rose above the shallow core elevation, the $\frac{Na}{Cl}$ values increased and $\frac{Br}{Cl}, \frac{Mg}{Cl}$ values decreased as a result of halite dissolution that was more advanced in the epilimnion due to its lower salinity.

The following shallow core samples suggest that the configuration of the stratified lake prevailed later on during the MIS 5a, documented by two samples from ~82 ka BP. These samples show similar values or slightly lowered/elevated in the epilimnion while the values in the hypolimnion gradually increased (in the $\frac{Na}{Cl}$)/decreased (in the $\frac{Br}{Cl}, \frac{Mg}{Cl}$) compare to MIS 5e-b values, testifying on a diluting lake that gradually dissolved halite also in its deep brine. The halite focusing mechanism did not took place in the lake any more at that time since the lake was not saturated with respect to halite anymore.

Glacial MIS 4-2: The following shallow core data comprise of individual sample from ~40.5 ka BP, a group of several samples from ~29-26.7 ka BP, and three samples from ~11-12 ka BP. All of them have lower $\frac{Na}{Cl}$/higher $\frac{Br}{Cl}, \frac{Mg}{Cl}$ values than the coeval deep core values, with an increased gap as the samples

gets younger. Unlike the previous shallow core samples that sank in the lake during the relatively dry MIS 5, these samples sank during the last glacial when the conditions in the drainage basin were much wetter and the characteristics of the lake were correspondingly different (except for the youngest group). The sample from 40.5 ka sank during MIS 3 that was relatively dryer and less stable than MIS 4 & 2 but its weather still sustained a lake that did not descend below ~330 m bmsl (Fig. 19 & Torfstein et al., 2013) and generally kept stratified (except for abrupt dry periods such as H3). The group of samples from ~29-26.7 ka sank during the extremely wet MIS 2, covering the period with the highest level in the lake, from ~200 m bmsl up to the highest peak of the LGM, reaching at 26.7 to ~180 m bmsl (Torfstein et al., 2013). Samples from 11-12 ka BP sank during the Holocene, at the onset of the massive salt precipitation in the deep basin.

A configuration in which the upper brine holds a $\frac{Na}{Cl}$ value that is lower and $\frac{Br}{Cl}$, $\frac{Mg}{Cl}$ values that are higher than the deeper brine is less familiar, and dose not coincide with the described configuration of MIS 5 and the processes that took place in the lake and observed today in the modern Dead Sea. Furthermore, during these periods the lake level was much higher and hence it is more reasonable that these samples from the shallow core does not represent the epilimnion but rather some elevation within the hypolimnion.

The scenario that described here imply on mild precipitation of halite that took place in the high part of the hypolimnion or lower part of epilimnion at the time of deposition. It is less likely that such a scenario occurred when considering several observations. Levy et al., (2018) calculated the degree of saturation with respect to halite (Ω_{NaCl}) in the extracted brines achieved from the deep core. The halite saturation curve along the deep core shows a distinct decrease to values that are well below halite saturation (below $\Omega_{NaCl} = 1$) in the section of 170-90 mblf, that correspond to ~70-12 ka BP. If the deepest brine in the lake was clearly undersaturated with respect to halite it imposes the brines atop it to be undersaturated as well, otherwise the upper brine will be saltier and hence heavier than the deeper brine and the steady state of light epilimnion that floats upon the heavier hypolimnion will not last. The absence of halite in the Lisan sediments from this period along with elemental concentrations and ratios that point on a diluting lake that dissolves halite (e.g., Mg, Br, $\frac{Na}{Cl}$. Levy et al., (2017, 2018) and this work) reinforce the idea that the lower $\frac{Na}{Cl}$/higher $\frac{Br}{Cl}$, $\frac{Mg}{Cl}$ values in the shallow core does not represent original halite precipitation in Lake Lisan.

Alternative scenarios can explain the lower $\frac{Na}{Cl}$/higher $\frac{Br}{Cl}, \frac{Mg}{Cl}$ values in the shallow core. One explanation will be the crystallization of halite in the sediments due to their exposure to the atmosphere during periods of low lake level. This scenario will discuss later on, as part of the marginal terraces' discussion.

The case of the three samples from ~11-12 ka BP is slightly different than the previous shallow core samples. These samples do coincide with the onset of the massive halite precipitation in the lake after the cessation of the Younger Dryas (marked by a dramatic drop in the $\frac{Na}{Cl}$/rise in the $\frac{Br}{Cl}, \frac{Mg}{Cl}$ values in the deep brine). Halite exists both in the sediments of the deep and shallow cores of this spell. During their time of deposition, the lake level already dropped dramatically. It is more reasonable that these shallow core samples represent the epilimnion or the upper brine in a mixed lake that could have precipitate halite in addition to the precipitation that took place in the deep lake. The lower values can be explained by two reasonable scenarios. Kiro et al., (2017) suggested that the basin geometry has an important influence on the halite deposition in the lake. When the lake reaches halite saturation while its level is higher than 400 m bmsl halite precipitates both at the margins and in the middle of the lake. In this configuration the upper brine precipitates a thicker section of halite than the lower brine. After the water level drops below ~400 m bmsl a lake is formed similar to the Dead Sea (or the Dead Sea itself). In such a lake halite dose not precipitates on the margins but rather dissolves while it intensively accumulates in the deep basin, as described by the mechanism of halite focusing presented in Kiro et al., (2017) and in greater details in Sirota et al., (2018). The shallow core samples from ~11-12 ka BP may testify on a lake with surface level higher than 400 m bmsl that accommodate epilimnion that used to precipitate halite more intensively than the hypolimnion and hence reached lower values of $\frac{Na}{Cl}$.

The brine in these sediments could have achieved intermediate low $\frac{Na}{Cl}$/high $\frac{Br}{Cl}, \frac{Mg}{Cl}$ values by precipitation of halite that took place in the lake, and later on these values were developed to become even lower due to the exposure of the sediments to the atmosphere, in a process that will be described later on.

7.2.3. Comparisons with marginal data

Finally, the marginal terraces $\frac{Na}{Cl}, \frac{Br}{Cl}, \frac{Mg}{Cl}$ data is placed atop the shallow and deep cores data (Fig. 20 A-C). This data comprises of the Mt. Sedom White Hill outcrop and the Perazim Valley PZ-1 outcrop.

Such a comprehensive comparison between the data sets reveals the simultaneous temporal variations of the chemical properties in Lake Lisan's water column in the deep, intermediate and shallow environments.

A prominent and significant observation that comes out of the $\frac{Na}{Cl}, \frac{Br}{Cl}, \frac{Mg}{Cl}$ comparisons, and from all other comparisons of the marginal, shallow and deep data, is the different behavior of the data of the deep core compare to the marginal sediments. While the soluble salts in the marginal sediments show frequent oscillations with remarkable amplitude the oscillations in the soluble salts data of the deep core are much smaller and scarce and the ratios' profiles display secular stable behavior along prolonged periods.

This observation strongly supports the theme of the soluble salts from the deep core sediments as representors of the hypolimnion's chemical composition whereas the soluble salts from the marginal terraces as representors of the epilimnion chemical composition. The shallow core data is too sparse to certainly being classified as noisy or stable, but with caution it is suggested to resemble the deep core data more than the marginal data, both in values and trends.

Oscillating values in the soluble salts' chemistry is what would be expected to find in the epilimnion since this upper brine is in direct contact with the local conditions, such as freshwater incomes, flash floods, freshwater and saline springs that discharge into the epilimnion, evaporation, seasonal variations and more. All of these impose their influence on the chemistry of the epilimnion and reflect in frequent variations with large amplitude. The deep hypolimnion on the other hand, kept greatly isolated along the last glacial period due to the stable stratified configuration of the lake that prevailed along it. Therefore, it was not influenced directly by the local conditions but rather buffered by the overlaying epilimnion. Accordingly, the stable values of the deep core with its secular trend, seems to suit with the deep brine.

Another important observation is the correlation between the results of Perazim valley PZ-1 outcrop to Mt. Sedom White Hill. There is some uncertainty on the ages of these two outcrops and their values variate frequently, so correlation cannot be certainly determined for specific samples. Nevertheless, these two adjacent sites show good accordance in their range of values and their trends. This correlation reinforces the validity of the results of each data set, the chronology of each site and suggest that the processes that took place in the lake across the area of Mt. Sedom and Perazim valley were locally uniform.

Next, the $\frac{Na}{Cl}, \frac{Br}{Cl}$ and $\frac{Mg}{Cl}$ variations, values and trends along the marginal Lisan sections require a discussion since they are clearly different from the deep and shallow cores data. As true for the rest of the data sets, the results of these ratios from the marginal terraces can express three different scenarios: 1. The observed values and trends represent chemical processes that took place in the lake, in this case in the epilimnion, and are part of the comprehensive and complex chemical development of Lake Lisan. 2. The data represent a local process that was restrict to the area of Mt. Sedom and Perazim Valley. 3. A

late diagenetic process has influenced the soluble salts values in the marginal terraces and altered the original values. Each scenario will be discussed separately.

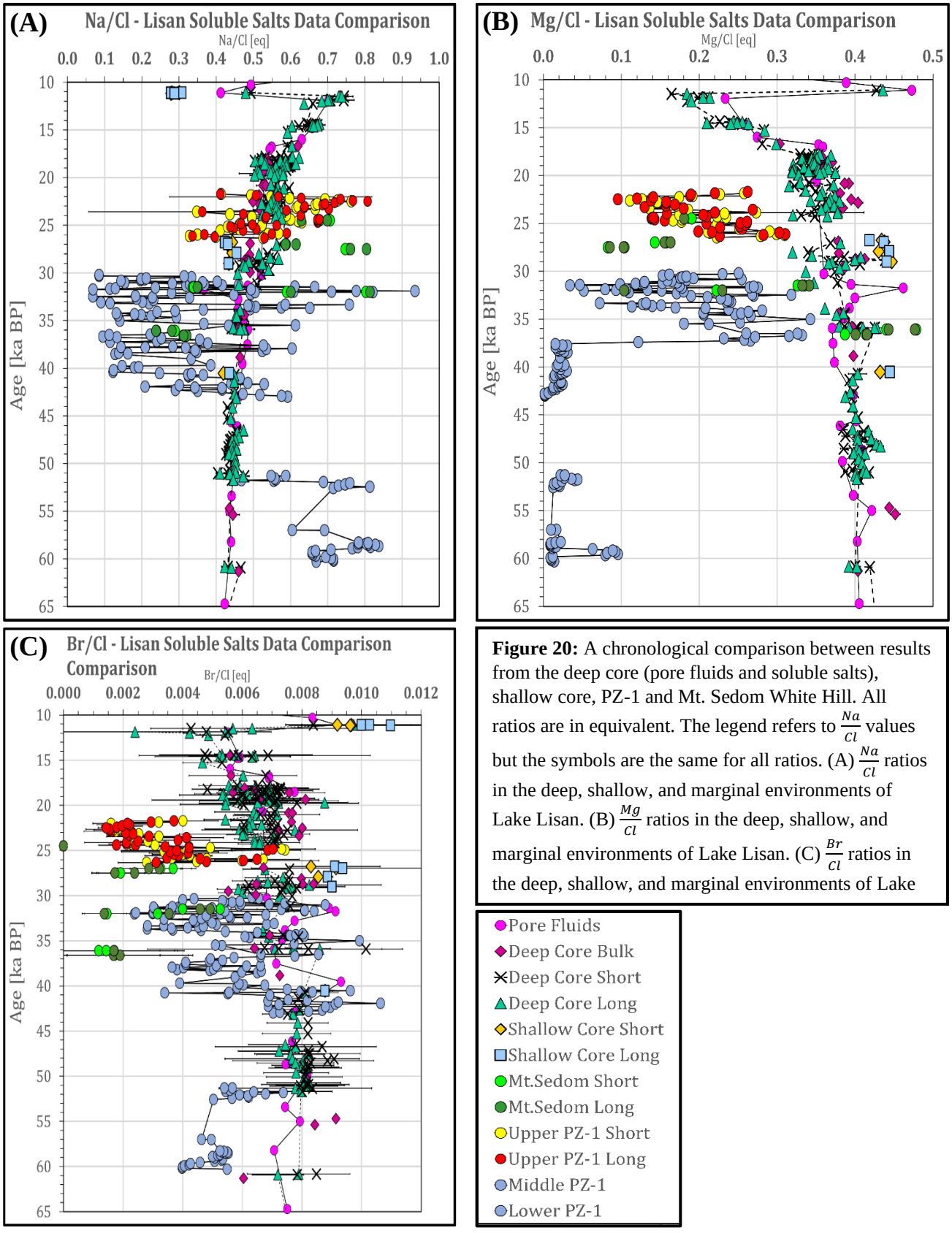

Figure 20: A chronological comparison between results from the deep core (pore fluids and soluble salts), shallow core, PZ-1 and Mt. Sedom White Hill. All ratios are in equivalent. The legend refers to $\frac{Na}{Cl}$ values but the symbols are the same for all ratios. (A) $\frac{Na}{Cl}$ ratios in the deep, shallow, and marginal environments of Lake Lisan. (B) $\frac{Mg}{Cl}$ ratios in the deep, shallow, and marginal environments of Lake Lisan. (C) $\frac{Br}{Cl}$ ratios in the deep, shallow, and marginal environments of Lake

1) <u>The marginal terraces data as integrative part of the entire lake:</u> The soluble salts values in the lower section of PZ-1 are higher than coeval ratios retrieved from the deep and shallow cores in the $\frac{Na}{Cl}$ ratio and lower in the $\frac{Br}{Cl}$ and $\frac{Mg}{Cl}$. The soluble salts from the middle and upper sections at the marginal terraces show frequent variations in all ratios. The $\frac{Na}{Cl}$ and $\frac{Br}{Cl}$ ratios oscillate between values that are higher to lower than the values retrieved from the deep and shallow cores while the $\frac{Mg}{Cl}$ data is constantly lower than the deep and shallow cores data.

If embracing the interpretation of these values as original values of the lake's brine the results of PZ-1 and Mt. Sedom (and several shallow core samples) arise a contradiction to the discussion so far.

Higher $\frac{Na}{Cl}$/lower $\frac{Br}{Cl}$, $\frac{Mg}{Cl}$ values in the soluble salts of the marginal sections are consistent with a more dilute epilimnion. A layered configuration with fresher epilimnion could persist for a long time. Yet, part of the PZ-1 and Mt. Sedom data show lower $\frac{Na}{Cl}$/higher $\frac{Br}{Cl}$ values than the deep and shallow cores (most notable are the lower $\frac{Na}{Cl}$ values). These low/high values imply on a more saline epilimnion than the deep brine, that could have reach halite saturation and precipitation. The frequent variations in the data imply that these conditions changed quickly, and halite deposition was followed by dissolution.

A configuration of a stratified lake that its epilimnion precipitates halite while its hypolimnion mildly dissolves halite or stays stable is not known in the lakes of the DSB or elsewhere. All the models of halite precipitation require the entire lake to be saturated to halite, with whether mixed or stratified water column, or having a saturated hypolimnion that precipitates halite simultaneously with an undersaturated epilimnion that is neutral or dissolves halite (Kiro et al., 2017; Sirota, 2016; Sirota et al., 2017, 2018). A water column with saturated epilimnion and an undersaturated hypolimnion will not sustain due to thermodynamic considerations. In such case the water column will mix due to the heavier epilimnion that placed upon the lighter hypolimnion. As mentioned before, Levy et al., (2018) calculated the degree of saturation with respect to halite in brines that were extracted out of the deep core sediments and found it to be well below saturation (below Ω_{NaCl}<1) during the period of ~70-12 ka BP. Accordingly, the epilimnion that covered the marginal terraces could not reach halite saturation at that time. Furthermore, if halite used to precipitate in the epilimnion of Lake Lisan it should have occur in the hypolimnion as well and it should be evident both in chemical and sedimentological traces. The $\frac{Na}{Cl}$, $\frac{Br}{Cl}$, $\frac{Mg}{Cl}$ records of the deep core along the Lisan period (both pore fluids and soluble salts) does not support halite precipitation. It rather suggests that the deep brine gradually dissolved halite throughout this period (Levy et al., 2017, 2018; Lazar et al., 2014). Along the 40 m of the marginal outcrop of PZ-1 several thin (few cm) halite

layers were observed by Machlus, (1996) in a sequence of thick primary gypsum (~30 cm) that followed by a thick clastic unit (~1 m) in which the halite layers appear. This sequence observed at a height of 23 m in the outcrop which correlates to the age of 35-34 ka BP. In the sediments of the deep core halite is absent as primary layers along the discussed spell. Inasmuch as halite is a highly soluble salt its precipitation could have been followed by dissolution. Such a scenario would be evident by fluctuating ratios in the soluble salts data, similar to the ratios behavior of the marginal terraces. If halite would have precipitate in Lake Lisan and later on dissolved the fluctuations in the $\frac{Na}{Cl}, \frac{Br}{Cl}, \frac{Mg}{Cl}$ values of the soluble salts in the deep brine should have be at least similar to those of the epilimnion, if not greater. Although, as discussed before, it is unreasonable that halite used to precipitate in the epilimnion routinely and massively while at the same time the hypolimnion dissolved halite.

To conclude, when considering the scenario of the marginal terraces the data is divided. $\frac{Na}{Cl}$ values that are higher and $\frac{Br}{Cl}, \frac{Mg}{Cl}$ values that are lower than the deep core values can be original and testify on the diluted epilimnion of Lake Lisan with the halite dissolution that took place in this upper brine. The proximity of PZ-1 and White Hill outcrops to the Mt. Sedom salt diapir increase the probability for dissolution of halite in the epilimnion, as indeed suggested by Levy et al., (2017, 2018, 2019). $\frac{Na}{Cl}$ values that are lower and $\frac{Br}{Cl}, \frac{Mg}{Cl}$ values that are higher than the coeval deep core values are contrarily rejected as an evident for halite precipitation that occurred in the epilimnion of Lake Lisan.

2) <u>Restricted environment:</u> Restricted environments that are disconnected from the main lakes could have accommodate separate processes that influenced the compositions of the soluble salts. The PZ-1 is located in the Amiaz Plain with Mt. Sedom salt diapir adjacent ~2.5 km to the east (Fig. 1&2). Thus, it is reasonable that their similar values represent the same local process if indeed occurred. The $\frac{Na}{Cl}, \frac{Br}{Cl}, \frac{Mg}{Cl}$ ratios vary sharply and frequently in the two sections and reach to advanced low/high values (~0.07-0.93 in the $\frac{Na}{Cl}$, ~0.002-0.011 in the $\frac{Br}{Cl}$ and ~0.034-0.343 in upper half of $\frac{Mg}{Cl}$. Fig. 18 & 20 A-C). In order to explain these extreme values and trends a process is required that will include phases of severe dry out accompanied with progressed halite precipitation that are followed by intense dilutions and the complete dissolution of the recently precipitated halite. A process is suggested here based on the observed ratios, the trends in the data of PZ-1 and Mt. Sedom sections and their topographic-geologic-lithologic characteristics.

PZ-1 section is located in a canyon that undermine in Lisan sediments which deposited from the lake on a relatively flat area. The top of the current Lisan sediments form a plain called Amiaz Plain that covers

the region between Mt. Sedom in the east to the Dead Sea valley escarpments in the west. The current elevation of Amiaz Plain in the proximity of PZ-1 is ~270-280 m bmsl, while the elevation of the current Perazim Valley floor is ~300-320 m bmsl (in PZ-1 proximity). The base of Lisan Fm. in this area lies ~1 m below the valley floor (Haase-Schramm et al., 2004, regard PZ-1). The suggested uplift rates of Mt. Sedom salt diapir lie between 3 to 8 $\frac{mm}{year}$ (Weinberger et al., 2007) implying that during the deposition of the Lisan's Lower Member (70-50 ka BP), the top of Mt. Sedom was at least several tens of meters below the elevation of the Amiaz Plain (~400 compare to ~310 m bmsl, respectively). By the time the Middle and Upper Members of the Lisan Fm. were deposited (~50-30 ka and 30-14 ka BP) the top of the diapir rose to elevations that are more or less aligned with the elevation of Amiaz Plain area (~350 to 280 m bmsl). By this alignment, the area of Mt. Sedom became part of the local plain.

This uplifted plain could serve as an area in which lake's brine pooled to form residual shallow lake. As long as the level of the main lake remained lower than the Amiaz -Mt Sedom plain, a residual lake could form and, under negative water balance, gradually desiccate and develop advanced degrees of evaporation, similar to the modern evaporitic ponds of the Dead Sea Works in the southern basin of the Dead Sea. Such residual lake which undergoes an advanced dry out could have reach saturation of gypsum, halite and even more progressed salts such as carnallite and bischofite. Periods of low lake level characterized with arid climate, and significant negative water balance that leads to a drop in the level of the main lake, and thus support the severe dry out of the residual lake as well. In addition to that, having the sprouting salt diapir at the surface of this area support the process as well by being a robust source of available halite for dissolution. As long as the brine of the residual lake remained above halite saturation, or some rain dropped on the area the dissolution of the diapir proceeds and the repository of dissolved ions of Na and Cl increased. This process buffered the salinity of this small lake, as suggested to occur in Lake Lisan by Levy et al., (2017) and maintained its salinity high. As long as the main lake did not rose and flooded the Plain the residual Amiaz lake remained highly saline and kept degree of saturation close to or above halite saturation. During these periods saline springs used to discharge back into the lake, as suggested previously (e.g., Machlus, 1996; Torfstein et al., 2008; Weber et al., 2018). These saline springs has their contribution of salts to the lake and the portion of those springs that discharged into the residual lake probably helped to sustain its high salinity. When Lake Lisan did ascend and covered the area during wetter periods the undersaturated brine of the epilimnion dissolved the halite that deposited by the residual lake. Such mechanism supports the observed fluctuations in the $\frac{Na}{Cl}$, $\frac{Br}{Cl}$ and $\frac{Mg}{Cl}$ values and can even explain the extremely low and high values of the marginal outcrops. The several halite layers in PZ-1 at ~35 ka BP strongly support this mechanism, especially when halite is absent in

the coeval sediments of the deep core. Finding the halite layers after a thick gypsum layer and within a clastic section reinforce this hypothesis by showing that the halite indeed precipitated at the end of an evaporating sequence, after gypsum saturation was achieved and the water level was so low that clastic material dominated the majority of the accumulating section due to the proximity to the shore. The lowest $\frac{Na}{Cl}$ value observed in the marginal terraces is ~0.068. Such a low value supports an almost complete desiccation of the brine. The lakes of the DSB never reached such a low $\frac{Na}{Cl}$ value, as known from independent works (e.g., Levy et al., 2018), which showed that the main lake reached its lowest $\frac{Na}{Cl}$ value of ~0.19 during the last interglacial. The $\frac{Na}{Cl}$ data of Mt. Sedom show another observation by fluctuating similarly to the PZ-1 data along the interval of the middle section, both in values and trends, while during the time of the upper section the data fluctuate in a range that is higher than PZ-1, deep and shallow cores data. This shift suggests that by the time the lake precipitated the Upper Member (30-14 ka BP) the diapir rose above Amiaz Plain and brine could not pool on top of it anymore. Instead, the residual lake was restricted to the area of the modern Amiaz Plain while on top of Mt. Sedom halite dissolution occurred broadly, but halite precipitation was quenched. According to the Lisan's lake level reconstruction (Fig. 19 & Bartov et al., 2002; Torfstein et al., 2013) its water surface indeed dropped several times below the level of Amiaz Plain (~320 to 280 m bmsl). Hence if indeed the topography allowed it a residual lake could have pool on top of the Plain.

This hypothesis seems plausible in many aspects on the one hand, nevertheless, there are several observations that contradict it.

Although seems more confined, stable and less frequent, the data of the lower and upper sections still show some clear drops in the values, both in PZ-1 and Mt. Sedom sections. According to the suggested model Mt. Sedom diapir was too low and too high during the deposition time of the Lower and Upper Members, respectively. The drops in the $\frac{Na}{Cl}$/rises in the $\frac{Br}{Cl}$, $\frac{Mg}{Cl}$ values are significant and imply on many events of halite precipitation that does not coincide with the model.

In addition, having a lone unit of halite in the entire section of PZ-1, that presumably precipitated significant amounts of halite seems deficient. Indeed, the process include an explanation for the dissolution of the halite, yet it is more reasonable that greater amount of halite would have been preserved in the section. Neev and Emery, 1995 investigated a core drilled in the southern basin of the Dead Sea. They found at least eight episodes of halite precipitation during the Lisan time interval in this core, with a total thickness of several meters. They suggested to correlate these salt units with dry climatic periods in the Dead Sea basin. The southern basin is as well a restricted plain, raised above the northern basin

with an average height of ~380 to 400 m bmsl. Today, this area is used as a convenient flooding plain for the Dead Sea Works evaporation ponds while in the past it was suggested to serve as a natural location for residual lakes that pooled during periods of lake level drop that were recede below the elevation of the southern basin (Neev and Emery, 1995; Machlus, 1996). After regaining positive water balance the lake reflooded the southern basin and the deposited halite potentially could have dissolve. The notable amount of halite that preserved in the Lisan sediments of the southern basin support the claim that the amount of halite in the PZ-1 section seems too little.

Furthermore, this model excludes the PZ-1 and Mt. Sedom sediments as integral part of Lake Lisan and suggests that portions of the middle section were deposited in a restricted environment. PZ-1 outcrop was extensively investigated in many previous works that treated its sediments as integral part of Lake Lisan (e.g., Machlus, 1996; Marco et al., 1996; Ron et al., 2006; Haase-Schramm et al., 2004; Stein et al., 1997; Haliva-Cohen et al., 2012). It will be highly unreasonable to deduce that all of these works actually investigated the sediments of a residual lake and their conclusions regard Lake Lisan were actually related to this residual lake.

Furthermore, The main feature of the residual lake mechanism is that it is local and could have occur only in areas that meet the required conditions. The flat topography of Amiaz Plain and similar places as the southern basin are obligated, while the coincidence correlated rise of Mt. Sedom seems to have played a key role in the formation of the marginal basin. These restrictions impose that soluble salts records from additional sites, that do not satisfy these terms, will show different behavior in their chemistry.

Soluble salts or sediments' chemistry were investigated in several additional marginal sites. Published data include soluble salts chemistry in the M1 outcrop located at the foot of the Masada archeological site (Katz and Kolodny, 1989; Torfstein, 2008) and chemistry of aragonite, detritus and bulk sediments from Masada M1 section and various additional sites (Katz et al., 1977; Machlus, 1996; Stein et al., 1997; Katz and Kolodny, 1989; Torfstein, 2008). Unpublished data include soluble salts chemistry from a Lisan outcrop in Lisan peninsula, first published in this work (achieved in a work of Amitai Katz and Mordechai Stein). A description of this outcrop can be found in Bartov, 1999. The chronology of the section at the Lisan Peninsula is not well established as the Haase-Schramm et al., (2004) age-heigh model of PZ-1. Nevertheless, the soluble salts' profiles from this site show some similarities to the PZ-1 and Mt. Sedom data (Fig. 26 A-C).

The $\frac{Na}{Cl}$ and $\frac{Br}{Cl}$ soluble salts records of the Lisan Peninsula section exhibit values within almost the same range as the PZ-1 values, ~0.08-1 and ~0-0.011 respectively (Fig. 26 A&B). These ratios vary with the similar frequent and pronounced behavior. The $\frac{Na}{Cl}$ values measured by Katz and Kolodny, (1989) in

soluble salts extracted from bulk sediments in M1 section variate in a similar range between 0.158 to 0.878. The samples number is little in this work, so the trend is not clear. Although having only few $\frac{Na}{Cl}$ values of the soluble salts along M1 section there are several comprehensive works that analyzed the chemical composition of sediments in this outcrop which demonstrate its similarity to PZ-1 and Mt. Sedom chemistry. If indeed the middle and upper sections of PZ-1 partly precipitated from a marginal separated lake some signature of this separation would be expected to reflect in its sediments, and accordingly its chemical record should show some discrepancies relative to remote sites. Nevertheless, the chemical correlation between PZ-1 to M1 and additional outcrops is remarkable. Machlus, (1996) measured the $\frac{Na}{Ca}$ and $\frac{Sr}{Ca}$ ratios in acid dissolved aragonite from PZ-1 and compared it to the equivalent ratios in M1 and Deir Shaman, measured by (Katz et al., 1977) (Fig. 5 in the introduction). This comparison reveals the highly similar trends and range of values of these ratios in the two sites, while the small variations in values were suggested to express analytical differences. Adi Torfstein measured as well the $\frac{Sr}{Ca}$ in acid dissolved aragonite from M1, as part of his PhD. He also received good accordance with Katz et al., (1977) M1 and Machlus, (1996) PZ-1 trends, and great similarity in its values. Katz et al., (1977) suggested that since the distribution coefficient of Sr between the brine and the aragonite crystals is ~1 and it is almost not dependent on salinity and temperature so the $\frac{Sr}{Ca}$ values in aragonite that precipitated from the brine represent the original ratio in the brine. The similarities in the $\frac{Na}{Ca}$ are reflected mainly in the highly correlated values since the trend is very noisy in all sections. This ratio was suggested to reflect salinity variations in the brine since the distribution coefficient of sodium between the brine and the aragonite crystals is salinity dependent (Katz et al., 1977; Machlus, 1996). Hence, the high similarity in the $\frac{Sr}{Ca}$ and $\frac{Na}{Ca}$ between the different sites suggest that the brine composition and salinity in the area of these sites were similar along the Lisan period.

In conclusion, the residual lake mechanism seems to valid in the Amiaz Plain-Mt. Sedom area as a secondary process that influenced the interstitial soluble salts.

At the time the Lower Member of the Lisan precipitated in PZ-1 the eastern side of the modern Amiaz Plain was too low to consist as a barrier and water could not pool atop the area during periods of descended lake level. This period was relatively wet and characterized with high lake level Bartov et al., (2002) and an undersaturated epilimnion that dissolved halite, which provided the high $\frac{Na}{Cl}$/low $\frac{Br}{Cl}$, $\frac{Mg}{Cl}$ values in the epilimnion. The period of the Middle Member was drier and less stable (Torfstein et al., 2015). By that time the Mt. Sedom salt diapir already aligned with the elevation of Amiaz Plain and

created a natural barrier that allowed the epilimnion brine to pool while the lake withdrew from the area. When formed, the residual lake covered both the area of Amiaz Plain and Mt. Sedom region, and when dried out reached halite saturation and precipitated this salt. After the lake level rose again most of the halite dissolved and this salt was removed from the sediments section. This process is evident by the advanced evaporation sequence at 35 ka BP in PZ-1 and probably occurred several additional times, but apparently not as many as the soluble salts data suggest by its $\frac{Na}{Cl}$ negative and $\frac{Br}{Cl}$, $\frac{Mg}{Cl}$ positive peaks.

During the deposition of the Upper Member Mt. Sedom diapir was already too high to allow water to accumulate on its peaks. Thus, the potential area for the residual lake shrank to the modern area of Amiaz Plain while on top of Mt. Sedom undersaturated brine dissolved halite from the diapir during periods of high lake level but retreat when lake level dropped.

In any case, the residual lake mechanism was not the solitary process that created the observed soluble salts values and trends in the marginal terraces. The restricted process of the residual lake is illustrated in Figure 21.

(Note: The $\frac{Mg}{Cl}$ ratio of the Lisan Peninsula oscillate frequently, as the other ratios, although the values are confined within the range of ~0-0.09 (Fig. 26 C). This range resembles the $\frac{Mg}{Cl}$ range of values in the lower half of PZ-1. The Lisan Peninsula section that presented here is thought to represent the lower section of the Lisan Fm. (Bartov, 1999). This observation suggests that the soluble salts Mg data of the lower half of PZ-1 may be correct. This work do not discuss whether this hypothesis is true or not and what mechanisms could have caused such a dramatic rise in the Mg content of the brine in the middle of the last glacial period).

3) <u>Diagenetic processes:</u> The third optional process that could influence the soluble salts chemistry is a diagenetic process that occurred after the deposition of the sediments. Such a diagenetic process would have to explain the high and low values and the frequent variations in the $\frac{Na}{Cl}$, $\frac{Br}{Cl}$ and $\frac{Mg}{Cl}$ profiles of PZ-1, Mt. Sedom and additional sites as Lisan peninsula and M1.

Katz and Kolodny, (1989) suggested that exposed sediments lose interstitial brine due to evaporation, while the water dry out faster from porous layers such as detritus and sand than from low permeability sediments such as aragonite. The evaporated brine reaches halite saturation and this salt crystalize in the pores. Due to the halite crystallization the $\frac{Na}{Cl}$ ratio drops and $\frac{Br}{Cl}$, $\frac{Mg}{Cl}$ rise and can reach values that are much lower/higher than the original values in the brine of the lake that the sediments precipitated from. In addition, a compensation diffusive flux of ions occur from the aragonite pores to the adjacent porous detritus or sand due to the non-uniform evaporation rate. This flux leads to a further reduce in the $\frac{Na}{Cl}$ and

a rise in the $\frac{Br}{Cl}, \frac{Mg}{Cl}$ values of the soluble salts in the aragonite. After the interstitial brine dried out completely this diagenetic process is ceased.

In the low permeable sections of the Lisan's, such as the aad sections, this process would be very slow. In sections with high content of clastic porous sediments, such as the Lisan's Middle Member, brine could evaporate and flow out of the pores more easily and hence it is likely that once exposed the process in such sediments will be more advanced.

Such a process would be expected to influence all the exposed marginal sediments of the Lisan Fm., with enhanced influence in more porous units. Furthermore, its influence will be expected to increase in sediments that are fully desiccated relative to recently exposed sediments. In accordance, it is supposed that in sediments that never exposed, this process is yet to occur. An examination of the soluble salts data strongly supports this scenario. First, the soluble salts ratios from different marginal sites show great resemblance between them, both in values' range and in the frequently variated behavior. This resemblance reinforces the diagenetic process feasibility due to its general validity in the marginal sediments. Second, the soluble salts data of PZ-1 and Mt. Sedom clearly present the influence of the porous sediments on this process. The lower and upper sections show $\frac{Na}{Cl}$ values that are more confined and higher, on average, than those of the middle section and also seems more stable. These differences are in accordance with the lithology of the members. The high clastic content of the Middle Member supports the more advanced influence of the diagenetic process in its sediments.

Another observation that agrees with the diagenetic process comes from the shallow and deep cores' data. It can be noticed that the $\frac{Na}{Cl}$ data of the shallow core of 40-11 ka BP is constantly lower than the deep core values, while the gap increase as the samples are more recent. $\frac{Br}{Cl}$ and $\frac{Mg}{Cl}$ data show the same (mirror) behavior. The shallow core sediments were exposed for limited periods before drilled, mostly along the Holocene, as known from the lithology of this core (Coianiz et al., 2019 & Corelyzer scans) and from the lake level curve (Torfstein et al., 2013; Bartov et al., 2002). It is likely to deduce that the deeper sediments of the shallow core (data points of 82 ka BP and older) were already buried beneath younger sediments until the location of the core was occasionally exposed, and therefore brine evaporation did not occur in these sediments, and they kept pristine. The younger sediments, on the other hand, were subjected to some brine evaporation due to exposure of the sediments to the atmosphere. The younger the sediments are, the more advanced its degree of desiccation due to their higher position in the core and proximity to the surface. The incomplete dry out initiate some halite crystallization in the pores, out of the drying brine and, in accordance, slightly reduced the $\frac{Na}{Cl}$ and increased the $\frac{Br}{Cl}, \frac{Mg}{Cl}$ values

in the soluble salts. The more advanced the dry out of the brine in the sediments, the greater the influence on the soluble salts' values. This hypothesis is further reinforced by the deep core data (both soluble salts and pore fluids) that shows a highly stable trend, without significant variations. These sediments were first exposed to the atmosphere during drilling and indeed their chemical behavior suggest that they were not influenced by evaporation and diagenetic processes.

To conclude, a diagenetic process of interstitial brine evaporation and halite crystallization in the pores seems the reasonable and main cause for low soluble salts values of $\frac{Na}{Cl}$ and high values of $\frac{Br}{Cl}$ and $\frac{Mg}{Cl}$ in sediments that exposed to the atmosphere. The earlier the exposure occurred, and the more porous the sediments are, the greater the influence of this diagenetic process on the chemistry of the soluble salts.

Differences between the $\frac{Na}{Cl}$ to the $\frac{Br}{Cl}$ & $\frac{Mg}{Cl}$ ratios: Additional observation that seems to require an interpretation is that despite showing great similarities, the $\frac{Br}{Cl}$ and $\frac{Mg}{Cl}$ marginal data does not show an exact mirror pattern as the $\frac{Na}{Cl}$, but rather show some differences that seem to be significant.

Many of the $\frac{Na}{Cl}$ values in the middle section are lower than the deep and shallow cores data and demonstrate large amplitude of variation, with negative peaks that get almost to 0. The coeval $\frac{Br}{Cl}$ however does not show an exact mirror pattern. Most of the $\frac{Br}{Cl}$ data located beneath the deep and shallow cores' data with few peaks that rise up above them. In the $\frac{Mg}{Cl}$ data even the highest peaks of the middle section does not exceed the deep and shallow cores' data.

This difference is most likely due to the Ca-chloride composition of the brine and the dynamics of halite precipitation. When halite extensively precipitates the Na in the remained brine can reaches to very low and even close to zero concentrations while the Cl reduces as well but its concentrations remain significantly higher. The Br and Mg on the other hand do not participate in the process and their concentrations in the brine remain steady. In such case the $\frac{Na}{Cl}$ values will drop down sharply and could reach close to zero while the $\frac{Br}{Cl}$ and $\frac{Mg}{Cl}$ will rise but not in a proportional way to the $\frac{Na}{Cl}$.

Therefore, it is suggested here that the rising peaks in the $\frac{Br}{Cl}$ values are the consequence of advanced evaporation that reached halite saturation in one of the two suggested mechanisms. At the same time, saturation of Br and Mg salts was not obtained or dwarfed by the halite precipitation that its reduced Cl dominant the ratio. A distinct and significant peak is observed at 35 ka BP that perfectly coincide with the sequence of advanced evaporation that was observed by Machlus, (1996) in PZ-1 section. It supports

the formation of a residual lake on Amiaz Plain at that time which reached advanced degrees of desiccation. The $\frac{Br}{Cl}$ value during this spell is ~0.01 which resembles the values during the last interglacial and the Holocene. Additional such high peaks are a testimony for highly advanced evaporation of the brine while lower peaks are an evidence for slightly milder evaporation processes, but still progressed enough to precipitate halite.

A similar picture is seen in the upper section of PZ-1, although in this case the data is clearly lower than the deep and shallow cores. This observation is in accordance with the rainier climate of this period, its high and stable lake level, the higher rate of halite dissolution (testified by the $\frac{Na}{Cl}$ data of this work and previous works (Levy et al., 2017, 2018; Lazar et al., 2014) and the low permeable sediments of this section.

The constant gap between the $\frac{Mg}{Cl}$ marginal data to the deep and shallow data may be due to the lower $\frac{Mg}{Cl}$ ratio in the epilimnion compare to the hypolimnion.

When observed in its entirety, the $\frac{Br}{Cl}$ record of PZ-1 seems to represent the general development of Lake Lisan better than the $\frac{Na}{Cl}$. Its mean trend shows the gradual freshening process of the lake.

The consequences of halite precipitation in the residual lake or in the pores after exposure of the sediments do create noise in the data, although, it left the $\frac{Br}{Cl}$ record of PZ-1 as a good representative of the development of the lake's brine. On the opposing side, the influence of halite precipitation on the $\frac{Na}{Cl}$ record seems to blur the original behavior of the brine (mostly during MIS 3) and hence to reflect a deceiving picture.

7.2.4. Mixing process in the epilimnion

Auxiliary plots of Na against Cl are used. These plots reveal some processes that took place in the lake and can also provide some clues regard the discussed three scenarios which could have influence the chemical properties of the soluble salts (Figure 22 A-C). The data of PZ-1 is presented, divided into the three sections. In each plot the data is distinguished between values that are higher and lower than the equivalent $\frac{Na}{Cl}$ value of the deep core, which determined as 0.45 for lower and middle sections and 0.52 for upper section. These plots display a distinct behavior. Data points that are higher than the coeval deep core values arrange on a linear line while points with lower values whether fit to the same linear line or sit below it without a clear order and with relatively low concentrations of Cl and even lower Na.

1. Configuration during deposition of Lake Lisan's **Lower** Member:

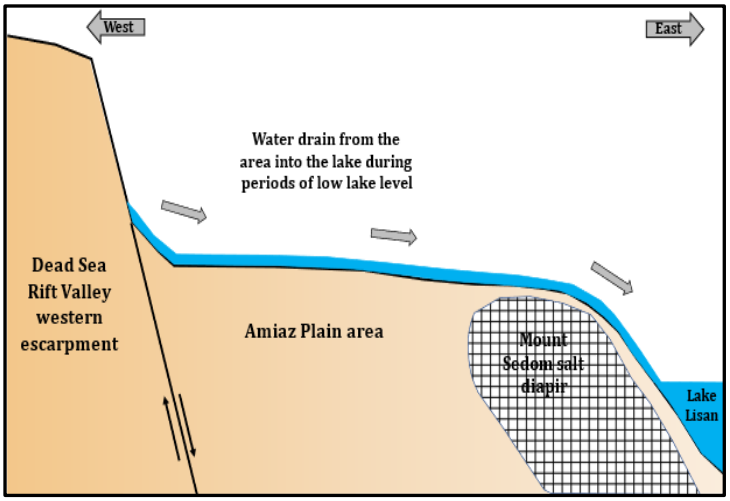

2. Configuration during deposition of Lake Lisan's **Middle** Member:

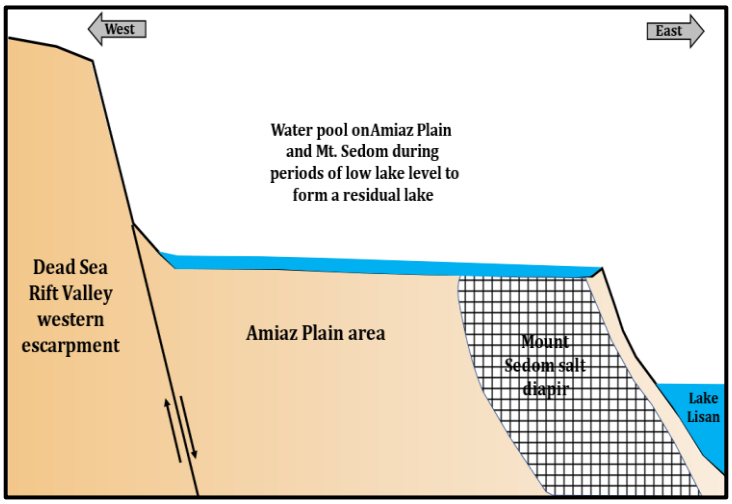

3. Configuration during deposition of Lake Lisan's **Upper** Member:

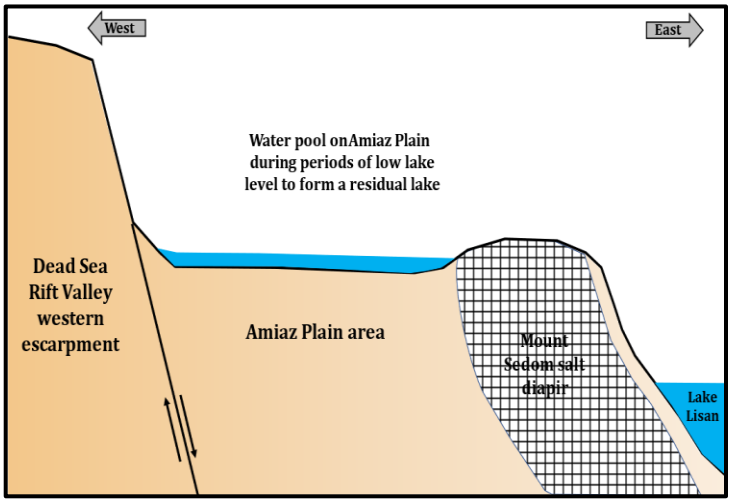

Figure 21: A schematic illustration of the geologic configuration that allowed the formation of a residual lake in the area of Amiaz Plain, as suggested in the text. 1. During the deposition of the lower member the diapir of Mt. Sedom was too low and water could not pool on the area. 2. Until the middle member was deposited Mt. Sedom aligned with Amiaz Plain and a residual lake could pool on the Plain during periods of low lake level. 3. At the time the upper member deposited the diapir of Mt. Sedom was too high and residual lake could form only upon the area of the modern Amiaz Plain. All three scenarios show the configuration during arid periods when lake level was lower than the elevation of Amiaz Plain. During wet periods with high lake level the salt diapir of Mt. Sedom supplied available halite for dissolution by the undersaturated brine of the lake.

In the lower section (Fig. 22 A) all values are higher than the deep core values thus they all correspond to a linear line with a fit of $R^2 = 0.9849$. The slope of the line is 0.6654 and it intersect at X=0, Y=0.311. In the middle section (Fig. 22 B) the data is less ordered. High values correspond to a liner line with fit of $R^2 = 0.8932$, a slope of 0.9049 and intersect at X=0, Y=-1.6567. Low values partly fit to the line or very close it while the rest sit beneath it, some with very low content of Na. In the upper section (Fig. 22 C) the high values fit well to a liner line with $R^2 = 0.9809$, slope of 0.8755 and intersect at X=0, Y=-23.63. Low values mostly fit to the line as well or slightly lower than it but show a distinct reduced content of Na and Cl relative to the high values.

An interpretation for these observations can be the following: the linear lines of the high values in all three sections are interpreted as mixing lines between two endmembers. The $\frac{Na}{Cl}$ values of the endmembers can be achieved from the edge of each line, as presented on the graphs. These values reveal that mixing occurred between a source with high $\frac{Na}{Cl}$ values (0.8-0.95) to a source with intermediate values (0.45-0.65). The intersect of the line in the lower section suggest that in this case it is a dilution line rather than a mixing line since the low end-member is highly poor in ions. Such a source can be freshwater with low salinity that used to wash into the lake. It could be that these waters entered the lake with high $\frac{Na}{Cl}$ value (~0.8), as occur today ($\frac{Na}{Cl}$ value in modern freshwater tributaries is ~1. Stein et al., 1997), or that they dissolved halite once entered the lake and gained the high values by that. The second end member hold a $\frac{Na}{Cl}$ value of 0.65 that is closer to the value of the hypolimnion, though slightly higher. Such a source could have been the diluted epilimnion brine that dissolved halite and gained a higher $\frac{Na}{Cl}$ value relative to the hypolimnion.

In light of that, the lower section of the Lisan Fm. deposited in the lake's margins from an epilimnion that was more diluted than the hypolimnion and hence was able to dissolve greater amounts of halite.

It constantly mixed with incoming freshwater that arrived with high $\frac{Na}{Cl}$ or gained it in the lake after halite dissolution. These sediments were not strongly influenced by the diagenetic processes due to the high content of low permeable sediments (*aad*) and since being the lowest sediments in the section and accordingly the most recent to expose to the atmosphere and desiccate. Drops in the $\frac{Na}{Cl}$ along this section can be part of the original mixing process with a period of dominance of the epilimnion source over the freshwater or a late diagenetic dry out that did occur and led to halite crystallization in the pores.

The middle section shows a more complex scenario. The high values present a mixing process as well that involved a source with high $\frac{Na}{Cl}$ value of 0.95 with a low $\frac{Na}{Cl}$ source of ~0.45 and possibly even lower

(since the threshold of 0.45 was an artificial approximation). This liner line seems to represent a similar mixing process between freshwater and brine. In this case the low end-member source could have been a more concentrated epilimnion (compare to the lower member), the hypolimnion itself and maybe there is some donation of the saline springs (with low $\frac{Na}{Cl}$ of ~0.32 by Weber et al., 2018) that used to discharge into the lake during episodes of low lake level that were common along this period (Torfstein et al., 2013). The lower fit to linear behavior in this period suggests that the mixing process was more complex than linear between two components. Several data points with low $\frac{Na}{Cl}$ may still fit to the mixing line but the majority of them show a clear shortage in Na and seemingly also Cl. These low and non-linear values could be the result of advanced halite precipitation in a residual lake or a late change of an originally linear fit values that were reduced and disordered by a diagenetic dry up and interstitial halite precipitation.

The data of this section also shows that as the Cl was reduced in samples with values lower than the deep core, its concentrations remained relatively much higher than the Na that gets close to zero in several samples. This observation reinforce a previous conclusion regard the impact of halite dissolution on $\frac{Na}{Cl}$ ratios that can lead to very low values while $\frac{Br}{Cl}$ and $\frac{Mg}{Cl}$ are less effected and their rise is more moderate when halite precipitate.

The upper section exhibits a similar scenario. Samples with values higher than 0.52 show good linear fit and support the same mixing scenario. The lower limit of this group was set to be 0.52, as the extrapolated pore fluids data of this section, but the lower end-member in this case holds a $\frac{Na}{Cl}$ value of 0.56 that correlate with the coeval soluble salts mean values. It may suggest that 0.56 was indeed the value of the deep brine at that time which served as the low endmember for the mixing process of the epilimnion. In samples with values lower than 0.52, data points that sit on the mixing line can vary well be part of the original mixing process. The several samples that sit a bit lower than the mixing line may affected by diagenetic or residual lake halite precipitation. During the period of the upper section Lake Lisan was in its highest position and hence there were much fewer opportunities for a residual lake to form on Amiaz Plain or for halite to crystallize in the pores (due to the low preamble sediments). In accordance, the $\frac{Na}{Cl}$ rarely drops below 0.4 and shows a more stable behavior.

According to these observations an additional conclusion is suggested. Weber et al., (2018) dated Ein Qedem brine with radiocarbon and radiokrypton methods. This brine is thought to be an ancient lake's epilimnion that penetrated into the adjacent aquifers during periods of high lake level (Weber et al., 2018; Torfstein et al., 2008). According to the received ages they estimated that Lake Lisan brine penetrated

into the adjacent aquifers during the high stand period of the Lisan (~31–17.4 ka). In addition, Weber et al., (2018) measured the $\frac{Na}{Cl}$ ratio in Ein Qedem brine and found it to be ~0.3-0.32.

According to that, discharge of saline springs could have been part of the mixing process in the epilimnion only until the onset of the upper member period (~30 ka BP). Such a discharge could have lowered the $\frac{Na}{Cl}$ values of the epilimnion down to 0.3-0.32. Lower values are probably the result of the discussed scenarios. The donation of the saline springs is apparently evident during the middle member, when lake level was often low and saline springs flew into it. During the lower member period, the impact of the saline spring is not evident, possibly due to high and stable lake levels or due to empty reservoir of brine in the aquifer after the previous arid interglacial.

Figure 22: Concentrations of Na against Cl [millimolar] in the 3 sections of Lisan Fm. of PZ-1. Data is divided between values that are higher and lower than the coeval mean deep core value (set as 0.45 for lower and middle sections and 0.52 for the upper section). Trendlines of the high values are presented with their equation and R^2. Black arrows show the 1:1 route of halite precipitation to demonstrate the effect of diagenetic halite crystallization in the pores on samples that originally fit to the mixing line. Values in gray rectangles show the $\frac{\text{Na}}{\text{Cl}}$ values of the adjacent samples, which are the endmembers of the mixing lines.

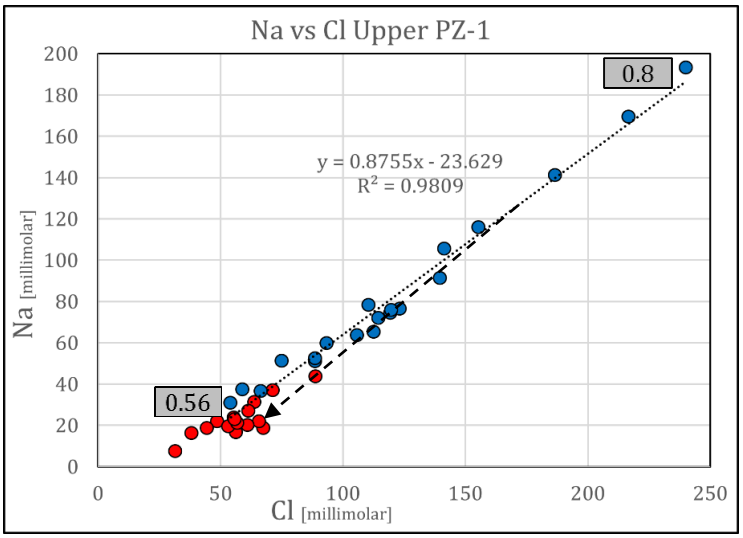

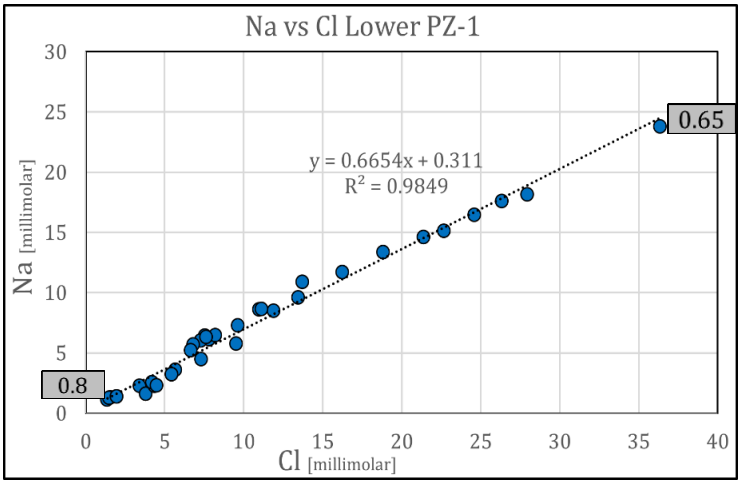

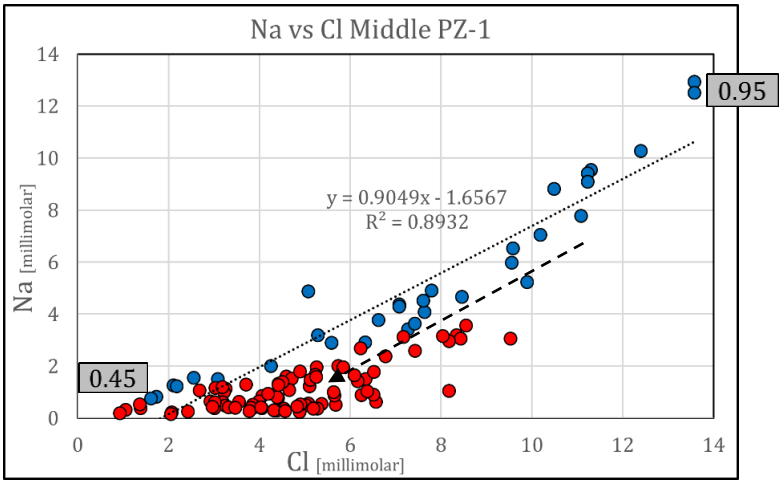

In summary, samples with $\frac{Na}{Cl}$ values that are higher/$\frac{Br}{Cl}$, $\frac{Mg}{Cl}$ values that are lower than the hypolimnion or equal to them are likely to show pristine original chemistry. This chemistry developed in Lake Lisan's epilimnion in the process of mixing between the lake's brine (deep brine or slightly diluted) with

incoming freshwater. During periods of low lake level, that were common mostly during the period of the middle section (MIS 3), saline springs discharged into the lake and, as part of the mixing process in the epilimnion, lowered its $\frac{Na}{Cl}$ and increased its $\frac{Br}{Cl}$, $\frac{Mg}{Cl}$ values. Samples with $\frac{Na}{Cl}$ values that are lower than the saline springs values (~0.3-0.32) testify on two possible processes. The main process is halite crystallization in the sediments' pores due to exposure and brine evaporation. In the specific case of Perazim Valley and Mt. Sedom sediments, several lower peaks could be the result of advanced halite precipitation in the residual lake of Amiaz plain.

7.2.5. Mixing process in the hypolimnion

Plots of Na against Cl of the deep core data are used in order to learn whether similar mixing processes controlled the development of the hypolimnion (Fig. 23). The data is roughly divided into the equivalent periods of the Lisan's three members: 98-60, 60-30, 30-14 ka BP. Figure 23 clearly shows that the data of each member fit to a linear line. The lower member fit is $R^2 = 0.9964$, the slope of the line is 0.3316 and it intersect at X=0, Y=4.15. The middle member fit is $R^2 = 0.9986$, the slope is 0.4496 and it intersect at X=0, Y=0.13. The upper member fit is $R^2 = 0.9877$, its slope is 0.5573 and it intersect at -1.21. All three lines originate from a similar origin.

The three linear lines are interpreted as mixing lines that describe the chemical development of the deep brine. It is suggested here that these lines reveal that the deep brine of Lake Lisan developed as well through a mixing process which occurred predominantly between two main components. It can be seen that the lower member begins with lower $\frac{Na}{Cl}$ values, inherited from the preceding arid interglacial. From there the $\frac{Na}{Cl}$ values increase along the mixing lines, each member with higher values.

Sirota et al., (2018) suggested that in a lake with stratified water column, diffusive fluxes occur between the upper and the lower brines. This model accounts for a halite-saturated hypersaline lake although it is highly reasonable that such fluxes will also occur between two brines with salinity gradient, even if both of them are undersaturated with respect to halite. Lazar et al., (2014) mentioned the turbulent mixing across the epilimnion-hypolimnion interface. It is suggested here that in the stratified Lake Lisan such diffusive fluxes and mixing took place between the diluted epilimnion to the more saline hypolimnion. By this process the higher $\frac{Na}{Cl}$ values of the epilimnion gradually assimilated in the hypolimnion and raised its values. This process strongly buffered the frequent chemical variations of the upper brine and delivered to the deeper brine only the average outcome of the various surface processes that influenced the epilimnion.

Another similar mechanism was suggested by Levy et al., (2019) that showed how halite used to dissolve from the salt diapir of Mt. Sedom by the undersaturated epilimnion of Lake Lisan. This dissolution rose the $\frac{Na}{Cl}$ value of the dissolving brine and increased its salinity and therefore also its density. This dense brine used to flow to the deep basin due to gravity and over there it mixed with the deep brine. Such a mechanism could decrease the $\frac{Na}{Cl}$ value of the hypolimnion along the Lisan period and hence could have been part of the mixing process that controlled the chemical development of the hypolimnion. It is reasonable that this process occurred simultaneously with the diffusive fluxes and mixing along the brines interface.

According to that, the hypolimnion of Lake Lisan developed along the last glacial period by mixing between the saline and concentrated deep brine, that was isolated from the surface to the overlaid epilimnion that in general held a higher $\frac{Na}{Cl}$ values. This mixing carried out through diffusive fluxes and turbulent mixing between the two brines that took place along the interface of the two water bodies.

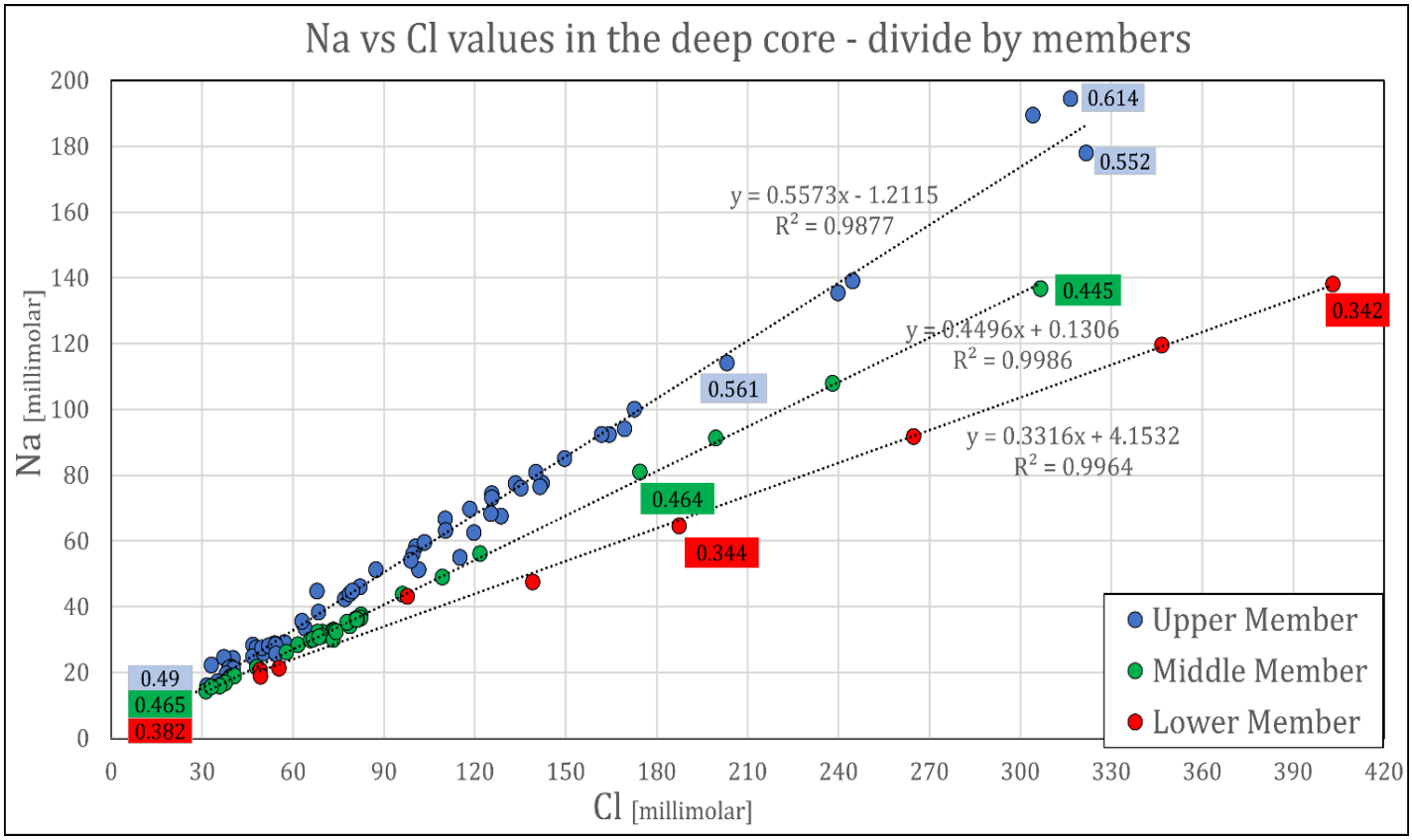

Figure 23: Concentrations of Na against Cl [millimolar] in the deep core data, divided into the three members of the Lisan Fm. Numbers in rectangles are the $\frac{Na}{Cl}$ values of the adjacent samples. Colors divide the members: red-lower member, green-middle member, blue-upper member.

At last, a plot of $\frac{Br}{Cl}$ against $\frac{Na}{Cl}$ is presented (Fig. 24), showing several of the discussed processes from a different perspective, and combining the $\frac{Br}{Cl}$ that reinforce these processes.

Zilberman et al., (2017) conducted several experiments that followed the chemical composition of evaporation Dead Sea and Ein Qedem brines, in terms of $\frac{Br}{Cl}$ vs $\frac{Na}{Cl}$ (Fig. 24).

These two groups of data are similar, and both show the advancement of the brines' chemical composition along the linear section that reflects the chemical development of the brines once halite began to precipitate. It can be seen that the Dead Sea brine precipitation path begins at $\frac{Na}{Cl} = \sim 0.24$ and $\frac{Br}{Cl} = \sim 0.011$ while Ein Qedem brine precipitation path begins at $\frac{Na}{Cl} = \sim 0.32 - 0.34$ and $\frac{Br}{Cl} = \sim 0.01$. As the halite precipitation proceed the $\frac{Na}{Cl}$ values decreased and the $\frac{Br}{Cl}$ values increased along the same linear path. After the precipitation process proceed the $\frac{Na}{Cl}$ of ~0.03 and $\frac{Br}{Cl}$ of ~0.014 in the residual brine the trend become steeper and turn to climb up along the $\frac{Br}{Cl}$ axis. The behavior of the data in this section is controlled predominantly by halite precipitation but could be influenced by the precipitation of additional, more advanced salts.

Soluble salts and pore fluids data from the deep core are presented on this graph together with PZ-1 soluble salts, divided to its 3 sections. The deep core soluble salts data covers the period of ~100-11 ka BP that was investigated by the deep core sediments, while the pore fluids data covers the period of ~150-11 ka BP that was investigated by the deep and shallow cores.

By extrapolating the linear line of Dead Sea and Ein Qedem precipitation path it crosses the deep core data and lower section of PZ-1 and shows a good fit both to the soluble salts and pore fluids. When drawn to the reversed direction and stretches between $\frac{Na}{Cl}$ =0 to 1 this line shows the complete linear path of halite precipitation-dissolution since these two processes follows the same 1:1 ratio of subtraction-addition of Cl and Na, respectively.

The fit of the deep core data to this linear line supports the gradual freshening of the hypolimnion that occurred in the lake since the end of the last interglacial and throughout the last glacial that induced halite dissolution in the lake. This dissolution is evident by the advancement of the deep core data from the edges of the Dead Sea and Ein Qeden data to the opposite direction on the precipitation-dissolution linear line. The fit of the lower section of PZ-1 to the linear line on the other edge of the deep core data may suggest that these were the $\frac{Na}{Cl}$ and $\frac{Br}{Cl}$ values of the epilimnion, which was more diluted and reached higher degrees of halite dissolution. The observation of the deep core data located between the diluted

values of the epilimnion to the concentrated values of the brine supports the mixing processes that dictated the development of the hypolimnion. These mixing processes provide a gradual smooth picture of halite dissolution in the hypolimnion.

The middle and upper sections of PZ-1 data mostly do not fit to the dissolution-precipitation line but rather located below it with a notable scatter. The cause for the deviation from the line and the scatter of the data cannot be certainly determined. A highly similar scatter of the Lisan Peninsula soluble salts data (Fig. 25) beneath the same linear line may suggest that it is mostly the diagenetic desiccation of the pore brine that led to the scatter and maybe also to deviation from an original fit to the linear line, due to the general validity of this process in the exposed marginal sediments of Lake Lisan. It seems that these are mostly the $\frac{Br}{Cl}$ values that were reduced in these samples (several samples of the Lisan Peninsula reach $\frac{Br}{Cl}$ values of zero) while the change in the $\frac{Na}{Cl}$ is milder. A process that leads to reduce in the $\frac{Br}{Cl}$ value in the soluble salts without having a proportional influence on the $\frac{Na}{Cl}$ values is not clear and such a mechanism is not suggested here.

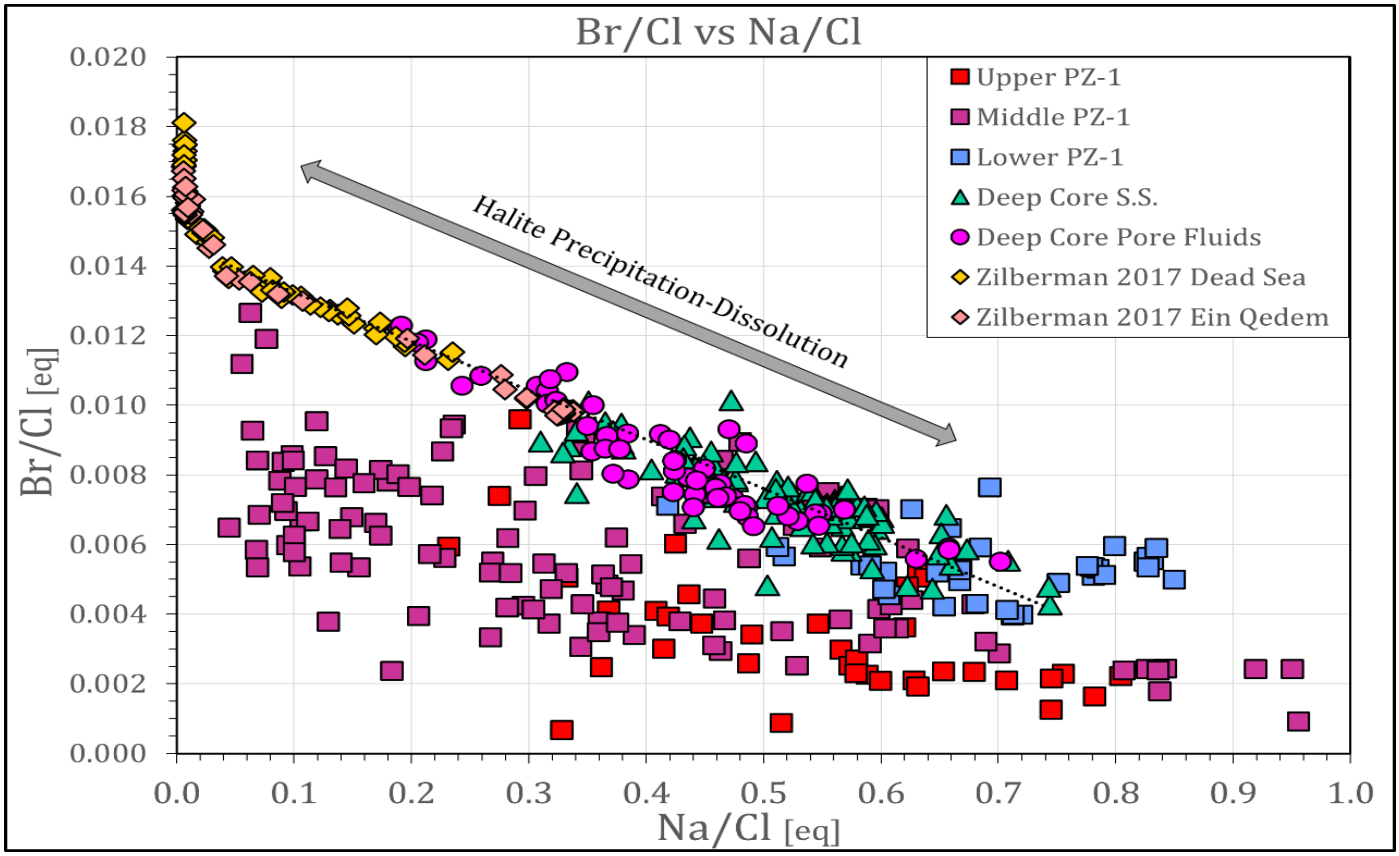

Figure 24: Soluble slats values of $\frac{Br}{Cl}$ vs $\frac{Na}{Cl}$ from the deep core and PZ-1, together with pore fluids data from the deep core. Dead Sea and Ein Qedem evaporation paths are attached from the work of Zilberman et al., (2017). The linear line shows the path of brines that precipitate or dissolve halite. Deep core and lower PZ-1 show good fit to the line while middle and upper PZ-1 data is scattered beneath it.

Figure 25: Soluble salts values of $\frac{Br}{Cl}$ vs $\frac{Na}{Cl}$ from the Lisan Peninsula. The linear line is the same line as in Fig. 24, showing the path of brines that precipitate or dissolve halite.

The data is scattered without a clear trend, but it all confined beneath the linear line.

Several samples with exceptionally low $\frac{\mathrm{Br}}{\mathrm{Cl}}$ values suggest that these are mainly these values that were reduced and led to the scatter.

This data achieved by Amitai Katz and Mordechai Stein and it is first published here.

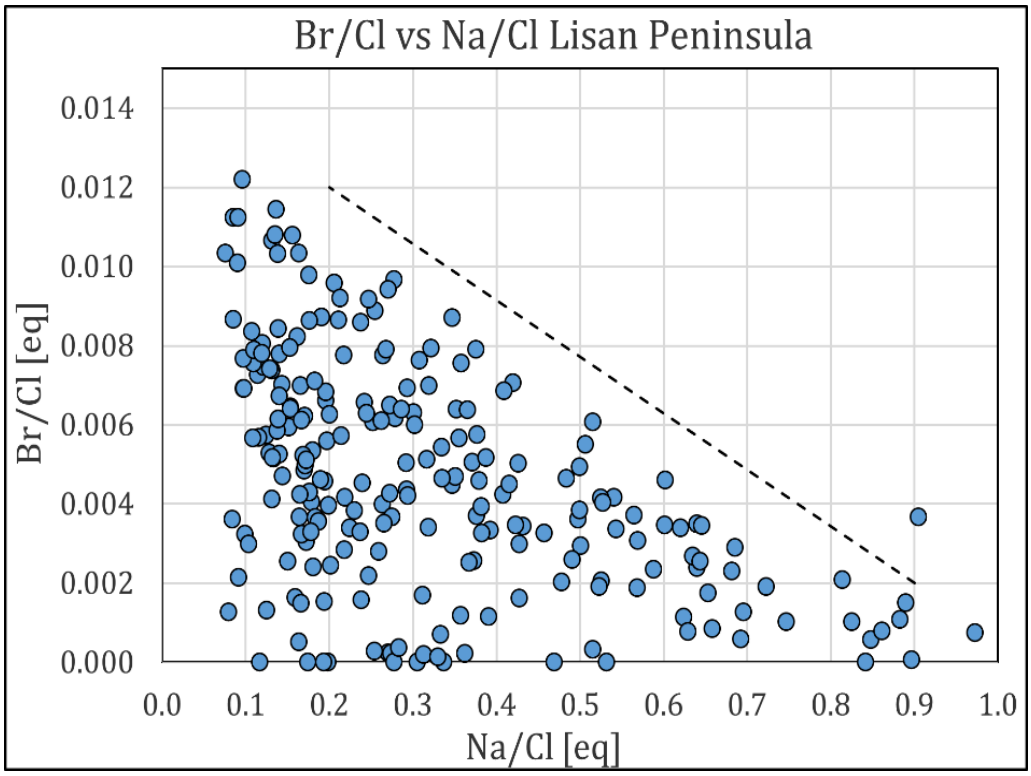

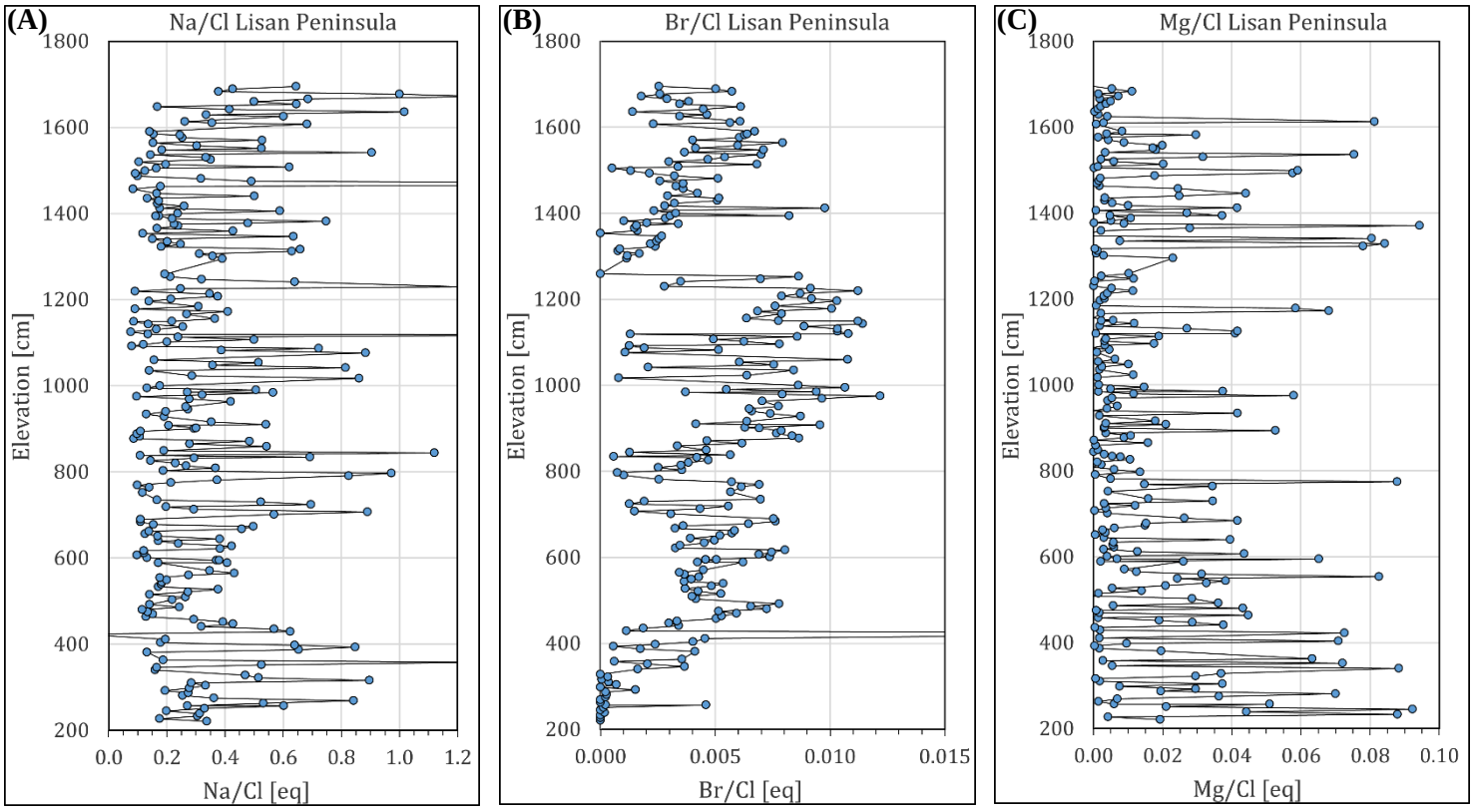

Figure 26: Ion ratios of soluble salts data that received from an outcrop of the Lisan Fm. in Lisan Peninsula (data first published here). All ratios are in equivalent. The chronology of this section is sparse, yet it seems to correlate with the Lower and Middle Members of the formation. (A) $\frac{Na}{Cl}$ ratio. (B) $\frac{Br}{Cl}$ ratio (C) $\frac{Mg}{Cl}$ ratio.

For additional details of this outcrop see Bartov, (1999).

7.3. Summary

This chapter establishes a high-resolution reconstruction of the chemical evolution of Lake Lisan's brine and former lakes of the DSB in their deep, intermediate, and marginal environments by using the ratios $\frac{Na}{Cl}$, $\frac{Mg}{Cl}$ and $\frac{Br}{Cl}$. These ratios were found in the previous chapter to be reliable tools for reconstructions of brine's composition. The main conclusions of this chapter are:

1. The $\frac{Na}{Cl}$ values of the soluble salts in the 5017-1-A deep core were found to steadily rise from 0.3, 100 ka ago to 0.7 at 12 ka BP, and then dropped sharply to 0.48 at 11 ka BP. $\frac{Mg}{Cl}$ and $\frac{Br}{Cl}$ ratios exhibit a mirror pattern during the same period, with $\frac{Mg}{Cl}$ values dropping from 0.5 to 0.2 and then peaking to 0.43 and $\frac{Br}{Cl}$ dropping from 0.01 to 0.005 and peaking to 0.008. The long-term variations of these ratios reveal the major wet climatic conditions in the drainage basin of the Lake Lisan during the last glacial period that led to its continuous dilution. This, in turn, induced dissolution of exposed halite in the lake, mainly from the emerging salt diapir of Mt. Sedom, that result in the accumulation of Na and Cl ions in the brine. Short-term variations reveal the sensitivity of these ratios and their ability to document changes in the lake that induced by significant climatic events that deviate from the general trend and last several thousand years, such as Heinrich events, glacial maximums, and the Younger Dryas.
2. The $\frac{Na}{Cl}$ values of the soluble salts in the 5017-3-C shallow core were found to variate in the range of 0.45-0.53 during the climax of the penultimate glacial (MIS 6) with a good correlation to the coeval pore fluids values. During the following interglacial of MIS 5 the shallow core values remain steady while the pore fluids of the deep core dropped dramatically to a minimum of 0.2. Following (sparse) values show a gradual decrease to values that become lower than the deep core data. The $\frac{Mg}{Cl}$ and $\frac{Br}{Cl}$ ratios show similar mirror patterns with values ranging between 0.34-0.58 and 0.007-0.011, respectively. These observations suggest that during glacial periods intermediate elevations in the lake were located within the hypolimnion due to the high and stable lake level. The simultaneous behavior of the last interglacial suggests that halite precipitation patterns in Lake Samra were similar to those occur today in the Dead Sea, where halite extensively precipitate and accumulate in the deep brine, year-round, while it mildly precipitates from the upper brine and later dissolves along the year without getting to accumulate a halite section in the shallow margins (this mechanism termed 'halite focusing').
3. Marginal data of PZ-1 and Mt. Sedom White Hill reveal an oscillating, unstable behavior that usually correlates between the two sites. The $\frac{Na}{Cl}$ variate frequently within the range of 0.07-0.93 with many values the are whether significantly higher or lower than the coeval deep and shallow cores' values. The

$\frac{Br}{Cl}$ data show a similar mirror behavior, oscillating between 0.0015 to 0.011, although its range is more confined with less distinct outliers. The $\frac{Mg}{Cl}$ data (upper half) show a similar behavior as the $\frac{Br}{Cl}$ yet its values are constantly lower than the coeval deep and shallow cores' data, ranging between 0.034-0.343. A comparison between the marginal soluble salts data to the deep and shallow coeval data provides various insights. First, the data was differentiated and values that seems to come from sediments that deposited from the main lake, and thus represent original values of the lake's brine, were point out. The rest of the values, that do not represent the original chemistry of the brine, are the result of the diagenetic crystallization of halite out of the pores' brine after the sediments were exposed and desiccated. A marginal residual lake that pooled on Amiaz Plain during periods of low lake level may deposited several restricted sections which their chemistry differ from the original chemistry of the lake.

Second, the development of the epilimnion and hypolimnion were investigated. It is shown that the chemical composition of the epilimnion was controlled by mixing between freshwater that nourished the lake with high $\frac{Na}{Cl}$ values of ~0.9 to the epilimnion's brine that held an intermediate $\frac{Na}{Cl}$ value of 0.45-0.65. This brine, that was relatively diluted, locally dissolved exposed halite and its density and $\frac{Na}{Cl}$ values were increased. Turbulent mixing and diffusive fluxes across the interface between the epilimnion to the hypolimnion and sinking of the dense halite-dissolving brine led to a slow transport of upper brine, and its chemical properties, down to the hypolimnion. This deep brine maintained lower $\frac{Na}{Cl}$ values, inherited from the last interglacial, and through these mixing prosses it was gradually diluted and its $\frac{Na}{Cl}$ values ascended. This gradual mixing with the deep hypolimnion buffered many surface processes that had an influence on the upper brine and led to oscillations in its chemical composition, leaving only the mean outcome of all these processes to seepage down and mix with the deep brine. Therefore, its chemical profile is much more stable and show a secular development compare to the noisy profile of the upper brine.

8. Using Ca^{2+}, SO_4^{2-}, Sr^{2+} as proxies for dissolution of primary minerals from the sediments and NO_3^- as proxy for oxidation conditions in the lake

This chapter deals with two separate issues that together complete the discussion over the results of the soluble salts that were achieved in the scope of this work.

First it deals with the results of the elements that do participate in some dissolution of primary minerals from the sediments, (such as gypsum and aragonite), in addition to their origination from soluble salts dissolution. These ions are Ca^{2+}, SO_4^{2-} and Sr^{2+}.

Second, it deals with the results of the NO_3^- that provide its own unique insights on the lake's chemistry, limnological configuration and oxidation states in the brines.

8.1. Results

In order to investigate the behavior of the Ca, SO_4 and Sr ion ratios will be used such as $\frac{SO_4}{Cl}$, $\frac{Sr}{Cl}$ and $\frac{Sr}{Ca}$. The data of these ratios that received form the soluble salts of the deep core are provided in chapter-1 (Figure 14 C,E,F). The data of the same ratios that received from the shallow core and the marginal terraces are presented below. All of the results that include Ca, SO_4 and Sr are first presented before any correction was performed on the data.

8.1.1. Data of the 5017-3-C Shallow Core

The $\frac{Sr}{Ca}$, $\frac{SO_4}{Cl}$ and $\frac{Sr}{Cl}$ ratios in the extracted soluble salts of the shallow core are presented in figure-27 A-C. The elements in the numerators of the ratios $\frac{SO_4}{Cl}$ and $\frac{Sr}{Cl}$ originated from dissolution of interstitial soluble salts and, also, from dissolution of primary minerals of the sediments. In the $\frac{Sr}{Ca}$ ratio both elements have this characteristic. The results of the soluble salts are compared with contemporaneous pore fluids data of the deep core.

The $\frac{Sr}{Ca}$ ratio: The behavior of the $\frac{Sr}{Ca}$ ratio along the core fluctuate as compared to the pore fluids from the deep core (Fig. 27 A). Several samples show good correlation with the values of the pore fluids from the deep core while other are significantly lower or higher than them. Samples from MIS 6 (~143.4-141.5 ka BP) mostly correlate with the pore fluids data while several samples are lower than the pore fluids (~2.2-12 versus 9.2-11.7, respectively). The $\frac{Sr}{Ca}$ ratios from the peak of MIS 6 and the transition to

MIS 5 (~137-127 ka BP) are similar to the pore fluids data of the deep core or show a slight deviation (~8-12 in both sets of data). A group of samples from the dry period of MIS 5, 117.3-113.8 ka BP, are either similar to the pore fluids or higher (~14 versus 11). Two younger samples from the end of the last interglacial, ~82.5 ka BP, show values that are lower than the pore fluids (~4-5 versus 11). In a group of samples from the wet period of the last glacial, ~40.5-26.7 ka BP, the trend shifts again, and the shallow core samples display values that are higher than the pore fluids (~8-12 versus 6-8). In the youngest group of samples, which was deposited already during the Holocene, after the Younger Dryas, ~11.1 ka BP, the values are again lower than the pore fluids (~3.7 versus 10.7).

The $\frac{SO_4}{Cl}$ ratio: The soluble salts $\frac{SO_4}{Cl}$ values of the shallow core (ranging from 0.03 to 1.26) are ~2 orders of magnitude higher than that of the pore fluids from the deep core (Fig. 27 B). The majority of the data plots in the range of ~0.05-0.3 with few values that peak higher than that range. Similar behavior was observed in the soluble salts data of the deep core as well (Fig. 14 E).

The $\frac{Sr}{Cl}$ ratio: The values of this ratio in the shallow core are constantly higher than those of the pore fluids from the deep core, ranging between 0.0015 to 0.004 compare to 0.0002-0.002, respectively (Fig. 27 C).

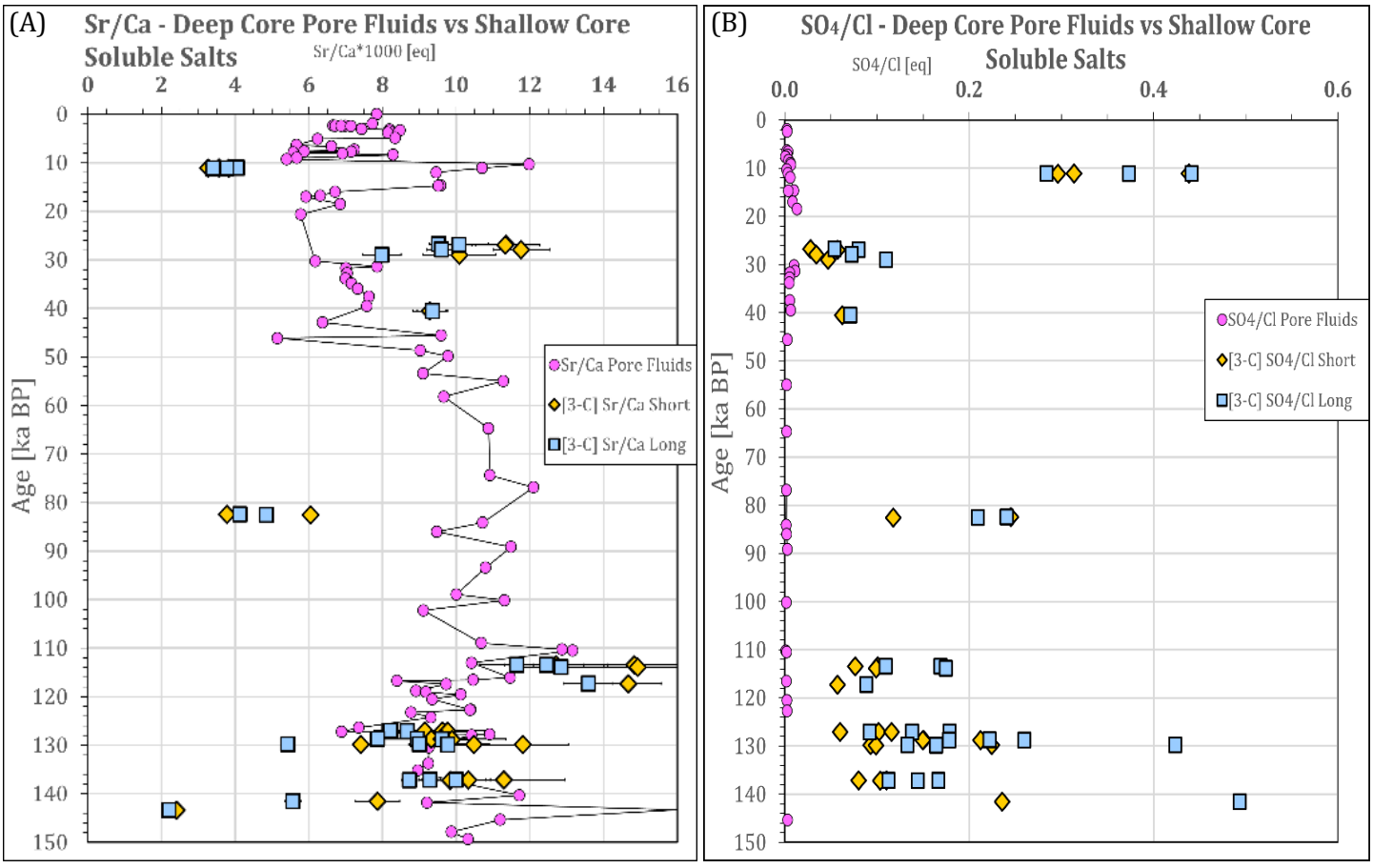

Figure 27: Soluble salts data of the shallow core compared with pore fluids data of the deep core. The presented ratios include one or two elements that dissolve primary minerals such as gypsum and aragonite in addition to their dissolution from soluble salts. (A) $\frac{Sr}{Ca}$, (B) $\frac{SO_4}{Cl}$, (C) $\frac{Sr}{Cl}$.

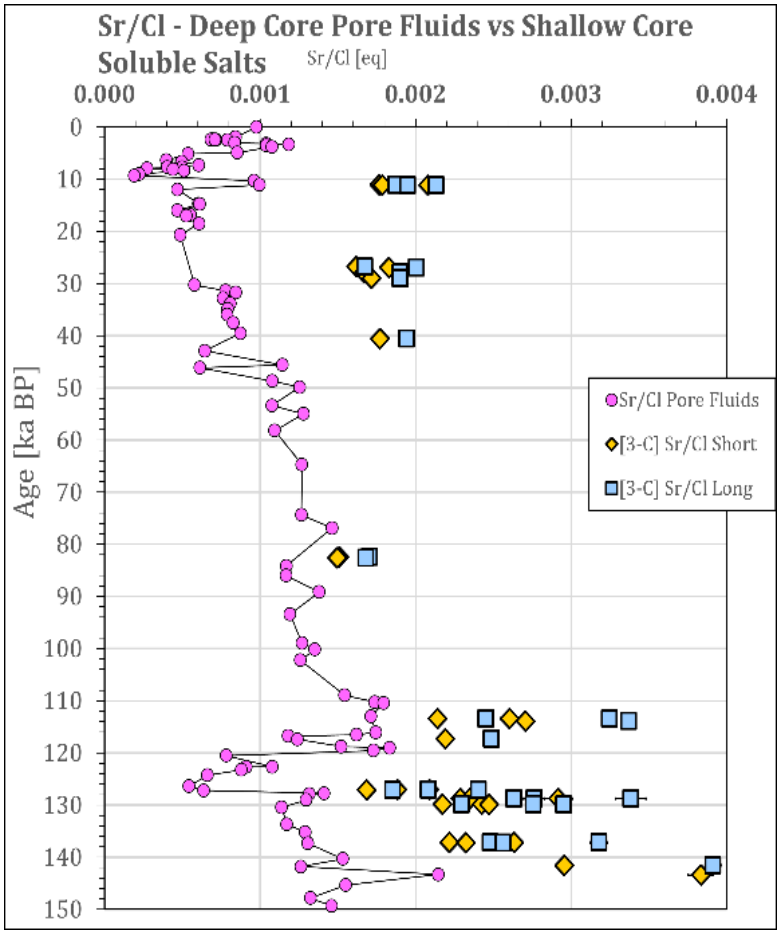

8.1.2. Data of the marginal terraces - PZ-1 and Mt. Sedom White Hill

The $\frac{Sr}{Ca}$, $\frac{SO_4}{Cl}$ and $\frac{Sr}{Cl}$ ratios in soluble salts that were extracted from PZ-1 and Mt. Sedom sections of the marginal terraces are presented here (Fig. 28 A-C).

The $\frac{Sr}{Ca}$ ratio: The range of the error bars in this ratio is larger than in other ratios while the long samples show error ranges that are slightly reduced compare to the short values (figure 28 A). Both the short and long samples are presented and reveal that in PZ-1 most of the long values are lower than the short values. Considering that both elements originate not solely from the interstitial brine but also from minerals in the sediments (e.g., gypsum and aragonite) the lower $\frac{Sr}{Ca}$ ratios in the long extractions probably indicate on excess contribution from the dissolving minerals present in the section, mainly gypsum/anhydrite. In Mt. Sedom, the long values are higher than the short values (which is a counterintuitive observation). The $\frac{Sr}{Ca}$ values variate frequently in the range of ~4 to 16. Many peaks of the short ratios, both positive and negative, correlate with distinct peaks in the long ratios. In the lower

section the $\frac{Sr}{Ca}$ values of PZ-1 variate in the widest range of 4.4 to 16. The general trend of this section seems to begin with the highest value of ~16 and reduce a little along the section to ~11. In the middle section the $\frac{Sr}{Ca}$ are not stable and variate often yet in a more confined range of 7 to 15. The general trend of this section seems to remain more or less stabilized on ~9-11, as the final values of the lower section. The upper section begins with values of ~9 and from there the mean trend gradually decline down to ~5-6. Mt. Sedom short values show good correlation with the coeval PZ-1 samples. Some of the long samples fit to the PZ-1 data while the others are a bit higher than it.

The $\frac{SO_4}{Cl}$ ratio: As seen in the deep and shallow cores, here as well, the samples seem to have a base value (~0.01-0.1) and from this base it abruptly rises to distinct positive peaks of up to ~1 (figure 28 B). In the lower section the $\frac{SO_4}{Cl}$ ratios rise from a low base value forming a distinct positive peak of almost 1. The PZ-1 data of the middle section is mostly concentrated within the low base range. It peaks twice to values of ~0.4 at the base and top of the section (43 and 31 ka BP). The data of the upper section behave differently in the short and long values. Short values are confined within the low base range (0.014-0.05) while long values are constantly higher than the short values and behave more as the high peaks (0.04-0.32). Increased values of $\frac{SO_4}{Cl}$ in the long compare to the short samples can be attributed to additional dissolution of gypsum/anhydrite during the longer dissolution. Mt. Sedom values show good correlation with the PZ-1 data. Its short and long values usually almost fit.

The $\frac{Sr}{Cl}$ ratio: The values of this ratio are unstable and variate frequently (Figure 28 C). In the lower section the oscillations rang between ~0.004 to 0.009 (mean value of ~0.006). The PZ-1 data of the middle section is the noisiest with ratios fluctuating within the range of ~0.002-0.01 (mean value similar to that of the lower section). The ratios of the upper section are distinctly lower, ranging between ~0.001-0.004. Short and long values are similar without a clear tendency between them. Mt. Sedom samples show a good correlation with the PZ-1 samples.

8.1.3. Nitrate in the deep core versus the marginal terraces

Results of the multiple washes experiment show that NO_3^- in samples of the marginal terraces (PZ-1) dissolved in distinct high concentrations of ~0.015-0.025 $\frac{mmol}{g}$ in the first wash and close to zero concentrations in all following washes, while NO_3^- concentrations in the deep core is almost zero in all washes (Fig. 29). The measurements of NO_3^- in the samples display the same behavior with

concentrations of ~0.01-0.06 $\frac{mmol}{g}$ NO_3^- in all the marginal samples (Mt. Sedom White Hill & PZ-1) while this ion is absent in all deep and shallow core samples.

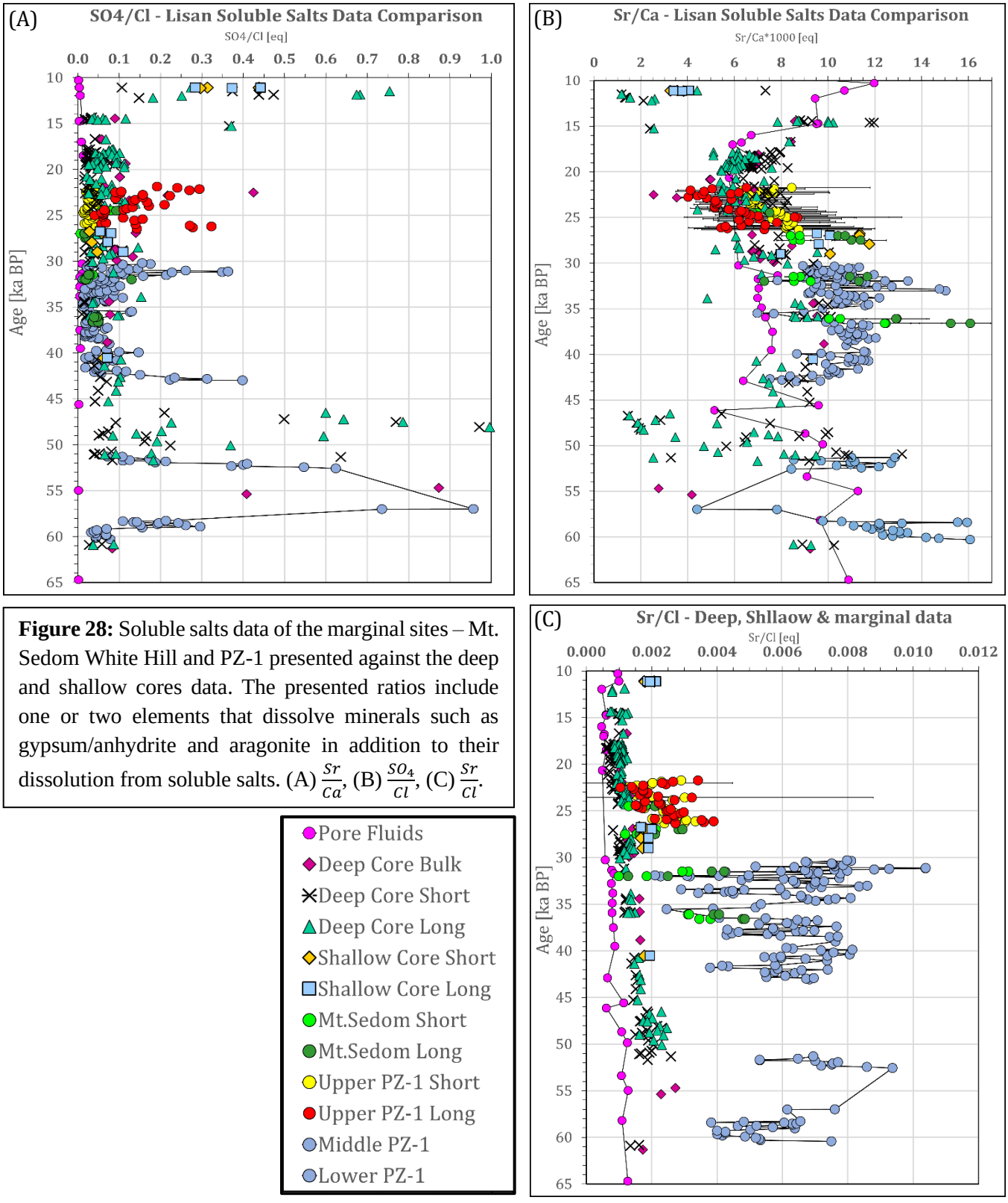

Figure 28: Soluble salts data of the marginal sites – Mt. Sedom White Hill and PZ-1 presented against the deep and shallow cores data. The presented ratios include one or two elements that dissolve minerals such as gypsum/anhydrite and aragonite in addition to their dissolution from soluble salts. (A) $\frac{Sr}{Ca}$, (B) $\frac{SO_4}{Cl}$, (C) $\frac{Sr}{Cl}$.

Figure 29: Nitrate concentrations in each of the five washes of the multiple washes experiment. The data is divided to a group of the marginal samples (PZ-1) and a group of the deep core samples.

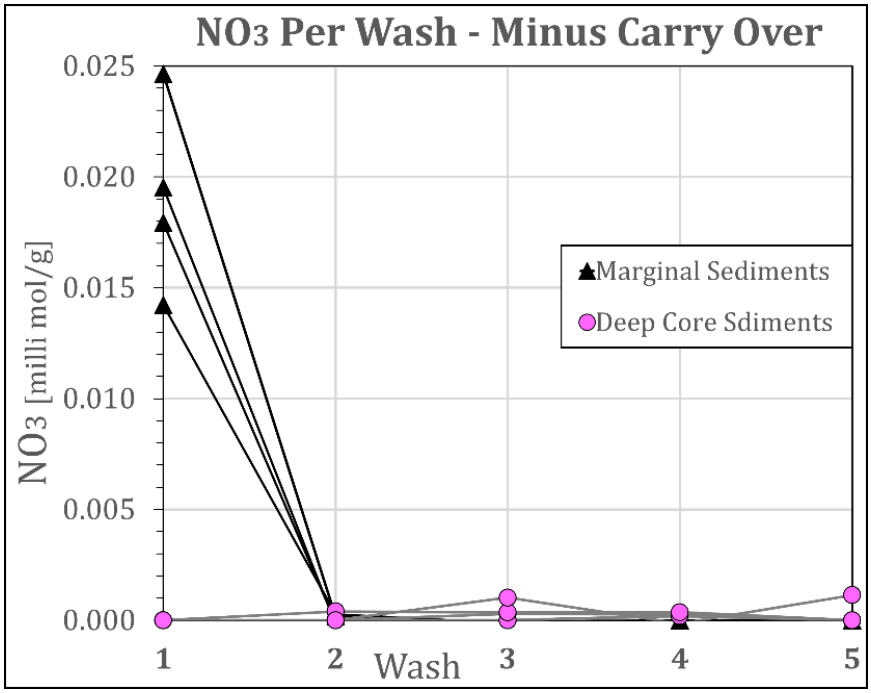

8.2. Discussion

8.2.1. Corrections for dissolution of sulfate and carbonate minerals

As shown previously, the multiple washes of the sediments and elemental ratios of the soluble salts demonstrate clearly that elements such as Na, Mg, Cl, Br originate mostly or solely from dissolution of soluble interstitial salts that represent the bottom brine at the location of the investigated sections. Other elements, such as Ca, Sr, SO_4^- originate from dissolution of interstitial salts and dissolution of authigenic sediments, mostly gypsum and aragonite. The origin of Ca and SO_4^-, besides the soluble interstitial salts, is mainly sedimentary gypsum and to lesser extent sedimentary aragonite. The Sr co-precipitates with aragonite (distribution coefficient of about 1) and to a smaller extent with gypsum (distribution coefficient smaller than 1).

Hence, elemental ratios of water extracted soluble salts containing one or two of the elements Ca, Sr and SO_4^- (e.g., $\frac{Sr}{Ca}, \frac{Sr}{Cl}, \frac{Na}{Ca}, \frac{Mg}{Ca}, \frac{SO_4}{Cl}$) have an inherent problem and can provide limited information before a reliable subtraction was conducted for the portion of each element that dissolved from sulfate and carbonate minerals.

Nevertheless, since these ratios are influenced by dissolution of minerals, mainly gypsum/anhydrite, they can provide some information regard these dissolutions before corrections are being conducted.

Peaks are observed in the $\frac{SO_4}{Cl}$ ratio of the deep core at ~95, 72, 50 (the last is the most prominent peak) and 11.5 ka (Fig. 14 E). The $\frac{SO_4}{Cl}$ values in the soluble salts of the deep core are much higher than the values in the pore fluids of this core. Moreover, a moderate excess in the $\frac{SO_4}{Cl}$ ratios (over these ratios in the pore fluids) is observed almost along the whole studied section of the deep core and the peaks in the $\frac{SO_4}{Cl}$ ratios can reach values that are about two orders of magnitude higher than these ratios in the pore fluids.

It is suggested here that the moderate constant excess of SO_4^{2-} originates mostly from dissolution of disseminated interstitial gypsum since no detectable gypsum laminae were observed in the majority of these sediments. The $\frac{SO_4}{Cl}$ peaks which coincide with gypsum laminae stem from dissolution of these laminae during extraction. Other peaks represent probably short periods of elevated SO_4^{2-} in the deep brine. Two scenarios are suggested for the short term rise of SO_4^{2-} in the deep brine of the lake (hypolimnion): 1. Enhanced mixing in the lake during dry periods, ventilate and enrich the deep brine with dissolved oxygen. The oxygen in turn oxidized dissolved sulfide and the sedimentary sulfur concretions, which accumulated in the deep lake during prolonged anoxic periods when the lake was stratified, to SO_4^{2-} (Torfstein et al., 2005, 2008). 2. Accumulation of SO_4^{2-} in the epilimnion of the stratified lake by inputs of SO_4^{2-} from freshwater during wet periods and the transport of this SO_4^{2-} to the hypolimnion by turbulent mixing and diffusion across the epilimnion-hypolimnion interface.

Further investigation is required in order to identify the mechanism causing the SO_4^{2-} increase in these peaks. The $\frac{SO_4}{Cl}$ distinct peaks are well correlated with minima in the $\frac{Sr}{Ca}$ ratios (Fig. 14 F), and with increased climaxes in the $\frac{Sr}{Cl}$ ratios (Fig. 14 C), which as well stem from gypsum dissolution. When gypsum (or anhydrite) dissolves, Ca is released to the solution in amounts that are much larger than the Sr and therefore the total value of the $\frac{Sr}{Ca}$ ratio is decreased.

The Ca^{2+} in the soluble salts was corrected for the presence of sedimentary gypsum and aragonite by subtracting the equivalent amounts of SO_4^{2-} and bicarbonate from the calcium, which accounts for the solid $CaCO_3$ and $CaSO_4$ present in the sample (as suggested by Katz and Kolodny, 1989):

$$Ca^{2+}_{\text{corrected}} = Ca^{2+}_{\text{measured}} - [\frac{1}{2} \cdot HCO_3^-{}_{\text{measured}} + SO_4^{2-}{}_{\text{measured}}]$$

This is an over-correction since it subtracts also the Ca^{2+} which may crystallize within the pores as soluble salts from the drying pores brine.

After this correction is applied ratios that compose of Ca and an element from the soluble salts group can be investigated such as $\frac{Na}{Ca}, \frac{Mg}{Ca}$ et cetera. Such a ratio is presented in Figure 30 after the correction for calcium was applied.

Additional correction was suggested by Katz and Kolodny, (1989) for the contribution of gypsum and aragonite dissolution to the elements Sr, Mg, Na and K. These elements were corrected by subtracting the product $\frac{M}{Ca} \cdot HCO_3$ from their total soluble concentrations, where $\frac{M}{Ca}$ is the equivalent ratio between the contaminating metal and calcium in the solid (For contribution of sulfate minerals additional correction with SO_4 instead of HCO_3 is required). Such a correction was not applied here because it requires to measure the ratios $\left(\frac{\text{ion}}{\text{Ca}}\right)_{\text{gypsum}}$ and $\left(\frac{\text{ion}}{\text{Ca}}\right)_{\text{aragonite}}$ (where ion refers to Sr, Mg, Na, K) in (acid dissolved) aragonite and gypsum mineral in each sample. Such a procedure was not conducted in this work.

Alternative method of correction is suggested here: By assuming that the pore fluids represent the pristine brine, the gap that is seen between pore fluids data to soluble salts data of ratios such as $\frac{Sr}{Cl}, \frac{SO_4}{Cl}$ express the excess of the contaminated element that originate from dissolution of gypsum and/or carbonate minerals. (The ratios has to include one 'contaminated element' and an element from the highly soluble group – Na/Cl/Br/Mg).

For instance, when Cl is used, the estimated amount of each ion contributed by the dissolution of the sediments in each sample can obtain from the difference:

$$\frac{\text{ion}_{\text{soluble salts}}}{\text{Cl}_{\text{soluble salts}}} = \frac{\text{ion}_{\text{measured}}}{\text{Cl}_{\text{soluble slats}}} - \frac{\text{ion}_{\text{pore fluids}}}{\text{Cl}_{\text{pore fluids}}}$$

assuming that all the Cl originate from the pore fluids/soluble salts, and nothing was contributed by the dissolving sediments.

This method have several drawbacks.

First, in case that some soluble salts crystallize from the interstitial brine, even in the unexposed deep core sediments, the extracted pore fluids will miss these salts, while the soluble salts on the other hand will include these salts in their dissolutions. In such case, it will be inaccurate to assume that the pore fluids represent the original chemistry of the brine. Second, there is some error on the soluble salts and pore fluids data. Thus, the gap between them can represent some error that does not induced from minerals dissolution.

Additionally, such a correction can be applied, in this case, only on the deep core data, where equivalent values of soluble salts and pore fluids are available.

There is a big interest to implement precise corrections for the excess of ions that dissolved form the sediments, especially for strontium and sulphate, since ratios such as $\frac{Sr}{Ca}$ can provide important insights and were investigated thoroughly in the marginal terraces in previous works. Such corrections are possible by applying the method suggested here although they are not presented in this work.

Figure 30: The $\frac{Na}{Ca}$ ratio before and after the correction for Ca was applied.

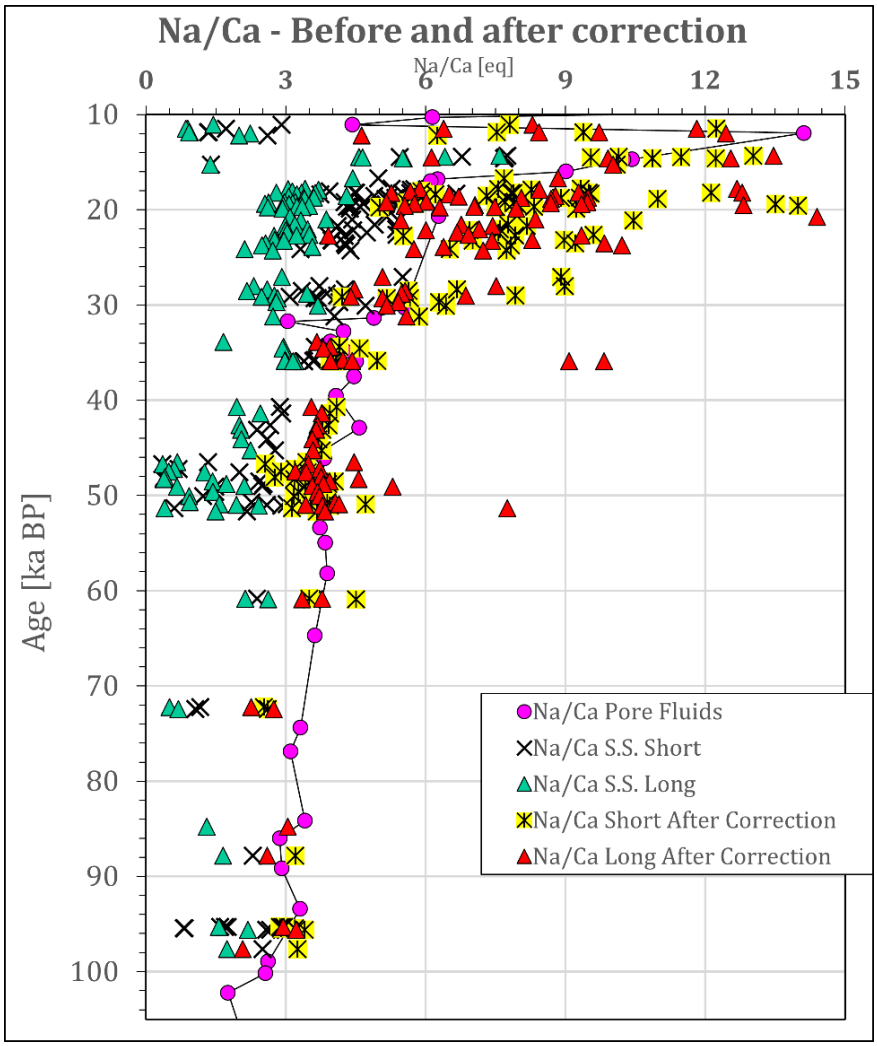

8.2.2. Nitrate in the soluble salts

As displayed in figure 29, NO_3^- is observed only in interstitial soluble salts of sediments from the marginal terraces while it is absent in the sediments of the deep and shallow cores. This may stem from "contamination" with nitrate of the exposed sediments on the marginal terraces. This nitrate could have been supplied by meteoric water which contained some nitrate or produced by oxidation of organic matter (by dissolved oxygen in the recharge waters), which was present in the sedimentary section.

This nitrate enrichment mechanism, however, can be rejected when considering the arid climate in the area and the low permeability of the Lisan Fm. sediments, both leading to limited flow of fresh groundwater and an excellent preservation of the aragonite minerals in the sedimentary sections, which otherwise would have quickly recrystallized to calcite (Katz et al., 1977). (Note that diagenetic processes in the exposed sediments of the Lisan that described in the previous chapter are all the consequence of brine desiccation and do not include seepage of water through the sediments). If considering a significant flow of freshwater through the Lisan sediments after their exposure the entire composition of the soluble salts in these sections is questionable, although this is not the working premise in this thesis.

Another clue for the origin of the nitrate in the soluble salts is its dissolution pattern in the multiple washes experiment, which is identical to the dissolution pattern of the elements from the highly soluble group. Altogether, it seems that nitrate indeed present in the pores of the marginal sediments as highly soluble salts such as $NaNO_3$.

The high content of nitrate in the marginal terraces may represents the oxidized epilimnion of the lake. According to this scenario, the epilimnion accumulated substantial amounts of nitrate and organic matter as weathering products that supplied by the freshwaters entering the lake from the drainage basin and by freshwater springs (Stein et al., 1997). Nitrate accumulated in the oxidized epilimnion, and the organic matter was slowly oxidized to nitrate as well (Thomas and Ariztegui, 2019) and was not consumed (assimilated) by the population of primary producers (phytoplankton). The reason for the low consumption is the epilimnion's high salinity (just about half the salinity of modern Dead Sea). Surface water may support phytoplankton blooms just during massive freshwater inflows (similarly to the case of the modern Dead Sea). As other ions, some of the accumulated nitrate transported down to the hypolimnion by turbulent mixing and diffusion (Lazar et al., 2014) and there it was slowly consumed by denitrifying bacteria present in the reducing deep brine layer.

The fact that nitrate behaves like the elements that clearly originated from soluble salts, e.g., Br, Cl also suggests that it originated from the soluble interstitial salts which represent the original epilimnic brine of Lake Lisan. The reducing brine of the saline springs which supplied (and are supplying at present) the lake with high content of dissolved salts, did not supply the lake with nitrate as indicated by the high ammonia content of the modern saline springs (e.g., Ein Qedem; Weber, 2021).

In summary, the presence of nitrate in the marginal terraces and its absence in the pore fluids and extracted soluble salts of the deep and shallow cores indicate that during the Lisan period the lake was stratified. Its epilimnion interact with the surface and hence kept oxidizing conditions and accumulated nitrate by freshwater incomes and oxidation of organic matter. Its hypolimnion was isolated from the

surface and hence developed reducing conditions and could not sustain nitrate that transported to it from the epilimnion since it was consumed by denitrifying bacteria.

Additional evidence for reducing hypolimnion is evident by massive layers of gypsum in the marginal sediments while the contemporaneous sediments of the deep and shallow cores contain mainly sulfur concretions (Torfstein et al., 2005, 2008).

8.3. Summary

This chapter deals with the effects of dissolution of primary minerals such as gypsum and aragonite on the investigated elemental ratios:

1. Before conducting any correction on the results of the soluble salts, the $\frac{SO_4}{Cl}$ ratio reveals a constant excess of SO_4 all along the deep, shallow, and marginal profiles. This excess is attributed to dissolution of disseminated interstitial gypsum, that consider as part of the soluble salts. Distinct positive peaks in this ratio, that observed in all profiles and can reach up to ~1.2, are correlated with contemporaneous positive peaks in $\frac{Sr}{Cl}$ that can reach up to ~0.004 and negative peaks in $\frac{Sr}{Ca}$ that can drop down to ~1.2. In several cases these peaks stem from dissolution of primary gypsum lamina that originally precipitated from the lake while in the others they testify on elevated concentrations of SO_4 in the brine. These elevated SO_4 concentrations may be the result of oxidation of sulfur concretions to dissolved SO_4 in the deep anoxic basin. This process occurred after oxygen was supplied to the deep brine by mixing of the water column of Lake Lisan that occurred during dryer periods. Alternatively, SO_4 could have accumulate in the upper brine during wet and stable periods and slowly transfer to the hypolimnion by turbulent mixing and diffusion across the epilimnion-hypolimnion interface.
2. A correction for Ca that originate from dissolution of sulfate and carbonate primary minerals is presented. This correction seems satisfactory. Furthermore, a method for the correction of Sr, SO_4, K and Mg is suggested that can be applied on the results of the deep core, although this correction is not implemented here.

The second section of this chapter deals with insights that can attain from the results of the nitrate in the soluble salts. The main conclusions of this section are:

Its presence in the marginal sediments while it is absent in the shallow and deep sediments constrain the lake to sustain stratified configuration during the last glacial with an upper oxidized epilimnion and a lower anoxic hypolimnion. The epilimnion accumulated substantial amounts of nitrate and organic matter as weathering products that supplied by the tributaries and freshwater springs. Bacteria that could

live in the diluted upper brine oxidized the organic matter to nitrate, while this in turn was not consumed (assimilated) by the population of primary producers due to the high salinity of the water that prevent their presence. Some of the nitrate transported down to the hypolimnion by turbulent mixing and diffusion and there it was slowly consumed by denitrifying bacteria present in the reducing deep brine layer.

9. Synthesis of the main conclusions

This thesis presents an investigation of the chemical properties of interstitial soluble salts that represent the brines that filled the Quaternary lakes of the Dead Sea Basin. The current study focuses mainly on the brines that filled the last glacial Lake Lisan (70-14 ka BP).

The studied soluble salts were extracted from sediments of the Lisan Fm. that were obtained from the DSDDP cores drilled in the depocenter of the DSB (5017-1-A) and at an intermediate depth (modern Dead Sea shore, 5017-3-C, containing several samples from the penultimate Amora Fm. and last interglacial Samra Fm.), and from sections of marginal outcrops in Perazim Valley and Mt. Sedom.

The soluble salts were extracted from the sediments by DDW rinses that were followed by leaches of the solutions with the dissolved salts to separate them from the residual sediments. These solutions were analyzed for the major elements compositions: Na^+, K^+, Ca^{2+}, Mg^{2+}, Sr^{2+}, SiO_2, Ba^{2+}, Cl^-, Br^-, NO_3^-, SO_4^{2-} and HCO_3^-. The results of these analyses from each core/outcrop were investigated separately and compared with each other, and with chemical compositions of pore fluids that extracted from the DSDDP deep core sediments, on the basis of their common chronology. This comprehensive investigation yields several important conclusions:

1. A robust validation for the soluble salts method as a tool for reconstructions of brine chemistry is achieved here for the first time by tracking the dissolution pattern of each element in the sediments rinses and by the comparison of the soluble salts to the pore fluids ionic ratios of the deep core. These comparisons revealed high correlation in ionic ratios that compose of elements that dissolve solely from soluble salts and confirmed that these ratios reliably show the original chemical composition of the brine, as the pore fluids do. The ions of this group are: Na^+, Mg^{2+}, Cl^-, Br^- and NO_3^-.
2. Ionic ratios that include Ca, Sr, SO_4 and K present some surpluses relative to equivalent pore fluids data. Surpluses of Ca, Sr and SO_4 originate mainly from dissolution of gypsum/anhydrite and secondly from dissolution of aragonite. Some portion of the dissolved gypsum is disseminated crystals of gypsum that exist all along the sediments' sections and are attribute to consider as part of the soluble salts. Additional portion are primary layers of gypsum that originally precipitate from the lake. The excess of K is less clear although it is suggested that a small portion of K originate from dissolution of potash salts that crystallized in the pores, such as carnallite or polyhalite, and join the portion that comes from soluble salts dissolution. Additional source can be the adsorption of K from clays during the sediments-water interactions of the soluble salts method.
3. A correction is conducted for the excess of Ca in the extracted solutions that seems to be satisfactory. Additional correction is suggested for the excess of Sr, SO_4, K and Mg.

This correction can be applied on the results of the deep core, although it is not implemented here.

4. A thorough investigation of ionic ratios that compose of elements that dissolve solely from soluble salts - $\frac{Na}{Cl}, \frac{Br}{Cl}, \frac{Mg}{Cl}$ provided several new insights:

   - The high-resolution profile of the soluble salts from the deep core (5017-1-A) revealed the sensitivity of this method that can document not only the major climatic event as glacial-interglacial oscillations but also short-term events such as the arid Heinrich events, and extreme wet periods such as glacial maximums and the Younger Dryas.

   - The soluble salts of the shallow core (5017-3-C) provided some insights on the lake from the period that precede the Lisan period, ~143-100 ka BP. Samples from the climax of the penultimate glacial, the shift to the last interglacial and the last glacial indicate on similar brine composition in the intermediate depth and the depocenter of the lake. Samples from the last interglacial suggest that in this period halite used to precipitate in a similar mechanism as observed in the modern Dead Sea. According to this mechanism such arid periods are characterized with simultaneous conditions in the deep and shallow environments. In the deep brine halite saturation was achieved due to the concentration of the brine and this salt massively precipitated and accumulated on the depocenter floor, while the upper brine remained, in general, undersaturated and did not sustain the accumulation of halite on the shallow margins.

   - The comparison between the deep, shallow, and marginal soluble salts data provide, for the first time, a high-resolution record of the chemical evolution of Lake Lisan's brine in the deep, intermediate, and marginal environments. This comprehensive integration provide the opportunity to compare the different limnological environments in the lake and to differentiate between the chemical properties of the upper and lower brines.

   - First, a clear difference is noticed between the stable and secular chemical evolution in the deep and shallow environments to the unstable behavior of the chemical profiles in the marginal sites. The marginal data was divided to samples that most likely sank form the epilimnion, as an integral part of the main lake and thus represent the original values of the local brine, to samples that sank in a local marginal restricted lake which pooled during periods of low lake level or samples that did sank in the main lake but were influenced by diagenetic processes after their exposure. The main diagenetic process that seems to influence the marginal sediments is the crystallization of interstitial halite due to the desiccation of the pores' brine. This process occurs faster in porose sections relative

to low permeable sections, and it is significantly more advanced in the long-exposed marginal sediments but can also be identified in recent sections of intermediate depth in the lake.

- Original values of the lake's brine were used to track its chemical development and to identify the processes that controlled it. It is shown that the chemical evolution of the epilimnion was dictated by mixing between freshwater that entered the lake by tributaries and springs and donate high $\frac{Na}{Cl}$ values of ~0.9 to the upper lake to the saline bring of the epilimnion that held an intermediate $\frac{Na}{Cl}$ value of 0.45-0.65. In addition, the upper brine was also influenced by the local environmental conditions (e.g., evaporation, seasonal variations, flash floods) that reduced its chemical stability and led to short-term variations.

- The hypolimnion on the other hand remained isolated during most of the Lisan period due to the stable stratification in the lake. This deep brine began the last glacial period with a highly saline composition and low $\frac{Na}{Cl}$ values that it inherited from the preceding last interglacial. From there it developed through diffusive fluxes and turbulent mixing along the interface with the upper diluted brine and gravity flows of local epilimnic brine that dissolved halite and sank to the deep basin. All of these processes led to the gradual dilution of the hypolimnion, the accumulation of large repository of Na and Cl ions in it and the increase of its $\frac{Na}{Cl}$ value. These mixing processes also buffered the short-term variations that occurred in the epilimnion and delivered only the mean outcome of the different inducers down to the deep brine. It resulted in a stable and secular development of the chemical properties in the hypolimnion that testified by its stable ionic ratios.

5. The presence of nitrate in the marginal sediments while it is absent in the deep and shallow sediments, and its dissolution pattern, that is identical to the soluble salts group, constrain the stable stratification in Lake Lisan that led to the anoxic conditions in the hypolimnion. In such configuration organic matter that washed into the lake from its freshwater sources could oxidize to nitrate by bacteria that lived in the diluted and oxide epilimnion. This nitrate was not consumed by primary producers due to the high salinity (~half of modern Dead Sea) that prevented their presence. This nitrate accumulated in the epilimnion together with the dissolved nitrate and additional ions that entered the lake with freshwater. Therefore, sediments that sank from this brine contain nitrate in their pores as a soluble salt. However, nitrate that transferred down to the hypolimnion was slowly consumed by denitrifying bacteria present in the reducing deep brine and thus its accumulation in the deep brine was prevented.

References

Barbier, M., 2017, Characterizing Polyhalite Plant Nutritional Properties: Agricultural Research & Technology: Open Access Journal, v. 6, doi: 10.19080/artoaj.2017.06.555690.

Bartov, Y., 1999. The geology of the Lisan Formation in Massada plain and the Lisan Peninsula. *Unpublished M. Sc. thesis. The Hebrew University of Jerusalem [In Hebrew with an English abstract]*.

Bartov, Y., Goldstein, S.L., Stein, M., and Enzel, Y., 2003, Catastrophic arid episodes in the Eastern Mediterranean linked with the North Atlantic Heinrich events: Geology, v. 31, p. 439–442, doi: 10.1130/0091-7613(2003)031<0439:CAEITE>2.0.CO;2.

Bartov, Y., Stein, M., Enzel, Y., Agnon, A., and Reches, Z., 2002, Lake Levels and Sequence Stratigraphy of Lake Lisan , the Late Pleistocene Precursor of the Dead Sea: v. 21, p. 9–21, doi: 10.1006/qres.2001.2284.

Begin, Z.B., Ehrlich, A., Nathan, Y., 1974. Lake Lisan, the Pleistocene precursor of the Dead Sea. Geological Survey of Israel Bulletin 63, 30.

Belmaker, R., Lazar, B., Beer, J., Christl, M., Tepelyakov, N., and Stein, M., 2013, 10Be dating of Neogene halite: Geochimica et Cosmochimica Acta, v. 122, p. 418–429, doi: 10.1016/j.gca.2013.08.033.

Bookman, R., Enzel, Y., Agnon, A., and Stein, M., 2004, Late Holocene lake levels of the dead sea: Bulletin of the Geological Society of America, v. 116, p. 555–571, doi: 10.1130/B25286.1.

Browman, A.A., and Hastings, A.B., 1937, Solubility of Aragonite in Salt Solutions: Journal of Biological Chemistry, v. 119, p. 241–246, doi: 10.1016/s0021-9258(18)74451-7.

Charrach, J., 2020, Comments on “Mount Sedom salt diapir - Source for sulphate replenishment and gypsum supersaturation in the last glacial Dead Sea (Lake Lisan)” by Levy EJ, Sivan O, Antler G, Lazar B, Stein M, Yechieli Y, Gavrieli I: Quaternary Science Reviews, v. 231, p. 106110, doi: 10.1016/j.quascirev.2019.106110.

Charrach, J., 2018, The Sdom evaporite formation in Israel and its relationship with the Messinian Salinity Crisis: Springer Berlin Heidelberg, v. 33, 727–766 p., doi: 10.1007/s13146-017-0410-1.

Coianiz, L., Ben-Avraham, Z., Stein, M., and Lazar, M., 2019, Spatial and temporal reconstruction of the late Quaternary Dead Sea sedimentary facies from geophysical properties: Journal of Applied Geophysics, v. 160, p. 15–27, doi: 10.1016/j.jappgeo.2018.11.002.

Enzel, Y., Bookman, R., Sharon, D., Gvirtzman, H., Dayan, U., Ziv, B., and Stein, M., 2003, Late Holocene climates of the Near East deduced from Dead Sea level variations and modern regional winter rainfall: Quaternary Research, v. 60, p. 263–273, doi: 10.1016/j.yqres.2003.07.011.

Feigenbaum, S., and Shainberg, I., 1975, Dissolution of Illite - a Possible Mechanism of Potassium Release.: Proc Soil Sci Soc Am, v. 39, p. 985–990, doi: 10.2136/sssaj1975.03615995003900050049x.

García-Veigas, J., Rosell, L., Zak, I., Playà, E., Ayora, C., and Starinsky, A., 2009, Evidence of potash salt formation in the Pliocene Sedom Lagoon (Dead Sea Rift, Israel): Chemical Geology, v. 265, p. 499–511, doi: 10.1016/j.chemgeo.2009.05.013.

Gavrieli, I., and Stein, M., 2006, On the origin and fate of the brines in the Dead Sea basin: Geological Society of America, v. 2401, p. 1–22, doi: 10.1130/2006.2401(12).

Goldstein, S.L., Kiro, Y., Torfstein, A., Kitagawa, H., Tierney, J., and Stein, M., 2020, Revised chronology of the

ICDP Dead Sea deep drill core relates drier-wetter-drier climate cycles to insolation over the past 220 kyr: Quaternary Science Reviews, v. 244, p. 106460, doi: 10.1016/j.quascirev.2020.106460.

Haase-Schramm, A., Goldstein, S.L., and Stein, M., 2004, U-Th dating of Lake Lisan (late Pleistocene dead sea) aragonite and implications for glacial east Mediterranean climate change: Geochimica et Cosmochimica Acta, v. 68, p. 985–1005, doi: 10.1016/j.gca.2003.07.016.

Haliva-Cohen, A., Stein, M., Goldstein, S.L., Sandler, A., and Starinsky, A., 2012, Sources and transport routes of fine detritus material to the Late Quaternary Dead Sea basin: Quaternary Science Reviews, v. 50, p. 55–70, doi: 10.1016/j.quascirev.2012.06.014.

Hazan, N., Stein, M., Agnon, A., Marco, S., Nadel, D., Negendank, J.F.W., Schwab, M.J., and Neev, D., 2005, The late Quaternary limnological history of Lake Kinneret (Sea of Galilee), Israel: Quaternary Research, v. 63, p. 60–77, doi: 10.1016/j.yqres.2004.09.004.

Jalali, M., 2006, Kinetics of non-exchangeable potassium release and availability in some calcareous soils of western Iran: Geoderma, v. 135, p. 63–71, doi: 10.1016/j.geoderma.2005.11.006.

Kagan, E., Stein, M., and Marco, S., 2018, Integrated Paleoseismic Chronology of the Last Glacial Lake Lisan: From Lake Margin Seismites to Deep-Lake Mass Transport Deposits: Journal of Geophysical Research: Solid Earth, v. 123, p. 2806–2824, doi: 10.1002/2017JB014117.

Katz, A., and Kolodny, N., 1989, Hypersaline brine diagenesis and evolution in the Dead Sea-Lake Lisan system (Israel): Geochimica et Cosmochimica Acta, v. 53, p. 59–67, doi: 10.1016/0016-7037(89)90272-X.

Katz, A., Kolodny, Y., and Nissenbaum, A., 1977, The geochemical evolution of the Pleistocene Lake Lisan-Dead Sea system: Geochimica et Cosmochimica Acta, v. 41, doi: 10.1016/0016-7037(77)90172-7.

Katz, A., and Starinsky, A., 2009, Geochemical history of the Dead Sea: Aquatic Geochemistry, v. 15, p. 159–194, doi: 10.1007/s10498-008-9045-0.

Katz, A., Starinsky, A., Taitel-Goldman, N., and Beyth, M., 1981, Solubilities of gypsum and halite in the Dead Sea and in its mixtures with seawater: Limnology and Oceanography, v. 26, p. 709–716, doi: 10.4319/lo.1981.26.4.0709.

Kinsman, D.J. and Holland, H.D., 1969. The co-precipitation of cations with CaCO3—IV. The co-precipitation of Sr2+ with aragonite between 16 and 96 C. *Geochimica et Cosmochimica Acta*, *33*(1), pp.1-17.

Kiro, Y., Goldstein, S.L., Garcia-Veigas, J., Levy, E., Kushnir, Y., Stein, M., and Lazar, B., 2017, Relationships between lake-level changes and water and salt budgets in the Dead Sea during extreme aridities in the Eastern Mediterranean: Earth and Planetary Science Letters, v. 464, p. 211–226, doi: 10.1016/j.epsl.2017.01.043.

Kiro, Y., Goldstein, S.L., Lazar, B., and Stein, M., 2016, Environmental implications of salt facies in the Dead Sea: Geological Society of America Bulletin, v. 128, p. 824–841, doi: 10.1130/b31357.1.

Kitagawa, H., Stein, M., Goldstein, S.L., Nakamura, T., and Lazar, B., 2017, Radiocarbon chronology of the dsddp core at the deepest floor of the dead sea: Radiocarbon, v. 59, p. 383–394, doi: 10.1017/RDC.2016.120.

Kolodny, Y., Stein, M., and Machlus, M., 2005, Sea-rain-lake relation in the Last Glacial East Mediterranean revealed by δ18O-δ13C in Lake Lisan aragonites: Geochimica et Cosmochimica Acta, v. 69, p. 4045–4060, doi: 10.1016/j.gca.2004.11.022.

Krumgalz, B.S., Magdal, E., and Starinsky, A., 2002, The evolution of a chloride sedimentary sequence-simulated evaporation of the Dead Sea: Israel Journal of Earth Sciences, v. 51, p. 253–267, doi: 10.1560/EL8J-PVU9-

EH88-M083.

Lazar, B., Sivan, O., Yechieli, Y., Levy, E.J., Antler, G., Gavrieli, I., and Stein, M., 2014, Long-term freshening of the Dead Sea brine revealed by porewater Cl- and δO18 in ICDP Dead Sea deep-drill: Earth and Planetary Science Letters, v. 400, p. 94–101, doi: 10.1016/j.epsl.2014.03.019.

Levy, E.J., Sivan, O., Antler, G., Lazar, B., Stein, M., Yechieli, Y., and Gavrieli, I., 2019, Mount Sedom salt diapir - Source for sulfate replenishment and gypsum supersaturation in the last glacial Dead Sea (Lake Lisan): Quaternary Science Reviews, v. 221, p. 105871, doi: 10.1016/j.quascirev.2019.105871.

Levy, E.J., Stein, M., Lazar, B., Gavrieli, I., Yechieli, Y., and Sivan, O., 2017, Pore fluids in Dead Sea sediment core reveal linear response of lake chemistry to global climate changes: Geology, v. 45, p. 315–318, doi: 10.1130/G38685.1.

Levy, E.J., Yechieli, Y., Gavrieli, I., Lazar, B., Kiro, Y., Stein, M., and Sivan, O., 2018, Salt precipitation and dissolution in the late Quaternary Dead Sea: Evidence from chemical and δ37Cl composition of pore fluids and halites: Earth and Planetary Science Letters, v. 487, p. 127–137, doi: 10.1016/j.epsl.2018.02.003.

Li, M., Fang, X., Galy, A., Wang, H., Song, X., and Wang, X., 2020, Hydrated sulfate minerals (bloedite and polyhalite): formation and paleoenvironmental implications: Carbonates and Evaporites, v. 35, p. 1–12, doi: 10.1007/s13146-020-00660-y.

Li, T., Wang, H., Zhou, Z., Chen, X., and Zhou, J., 2015, A nano-scale study of the mechanisms of non-exchangeable potassium release from micas: Applied Clay Science, v. 118, p. 131–137, doi: 10.1016/j.clay.2015.09.013.

Lu, Y., Bookman, R., Waldmann, N. and Marco, S., 2020. A 45 kyr laminae record from the Dead Sea: Implications for basin erosion and floods recurrence. *Quaternary Science Reviews*, *229*, p.106143.

Lüthi, D., Le Floch, M., Bereiter, B., Blunier, T., Barnola, J.M., Siegenthaler, U., Raynaud, D., Jouzel, J., Fischer, H., Kawamura, K. and Stocker, T.F., 2008. High-resolution carbon dioxide concentration record 650,000–800,000 years before present. *nature*, *453*(7193), pp.379-382.

Machlus, M., 1996, Machlus_MSc_thesis.pdf:

Machlus, M., Enzel, Y., Goldstein, S.L., Marco, S., and Stein, M., 2000, Reconstructing low levels of Lake Lisan by correlating fan-delta and lacustrine deposits: v. 74, p. 137–144.

Migowski, C., Agnon, A., Bookman, R., Negendank, J.F.W., and Stein, M., 2004, Recurrence pattern of Holocene earthquakes along the Dead Sea transform revealed by varve-counting and radiocarbon dating of lacustrine sediments: Earth and Planetary Science Letters, v. 222, p. 301–314, doi: 10.1016/j.epsl.2004.02.015.

Migowski, C., Stein, M., Prasad, S., Negendank, J.F.W., and Agnon, A., 2006, Holocene climate variability and cultural evolution in the Near East from the Dead Sea sedimentary record: Quaternary Research, v. 66, p. 421–431, doi: 10.1016/j.yqres.2006.06.010.

Morse, J.W., Mucci, A., and Millero, F.J., 1980, The solubility of calcite and aragonite in seawater of 35%. salinity at 25°C and atmospheric pressure: Geochimica et Cosmochimica Acta, v. 44, p. 85–94, doi: 10.1016/0016-7037(80)90178-7.

Neev, D. and Emery, K.O., 1967. The Dead Sea: depositional processes and environments of evaporites.

Neev, D. and Emery, K.O., 1995. *The destruction of Sodom, Gomorrah, and Jericho: geological, climatological, and archaeological background*. Oxford University Press.

Neugebauer, I., Brauer, A., Schwab, M.J., Waldmann, N.D., Enzel, Y., Kitagawa, H., Torfstein, A., Frank, U., Dulski, P., Agnon, A., Ariztegui, D., Ben-Avraham, Z., Goldstein, S.L., and Stein, M., 2014, Lithology of the long sediment record recovered by the ICDP Dead Sea Deep Drilling Project (DSDDP): Quaternary Science Reviews, v. 102, p. 149–165, doi: 10.1016/j.quascirev.2014.08.013.

Palchan, D., Stein, M., Goldstein, S.L., Almogi-Labin, A., Tirosh, O., and Erel, Y., 2018, Synoptic conditions of fine-particle transport to the last interglacial Red Sea-Dead Sea from Nd-Sr compositions of sediment cores: Quaternary Science Reviews, v. 179, p. 123–136, doi: 10.1016/j.quascirev.2017.09.004.

Ron, H., Nowaczyk, N.R., Frank, U., Marco, S. and McWilliams, M.O., 2006. Magnetic properties of Lake Lisan and Holocene Dead Sea sediments and the fidelity of chemical and detrital remanent magnetization. *New frontiers in Dead Sea paleoenvironmental research*, *401*, p.171.

van der plicht, J., Beck, J.W., Bard, E., Baillie, M.G.L., Blackwell, P.G., Buck, C.E., Friedrich, M., Guilderson, T.P., Hughen, K.A., Kromer, B., McCormac, F.G., Bronk Ramsey, C., Reimer, P.J., Reimer, R.W., et al., 2004, Notcal04-Comparison/calibration 14C records 26-50 cal kyr BP: Radiocarbon, v. 46, p. 1225–1238, doi: 10.1017/S0033822200033117.

Shmuel Marco, Mordechai Stein, A.A., 1996, earthquake clustering : record in the Dead Sea Graben L _ To pLisan Plate: v. 101.

Sirota, I., 2016, Seasonal variations of halite saturation in the Dead Sea:, doi: 10.1002/2016WR018974.Received.

Sirota, I., Enzel, Y., and Lensky, N.G., 2018, Halite focusing and amplification of salt layer thickness: From the Dead Sea to deep hypersaline basins: Geology, v. 46, p. 851–854, doi: 10.1130/G45339.1.

Sirota, I., Enzel, Y., and Lensky, N.G., 2017, Temperature seasonality control on modern halite layers in the Dead Sea: In situ observations: Bulletin of the Geological Society of America, v. 129, p. 1181–1194, doi: 10.1130/B31661.1.

Starinsky, A., 1974. Relationship between Ca-chloride brines and sedimentary rocks in Israel. PhD. diss., Department of Geology, Hebrew University, Jerusalem.

Stein, M., 2001, The sedimentary and geochemical record of Neogene- Quaternary water bodies in the Dead Sea Basin – inferences for the regional paleoclimatic history: Journal of Paleolimnology, doi: 10.1023/A:1017529228186.

Stein, M., Agnon, A., Katz, A., and Starinsky, A., 2002, Strontium isotopes in discordant dolomite bodies of the Judea Group, Dead Sea basin: Israel Journal of Earth Sciences, v. 51, p. 219–224, doi: 10.1560/61UM-UMQF-YU86-JNU0.

Stein, M. and Goldstein, S.L., 2006. U-Th and radiocarbon chronologies of late Quaternary lacustrine records of the Dead Sea basin: methods and applications. *SPECIAL PAPERS-GEOLOGICAL SOCIETY OF AMERICA*, *401*, p.141.

Stein, M., Ben-Avraham, Z., and Goldstein, S.L., 2011, Dead Sea deep cores: A window into past climate and seismicity: Eos, v. 92, p. 453–454, doi: 10.1029/2011EO490001.

Stein, M., Starinsky, A., Agnon, A., Katz, A., Raab, M., Spiro, B., and Zak, I., 2000, The impact of brine-rock interaction during marine evaporite formation on the isotopic Sr record in the oceans: Evidence from Mt. Sedom, Israel: Geochimica et Cosmochimica Acta, v. 64, p. 2039–2053, doi: 10.1016/S0016-7037(00)00370-7.

Stein, M., Starinsky, I.A., Katz, I.A., Goldstein, J.S.L., Machlus, M., Schramm, A., Starinsky, A., Katz, A., and

Goldstein, S.L., 1997, for the evolution of Lake Lisan and the Dead Sea: Geochimica et Cosmochimica Acta, v. 61, p. 3975–3992.

Stein, M., Torfstein, A., Gavrieli, I., and Yechieli, Y., 2010, Abrupt aridities and salt deposition in the post-glacial Dead Sea and their North Atlantic connection: Quaternary Science Reviews, v. 29, p. 567–575, doi: 10.1016/j.quascirev.2009.10.015.

Stein, M., 2014. The evolution of Neogene-Quaternary water-bodies in the Dead Sea rift valley. In *Dead Sea Transform fault system: reviews* (pp. 279-316). Springer, Dordrecht.

Thomas, C., and Ariztegui, D., 2019, Fluid inclusions from the deep Dead Sea sediment provide new insights on Holocene extreme microbial life: Quaternary Science Reviews, v. 212, p. 18–27, doi: 10.1016/j.quascirev.2019.03.020.

Torfstein, A., 2008, Brine–Freshwater Interplay and Effects on the Evolution of Saline Lakes: the Dead Sea Rift Terminal Lakes: Geological Survey of Israel, Report GSI/20,.

Torfstein, A., Gavrieli, I., Katz, A., Kolodny, Y., and Stein, M., 2008, Gypsum as a monitor of the paleo-limnological-hydrological conditions in Lake Lisan and the Dead Sea: Geochimica et Cosmochimica Acta, v. 72, p. 2491–2509, doi: 10.1016/j.gca.2008.02.015.

Torfstein, A., Gavrieli, I., and Stein, M., 2005, The sources and evolution of sulfur in the hypersaline Lake Lisan (paleo-Dead Sea): Earth and Planetary Science Letters, v. 236, p. 61–77, doi: 10.1016/j.epsl.2005.04.026.

Torfstein, A., Goldstein, S.L., Kagan, E.J., and Stein, M., 2013, Integrated multi-site U-Th chronology of the last glacial Lake Lisan: Geochimica et Cosmochimica Acta, v. 104, p. 210–231, doi: 10.1016/j.gca.2012.11.003.

Torfstein, A., Goldstein, S.L., Kushnir, Y., Enzel, Y., Haug, G., and Stein, M., 2015, Dead Sea drawdown and monsoonal impacts in the Levant during the last interglacial: Earth and Planetary Science Letters, v. 412, p. 235–244, doi: 10.1016/j.epsl.2014.12.013.

Torfstein, A., Goldstein, S.L., Stein, M., and Enzel, Y., 2013, Impacts of abrupt climate changes in the Levant from Last Glacial Dead Sea levels: Quaternary Science Reviews, v. 69, p. 1–7, doi: 10.1016/j.quascirev.2013.02.015.

Torfstein, A., Haase-Schramm, A., Waldmann, N., Kolodny, Y., and Stein, M., 2009, U-series and oxygen isotope chronology of the mid-Pleistocene Lake Amora (Dead Sea basin): Geochimica et Cosmochimica Acta, v. 73, p. 2603–2630, doi: 10.1016/j.gca.2009.02.010.

Waldmann, N., 2002. *The geology of the Samra formation in the Dead Sea basin*. Hebrew University of Jerusalem.

Waldmann, N., Starinsky, A., and Stein, M., 2007, Primary carbonates and Ca-chloride brines as monitors of a paleo-hydrological regime in the Dead Sea basin: Quaternary Science Reviews, v. 26, p. 2219–2228, doi: 10.1016/j.quascirev.2007.04.019.

Waldmann, N., Stein, M., Ariztegui, D., and Starinsky, A., 2009, Stratigraphy, depositional environments and level reconstruction of the last interglacial Lake Samra in the Dead Sea basin: Quaternary Research, v. 72, p. 1–15, doi: 10.1016/j.yqres.2009.03.005.

Weber, N., 2021, The Ein Qedem springs, Dead Sea –Geological history and key role in depositing prominent gypsum structures during the Holocene: the Hebrew University of Jerusalem.

Weber, N., Lazar, B., Gavrieli, I., Yechieli, Y., and Stein, M., 2021, Gypsum Deltas at the Holocene Dead Sea Linked to Grand Solar Minima: Geophysical Research Letters, v. 48, p. 1–10, doi: 10.1029/2020GL091034.

Weber, N., Yechieli, Y., Stein, M., Yokochi, R., Gavrieli, I., Zappala, J., Mueller, P., and Lazar, B., 2018, The circulation of the Dead Sea brine in the regional aquifer: Earth and Planetary Science Letters, v. 493, p. 242–261, doi: 10.1016/j.epsl.2018.04.027.

Weinberger, R., Bar-Matthews, M., Levi, T., and Begin, Z.B., 2007, Late-Pleistocene rise of the Sedom diapir on the backdrop of water-level fluctuations of Lake Lisan, Dead Sea basin: Quaternary International, v. 175, p. 53–61, doi: 10.1016/j.quaint.2007.03.007.

Yechieli, Y., Magaritz, M., Levy, Y., Weber, U., Kafri, U., Woelfli, W., and Bonani, G., 1993, Late quaternary geological history of the dead sea area, Israel: Quaternary Research, v. 39, p. 59–67, doi: 10.1006/qres.1993.1007.

Yermiyahu, U., I. Zipori, C. Omer, Y.B., 2019, Research findings.: Nursing times, v. 80, p. 21, doi: 10.7748/en.12.7.8.s10.

Zak, I., 1967. *The geology of Mt. Sedom* (Doctoral dissertation, PhD Thesis) Hebrew University, Jerusalem).

Zilberman, T., Gavrieli, I., Yechieli, Y., Gertman, I., and Katz, A., 2017, Constraints on evaporation and dilution of terminal, hypersaline lakes under negative water balance: The Dead Sea, Israel: Geochimica et Cosmochimica Acta, v. 217, p. 384–398, doi: 10.1016/j.gca.2017.08.040.

המכון הגיאולוגי
משרד האנרגיה

ההתפתחות הגיאוכימית של תמלחת אגם הלשון מתוך הרכב המלחים המסיסים שבתווך הנקבובי

עומרי כליפא

חיבור לשם קבלת התואר 'מוסמך'

הוגש לסנט האוניברסיטה העברית בירושלים

העבודה נעשתה בהדרכתם של:

פרופ' מרדכי שטיין, האוניברסיטה העברית בירושלים, המכון הגיאולוגי לישראל

פרופ' בעז לזר, האוניברסיטה העברית בירושלים

דוח מס' GSI/10/2021

נובמבר 2021

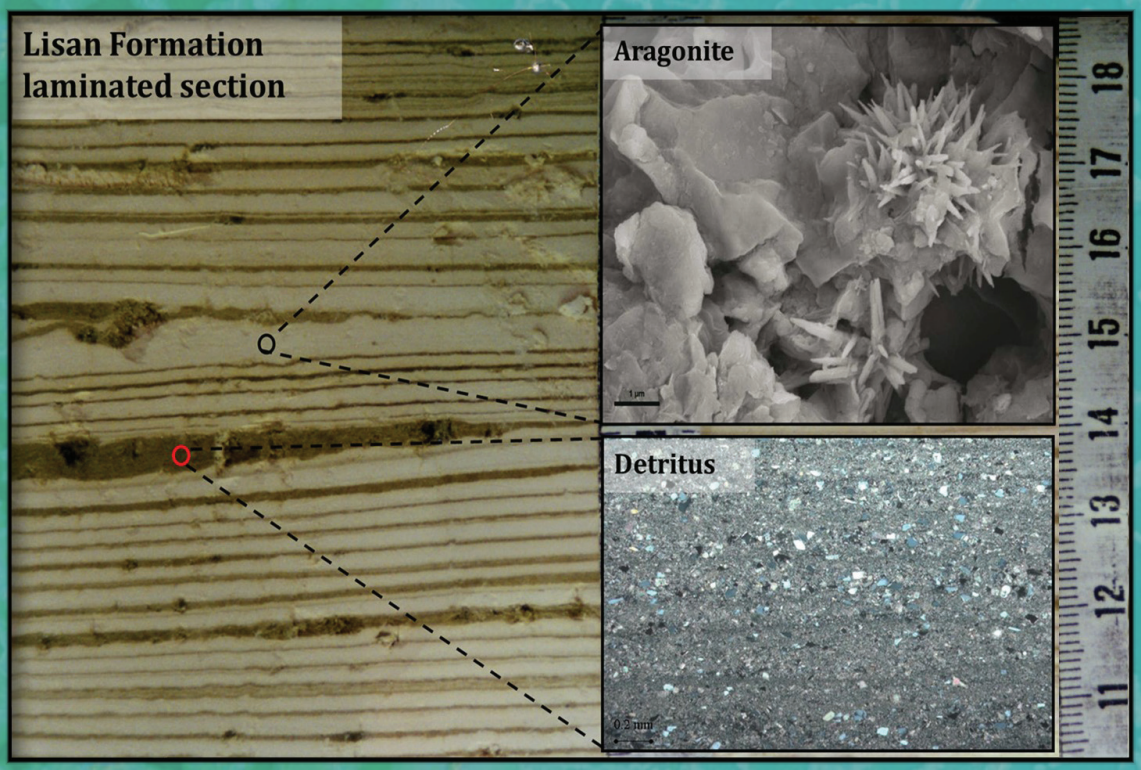
Lisan Formation
laminated section
Aragonite
1 µm
Detritus
0.2 mm
11
12
13
14
15
16
17
18